Robust output-feedback control of 3D directional drilling systems

Octavio A. Villarreal Magaña

Master of Science Thesis

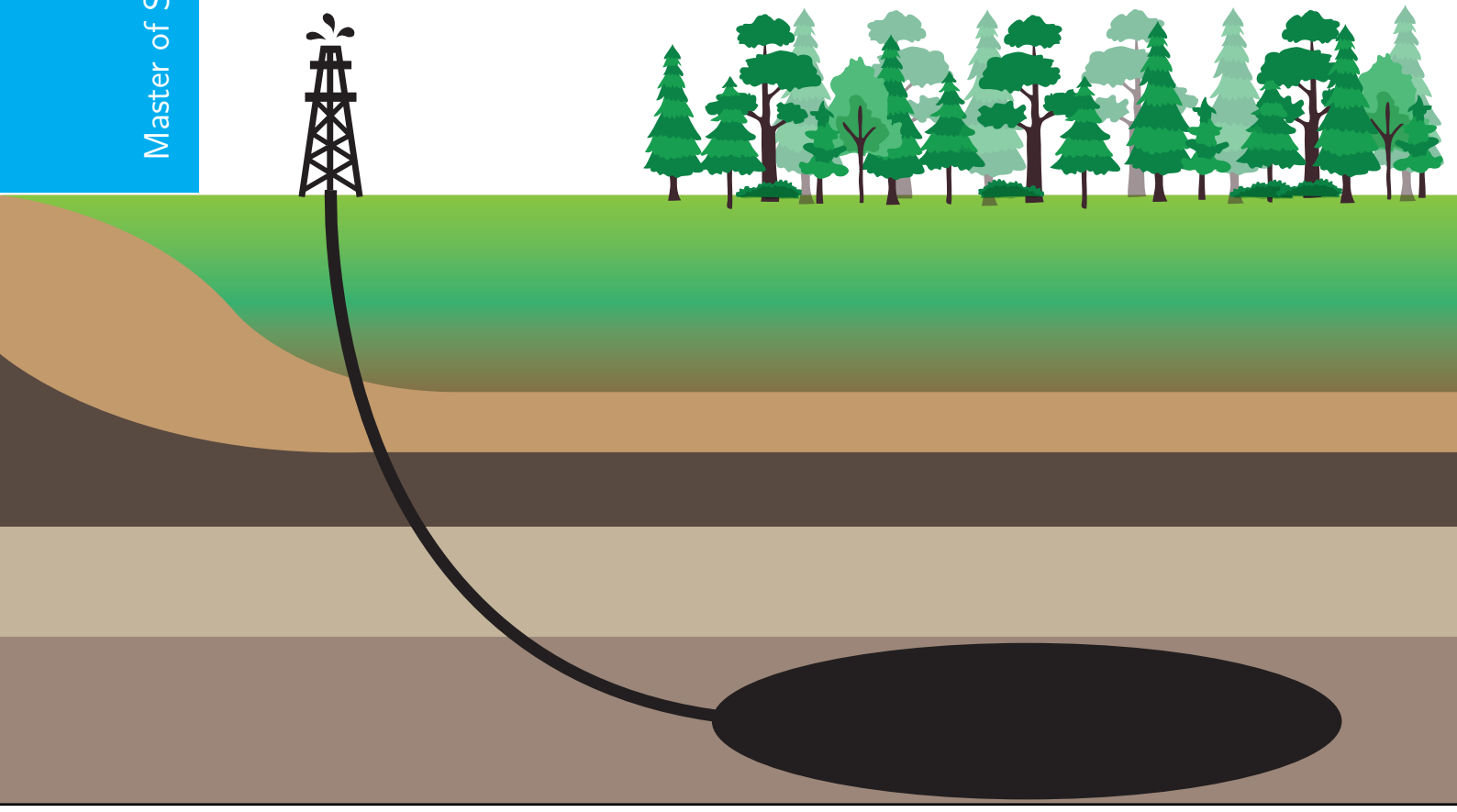

TU Delft Delft University of Technology

Delft Center for Systems and Control

Robust output-feedback control of 3D directional drilling systems

Master of Science Thesis

For the degree of Master of Science in Mechanical Engineering at Delft University of Technology

Octavio A. Villarreal Magaña

July 12, 2016

Faculty of Mechanical, Maritime and Materials Engineering (3mE) · Delft University of Technology

This project was done in collaboration with the University of Minnesota.

Delft University of Technology
Department of
Delft Center for Systems and Control (dcsc)

The undersigned hereby certify that they have read and recommend to the Faculty of Mechanical, Maritime and Materials Engineering (3mE) for acceptance a thesis entitled

Robust output-feedback control of 3D directional drilling systems

by

Octavio A. Villarreal Magaña

in partial fulfillment of the requirements for the degree of

Master of Science Mechanical Engineering

Dated: July 12, 2016

Supervisor(s):

prof.dr.ir. Nathan van de Wouw

prof.dr. Emmanuel Detournay

Reader(s):

dr.ir. Manuel Mazo Jr.

Abstract

The amount of mineral and energy resources in conventional reservoirs has been drastically diminished in recent years. This has led to the development of techniques to reach reservoirs which are not easy to access and, more specifically, where boreholes with complex geometries need to be drilled. Directional drilling allows to accomplish such complex boreholes. Although this process is not new to the industry, its complex dynamics have been responsible for the development of both numerical models and closed-form models in terms of delay differential equations. Such models can be used to predict the evolution of a borehole or to develop control strategies.

Current state-of-practice control methods are basically open-loop techniques, where an operator has the task to steer the drilling system while trying to follow a reference for the borehole trajectory. This usually generates undesired behavior such as borehole spiraling and kinking. In order to provide a way to avoid these undesired effects, novel control strategies need to be designed to improve the directional drilling process.

In order to improve the performance of this type of processes, some efforts have been made to propose a control strategy. One of the most recent approaches makes use of the model developed by Perneder and Detournay (PD) at the University of Minnesota, which describes the three-dimensional evolution of the borehole, with a set of nonlinear delay differential equations. The proposed control strategy implements a state-feedback controller to this model; hence it relies on availability of full-states measurements, which are not available in practice.

The goal of this thesis project is to extend this controller design making use of only local measurements of the orientation of the bottom-hole assembly. This is accomplished by including an observer in the control structure. Furthermore, the proposed controller design is robust against parameter uncertainty. The approach taken considers initially the case where the bit does not exhibit the so-called bit walk, simplifying the controller design. The effectiveness of the resulting robust output-feedback control approach is illustrated on realistic drilling scenarios.

Contents

List of Figures

List of Tables

Acknowledgements

I would like to thank first and foremost of all to my family. They are the reason I have been able to be here, doing what I'm most passionate about. Their restless support and trust in every decision I have ever made, has been the driving force that has guided me up to this point.

Gracias mamá por siempre confiar en mí y hacerme sentir que puedo cambiar el mundo, no podría pedir mejor fan número uno. Papá, te agradezco el apoyo incondicional que siempre has mostrado, la voluntad de entenderme y enseñarme el aprecio por el conocimiento. Gracias Alfredo, por seguir siendo una inspiración para mí, por siempre dar el consejo más atinado y honesto cuando lo necesito.

Secondly, I would like to thank my supervisors Prof.Dr.Ir. Nathan van de Wouw and Prof.Dr. Emmanuel Detournay. From the very beginning of this project and even today, they have always shown an extraordinary willingness to help me, not only with my thesis project but also with other aspects of my career. They have set an example for me regarding research work. Despite their numerous occupations and projects, they always made time on their agendas to provide meaningful advice. I sincerely hope we can keep in touch in the future.

My friends, both in Mexico and The Netherlands, have been constantly present throughout this Master's Program. New people have become part of my life; we shared the load of this new stage in our lives and, I had the chance to exchange experiences and get to know different cultures. I will always say, that the best experiences of traveling and living abroad are related to people. Also thanks to all of my lifelong friends, whom have kept on providing a positive inflence in my life despite the different paths we have taken in life.

I would like to thank María. You have always been since the day I met you, the spark that gives me the confidence to dare and believe that I can succeed. I feel proud of what we have both achieved together and I am sure that we will keep on changing each others lives.

Finally, I have to acknowledge the "Consejo Nacional de Ciencia y Tecnología" (CONACyT) for providing me with the financial support to perform my Master studies in The Netherlands.

Delft, University of Technology — Octavio A. Villarreal Magaña
July 12, 2016

Chapter 1

Introduction

The exhaustion of conventional supplies of mineral and energy resources has become an increasing and well-known problem in the past decades. This has lead to the development of new drilling techniques, which provide the possibility to exploit more difficult-to-reach reservoirs of these resources, as well as preventing and reducing environmental costs. An important breakthrough in this matter is directional drilling, a technology that allows to drill wells with complex geometries in order to access unconventional reservoirs of energy resources and minerals.

Directional drilling has proven to be a successful and cost-efficient process in important applications (see Figure 1-1), such as:

(a) Drilling to reservoirs, which are inaccessible using conventional techniques, such as resource deposits under a city or a natural area, providing a smaller environmental and social impact (Figure 1-1a).

(b) Multiple wells can be drilled from the same drill rig, reducing economic and environmental costs compared to drilling processes that require to drill separate boreholes from a different rig (Figure 1-1b).

(c) Drilling relief wells to release pressure in hazardous situations when control over a well is lost. This was demonstrated at the gulf of Mexico Deepwater Horizon oil spill in 2010, when two reliefs wells where drilled in order to seal the failure (Figure 1-1c).

(d) If a reservoir is close to a geological fault, directional drilling can be used to drill away from the fault plane avoiding damage to the well caused by fault slippage (Figure 1-1d).

In order to steer the drilling system and therewith the borehole generation, different methods have been implemented [6].

Conventionally, steerable motors were used to change direction during the drilling process. This motors have two modes: rotating and sliding. In the first mode, the whole drill rotates as in conventional drilling in a straight direction. In order to change direction, the drillstring

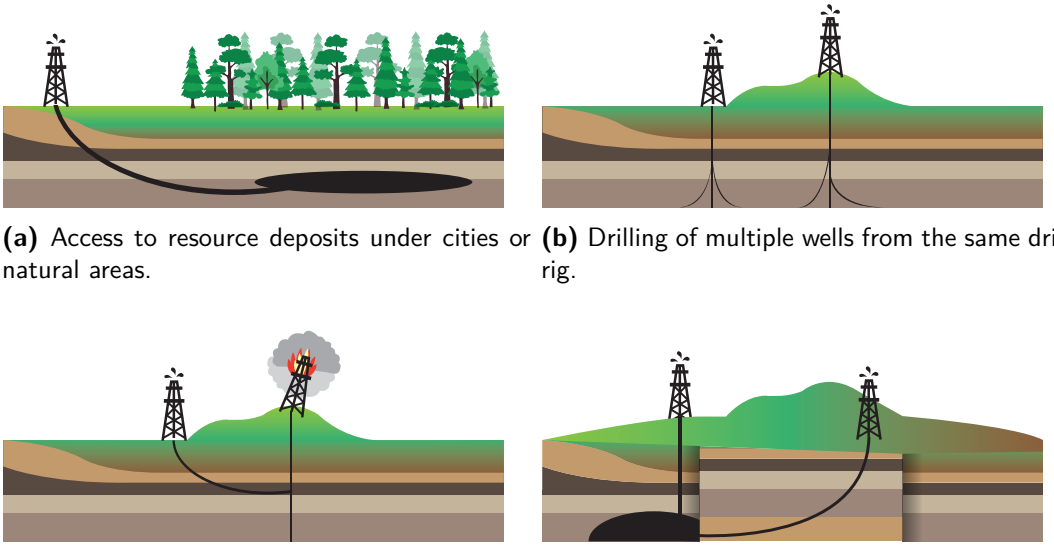

(a) Access to resource deposits under cities or natural areas.

(b) Drilling of multiple wells from the same drill rig.

(c) Drilling of relief wells in hazardous situations.

(d) Avoid drilling close to geological fault.

Figure 1-1: Applications of directional drilling.

is halted and a downhole motor is used, which is powered by drilling muds in order to point the bit in the desired drilling direction, the two modes are shown in Figure 1-2. This method proved to be very challenging, requiring a lot of skill from the drill operators and, as the complexity of boreholes was increased, the quality diminished due to the crookedness in the borehole induced by the rotating mode. Because of the previously mentioned issues, a new method to steer the direction of the drill was developed, namely the Rotary Steerable System (RSS). This type of technology allows the system to change direction while drilling, reducing borehole tortuosity, drilling time as well as increasing the Rate of Penetration (ROP). These are the type of steering mechanisms that will be considered in this research, due to their extensive use in industry nowadays.

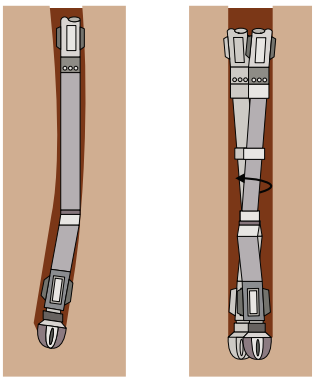

(a) Sliding.

(b) Rotating.

Figure 1-2: Drilling modes of a steerable motor.

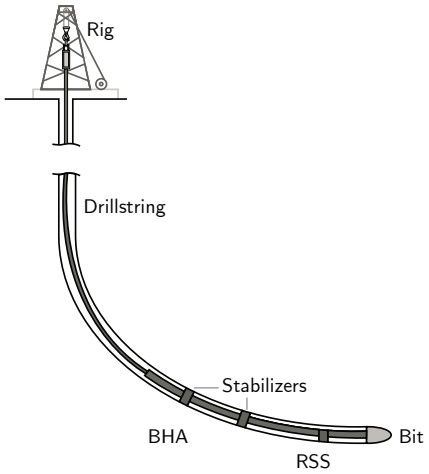

Figure 1-3: General description of a directional drilling system.

1-1 General description of the directional drilling system

A directional drilling system consists of the elements depicted in Figure 1-3. The drillsting (generally of a length in the order of kilometers) is the assembly of components from surface to bottom. Along this, power is transmitted to provide axial force and rotational speed imposed at the drilling rig. For the upper part of the drillstring, the axial force (commonly known as hook-load) along with its own weight, provide tension in the drillstring to prevent buckling. The Bottom Hole Assembly (BHA) constitutes the lower part of the drillstring and is usually in the order of hundreds of meters long. The BHA is in compression, in contrast with the upper part of the drillstring, to induce an axial force transmitted to the drill bit, called weight on bit. The BHA is commonly equipped with 3 to 5 stabilizers. These stabilizers center the BHA in the borehole, prevent for buckling as well and minimize torsional vibrations of the BHA. Between the first stabilizer and the bit, the previously mentioned RSS is placed. It is equipped with mud actuators and sensors to provide inclination and azimuth control of the borehole. There exist two main types of RSS: push-the-bit and point-the-bit systems. The first one applies lateral force, pushing against the borehole using pads actuated by mud diverted with a disk valve. In point-the-bit systems, the bit is tilted relative to the rest of the tool to achieve the desired trajectory [6]. In recent years, a new type of RSS is being researched on [7]. This type of mechanism (called hybrid RSS) combines the principles of point-the-bit and push-the-bit systems. Despite this, the most widely implemented type of RSS is the push-the-bit type and its functioning is demonstrated in Figure 1-4.

Along the process to achieve complex geometries using directional drilling systems, effects like kinking, rippling or spiraling may appear. The latter one has become an important subject of study in recent years, and it refers to the generation of undesired spiraling patterns along the borehole walls [8], see Figure 1-6. Reducing this borehole spiraling effect is one of the main challenges in the directional drilling industry in recent years. All of the previously mentioned effects may be harmful to the process and can potentially cause:

(a) An increase of frictional resistance of the borehole, which reduces the ROP, considerably affecting drilling times.

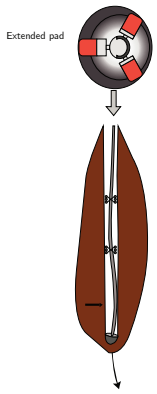

Figure 1-4: RSS push-the-bit system.

Figure 1-5: PDC drill bit [1].

(b) Reduced target-reach accuracy.

(c) Difficulty in the insertion of the casing after the borehole has been drilled.

(d) In a severe case, instability of the borehole evolution.

In most cases for directional drilling, Polycrystalline Diamond Compact (PDC) bits are used, an example of these is shown in Figure 1-5. This type of bit rotates at the end of the BHA and it is, in particular, laterally aggressive while drilling a borehole. The latter characteristic, among other causes, can produce a commonly known phenomenon called bit walk tendency, which is the natural behavior of the bit to deviate from its original path due to the lateral forces present while drilling.

In addition to the RSS, directional drilling systems nowadays are equipped with Measurement While Drilling (MWD) systems, that allow the driller to receive information from the down-hole elements to the surface at the same time as the drilling process takes place. Current MWD systems (mud pulse based systems) use the fluid flowing from inside the borehole, propagating it up to the top of the drillstring, which in practice generates a slow transmission of information (at a rate of the order of 10 bits per second [3]).

The control process of the RSS is generally conducted by three control loops:

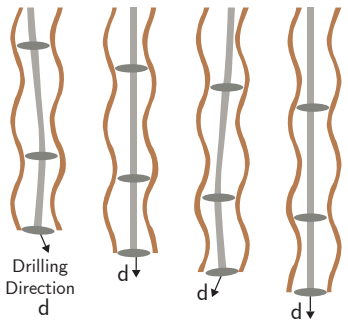

Figure 1-6: Borehole spiraling mechanism [2].

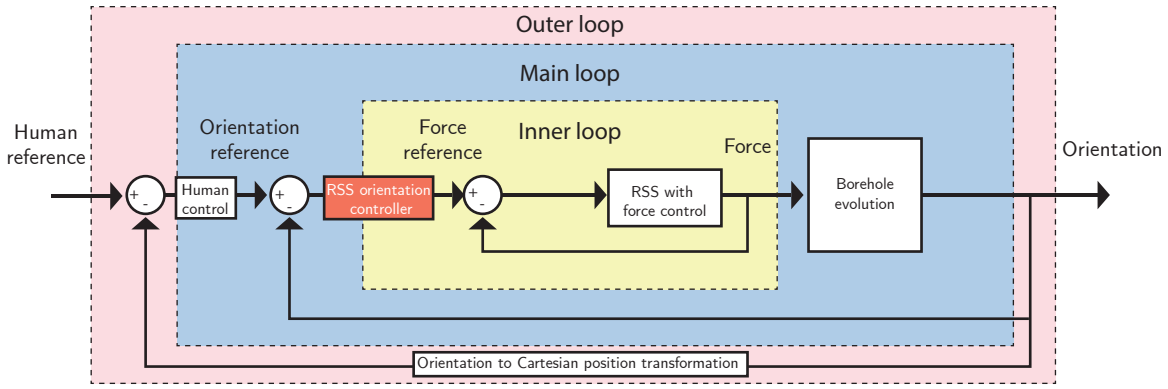

Figure 1-7: Control loops of a directional drilling system.

1. The main control loop, which sends commands for the actuation forces of the RSS in order to steer the borehole in a desired orientation.
2. An inner control loop which translates the incoming commands of the main loop into the RSS valve system.
3. An outer control loop which is in charge of correcting possible deviations in Cartesian coordinates of the borehole; these corrections are generally operated by a human.

A schematic block diagram of the three control loops is shown in Figure 1-7. At present, the most common practice for RSS type of systems is to apply constant force, expecting to obtain a constant curvature, which is generally not the case. The focus of this research will be on the main control loop, as this is the most involved level of control when steering the system. Furthermore, it is believed that borehole spiraling can be corrected at the level of this loop by implementing an RSS orientation controller.

There is not much research on control of directional drilling with a RSS, in part because it is relatively new to the industry [6]. As a consequence of this novelty, there are still discrepancies between the models that describe it. In most situations, developed controllers are designed for two-dimensional models, for which the effects that couple the responses of the two orientation variables (inclination and azimuth) are not considered. This is highly disadvantageous since some of the previously mentioned undesired effects can be a consequence of this coupling.

1-2 Literature review on directional drilling

To start studying the next steps to be taken regarding controller design of a directional drilling system, the available literature on the topic was analyzed. One of the most important tools for control engineers is the mathematical model representation of the dynamical systems to be controlled. In this regard, it was found that the most reliable way of representing the evolution of a borehole being drilled with this type of systems, is described by models in terms of delay differential equations, although other representations were also found during this literature review. These different models have a great effect on the chosen control strategies that have

been implemented throughout time. Despite the fact that currently most of the processes are being performed with essentially open-loop techniques, there are different control strategies, in the literature, based on different model types.

This section aims to give a general overview of these models and control strategies in order to set the stage to start developing new ways to cope with the current challenges in the field such as the avoidance of undesired borehole spiraling behavior and robustness to parametric uncertainty.

1-2-1 Modeling of directional drilling systems

As directional drilling technology arose, the need to describe its behavior, and predict the trajectories that a borehole would take, became more important due to the fact that in order to achieve a desired trajectory, experience of the driller was fundamental. This imposed a "trial and error" approach to the process. To overcome this problem, the most common way to assess the issue was to obtain a numerical model for the borehole propagation.

The works of [9], [10] and [11] are a few examples where finite element methods, combined sometimes with finite difference methods to solve the differential equations that describe the model, were used. Nevertheless, these examples do not contain crucial information related to the development of controllers, since most of the properties of the borehole propagation phenomena are not described in detail.

In recent years, Schlumberger® developed a finite element analysis model called "ST2", made to calculate trajectories of wells formed using a defined BHA, a bit and steering unit forces [12]. This model has been mainly used to compare the prediction of the borehole evolution from first principle models such as [13], showing in [14] a good match between the two models. Nevertheless the "ST2" model has not been directly used to develop control algorithms. Due to the complexity in finite element models, stability analysis and the influence forces and moments on the orientation of the borehole is not as evident as in first principles models. This aspect of numerical models makes controller design highly complex, since most of the control strategies are based on mathematical properties of a system or process, in order to give a physical interpretation of how these properties determine its behavior. One could use this numerical models to implement a method where depending on the current configuration, the right input (RSS forces) for the system in order to achieve a specific orientation could be computed, in a similar way as a "lookup" table. However, in numerical models the computational effort to predict the borehole evolution is much greater. This high demand for calculations, would make the implementation of an on-line closed-loop controller almost impossible, since it would have to compute the inputs at every instant using the complex numerical model. In summary, due to the transparency for the analysis, the reduced computational effort and the possibility to implement closed-loop control strategies on-line, first principles models are preferred.

A different type of models are the ones based on input-output correlations, for example neural-networks or polynomial correlations. These models are used to implement controllers in [12]. Since the circumstances where directional drilling systems are used may vary (due to factors such as type of soil, task to be performed, BHA configuration), the development of these type of models is not general since it is based on experimental data, meaning that a model should be built from scratch for every situation. Furthermore, these models are generally complex

and the inner physical effects in the system are not evident. Because of these reasons, it becomes difficult to perform stability and performance analysis. Finally, in the case of the controller developed in [12], there is no clear explanation about the behavior and the influence of forces in the model or the controller itself.

Regarding models useful for control, one of the approaches found in literature for the modeling of directional drilling systems is the one taken in [15] and [16], where the effects of lateral and torsional forces on the BHA and the drillstring are disregarded, considering that they are much faster than the borehole propagation. These models rely on kinematic coordinate transformations, presenting very simple descriptions of the directional drilling system. This simplicity provides the advantage that several type of conventional methods for controller design can be applied. Despite this, since the model has not yet been validated with field or experimental data, it can not be proven that the considered assumptions hold in general. Besides, the models that use delay differential equations and take into account forces and moments of the system, present a good match with both numerical and experimental data ([14], [17]), which can lead to the conclusion that these effects are important to the borehole evolution.

Neubert and Heisig developed a model in [18], which is considered one of the pioneering steps in first-principle-based modeling for directional drilling nowadays. The key elements that were introduced are the use of delay differential equations to describe the borehole evolution, analysis of kinematics and the deduction of a new bit/rock interaction that takes into account both axial and lateral effects. Despite this, there is only a small number of publications regarding this model and the international published paper on this model is not detailed enough in order to reproduce their results, and analyze the methods they used to develop controllers. Because of this, it is difficult to comprehend the exact underlying mechanisms in the model. The basic principles behind this model are extended by other models ([3], [13]).

One of the models that is most commonly found in literature is the one developed by Downton in [13]. A great advantage of this model is that its match with a specific numerical model has been tested with promising results [14]. Also, a transfer function representation can be obtained to use as a basis for controller design. Nevertheless, the bit/rock interaction is not as detailed as in other models. Another important aspect lies in the fact that this model has been derived only for a two-dimensional drilling system, although it has been mentioned in [13] that it could be extended to 3D. This is a major disadvantage since, some of the crucial causes of borehole spiraling take place due to the effects on three dimensions (i.e., bit walk). The model is derived in terms of deformation from an initial configuration, restricting the model to small angle rotations.

Finally, the so-called PD Model, developed by Perneder and Detournay in [3] (hence its name) at the University of Minnesota, is one of the most complete models developed up to this day. It possesses a more detailed bit/rock interaction model (compared to the one of Neubert and Heisig) and it also captures the delayed nature of the process. Furthermore, the model is developed for a three-dimensional system, and it is not restricted to small angle rotations. Also, a convenient state-space representation has been worked out in order to develop controllers in [5] and the model has been validated with field data in [17]. Despite these advantages, as most of the models developed up to this point, it lacks the inclusion of nonlinear effects such as bit-tilt saturation (although, bit-tilt saturation has been considered recently in [19]) and relies on assumptions such as borehole contact with the stabilizers at all

times.

1-2-2 Control of directional drilling systems

Current state-of-practice control methods are mostly open-loop, which in essence means that a constant RSS force is applied to the BHA, expecting a constant curvature of the borehole. This is generally not the case and undesired effects such as borehole spiraling, rippling and kinking are present when implementing this kind of strategies.

Because of this, some efforts have been made in order to implement more reliable methods to achieve a desired borehole trajectory. As in most cases in controller design, there is a close relation between the mathematical models and the controllers that have been developed to describe the process. As a result of this, the designed algorithms differ depending on the model that was used as a basis for design.

Due to the simplicity of the previously mentioned models developed in [15] and [20], various strategies to control the attitude of the bit have been implemented, such as linear feedback controllers with integral action and Model Predictive Control (MPC) [21], although the same problem regarding the unreliability of the model description remains. In the case of the model developed by Downton in [13], two controllers have been derived, one simple proportional controller in order to test the closed-loop stability of the system [14], and a more interesting $\mathcal{L}_1$ adaptive controller in order to deal with uncertainty [22]. These two controllers though, face the problem of only being derived for a 2D model, which does not consider effects on the azimuthal plane, which are crucial in borehole spiraling. This 2D limitation is not present in the pioneer model developed by Neubert and Heisig, for which two control algorithms were implemented by using a stabilizer with variable eccentricity. One is just a simple proportional controller, and the other is a proportional-derivative controller, that uses the tangent vector of the borehole trajectory at the bit as control variable in order to follow a trajectory [18]. The issue with this controller is not only the unavailability of publications, but also that the actuation is through the variable eccentricity, which is a suitable description for a point-the-bit system, and not for a push-the-bit system, the latter of which is studied in this thesis project.

Finally, there exist two recent works related to the development of control algorithms for the PD model; initially the control strategy was derived for the 2D case ([23], [24]), which constituted a first step towards a 3D control strategy [5]. A key element in the 3D model is the inclusion of what is called the bit walk tendency, which is the trend of the bit to drift in a lateral direction due to lateral forces acting in a different axis than the lateral penetration of the bit. It is important to notice that the controller in [5] is designed for the two stabilizers case. This does not yield loss of generality since the evolution of the system is not critically affected and the presented methodology can be applied to a higher number of stabilizers [5]. This controller seems to be highly advantageous in comparison with the previously presented ones. First of all, it is synthesized for the three-dimensional case of a directional drilling system, which takes into account the effects caused by bit walk, tackling the compensation for borehole rippling for both orientation variables of the system (azimuth and inclination). Furthermore, it considers the possibility of not being able to directly measure the states of the system, for which it gives an initial approach to an observer design. However, a stability analysis for the observer and the resulting output-fedback control strategy is lacking.

Moreover, the controller design in [5] does not yield "a priori" robust stability guarantees in the presence of uncertainties in e.g. the weight-on-bit and the bit walk angle.

1-3 Research objectives

Considering the previously mentioned aspects, the purpose of this thesis project is to develop a robust output-fedback control strategy for 3D directional drilling processes. Most of the existing control strategies, rely on the fact that there is access to all the states of the system (see Section 1-2). One of the main sub-goals is therefore to propose a control strategy for a 3D directional system to follow a desired borehole trajectory, which only relies on local measurements of the BHA orientation. In other words, the research aims to develop an observer-based controller design for a 3D directional drilling system.

Moreover, this design should take into account the fact that there is uncertainty in the process, so a strategy that can guarantee stability despite the variation of the parameters of the system is also a second sub-goal of high importance. The controller design should be robust to changes in the active weight on bit and the bit walk angle, and be able to reject disturbances present in the system.

1-4 Outline

The outline of this thesis will be given according to the following structure. Chapter 2 aims to describe the model that it is going to be used for controller design, namely the PD model. This chapter describes the key elements of the model and formulates this model in terms of a state-space delay system description suitable for controller design. Furthermore, in this section the neutral bit walk model, which will be used for controller design in later chapters is derived. This chapter also details the open-loop response of the system, in order to give a better understanding of the underlaying dynamics of the process and its deficiencies, based on a benchmark drilling system configuration.

Controller design for the case with no parameter uncertainty will be described in Chapter 3. The developed controller considers the neutral bit walk case, which only presents unilateral coupling from the inclination to the azimuth. Chapter 4 will use the analysis of the nominal case as a basis to develop a robustly stable control strategy against parameter uncertainty on the active weight on bit. The effectiveness of the proposed control strategy is shown in simulations for both the neutral and non-neutral bit walk model.

The final chapter details the conclusions of the developed control strategies and gives recommendations for further improvement on this work.

Chapter 2

Model of a 3D directional drilling system

From the literature review, it became evident that the most suitable model for controller design is the one developed by Perneder and Detournay. In this chapter, a general outline of the model derived in [3] is considered. Added to this, the state-space description of the system obtained in [5] is shown along with the neutral bit walk model that is used in the following chapters. Also the benchmark parameters that are used for the simulations performed during the research is provided. Finally, the chapter ends with the open-loop simulations of the model to verify its behavior for the different conditions considered in this thesis and to highlight the key deficiencies in the open-loop behavior that should be resolved by the control strategy to be developed.

2-1 Model description

The PD model was developed by Perneder and Detournay in [3], [25], [26] and [4], hence its name. It is formulated in terms of delay differential equations. A general description of the system is provided in Section 1-1. The delayed nature comes from the fact that the drillstring has to fit inside the borehole that has already been drilled. The geometric description for this model is shown in Figure 2-1. The elements of the geometric description of the model are listed below:

1. The earth-fixed coordinate basis is given by $(\vec{e}_x, \vec{e}_y, \vec{e}_z)$. It is located at the drill rig and vector $\vec{e}_z$ points in the direction of gravity and is perpendicular to $\vec{e}_x$ and $\vec{e}_y$ for a right-handed system.

2. The borehole is described as a function of the curvilinear coordinate S, with $0 \leq S \leq L$ where 0 is the value of the coordinate at the surface and L is the total length of the borehole.

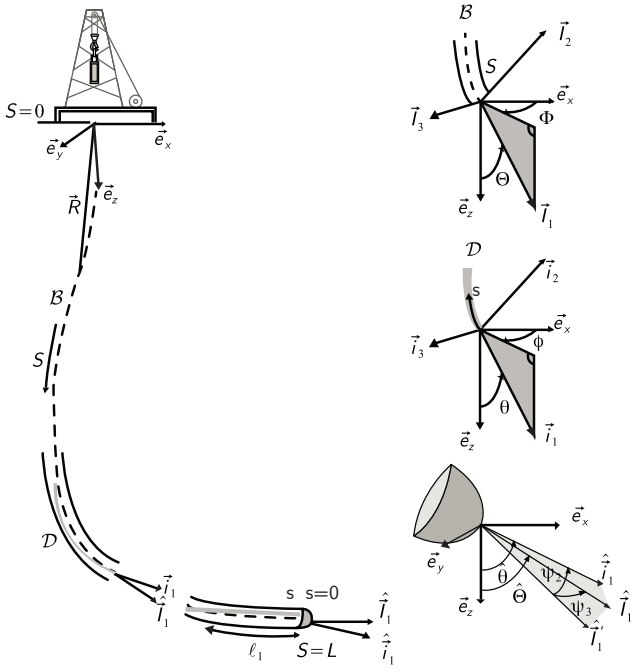

Figure 2-1: Geometric description of directional drilling system.

3. The borehole axis $\mathcal{B}$ is defined as the trajectory of a reference point at the bit.

4. The vector function $\vec{R}(S)$ for $S \in [0, L]$ describes the borehole axis $\mathcal{B}$ as a function of S in the earth-fixed basis.

5. At a certain position along the borehole, the direction of the borehole can be locally defined by the tangent vector of the borehole axis $\vec{I}_1 = \frac{d\vec{R}}{dS}$. Using this vector, a local basis $(\vec{I}_1, \vec{I}_2, \vec{I}_3)$ for the borehole can be defined by stating that $\vec{I}_2$ is in the same vertical plane as $\vec{I}_1$ and $\vec{I}_3$ is necessarily parallel to $\vec{e}_y$ (i.e., $\vec{I}_1 \times \vec{I}_2 = \vec{I}_3$ and $\vec{I}_3 \cdot \vec{e}_y = 0$) and defining the frame as right-handed.

6. The borehole inclination Θ is the angle between vector $\vec{e}_z$ and $\vec{I}_1$ as a function of the curvilinear coordinate S.

7. The borehole azimuth Φ is the angle between $\vec{e}_x$ and the projection of $\vec{I}_1$ to the plane spanned by $\vec{e}_x$ and $\vec{e}_y$.

8. The BHA axis is described as a function of the curvilinear coordinate $s \in [0, L_{BHA}]$ where 0 is the position of the drill bit and L_{BHA} is the length of the BHA.

9. The BHA axis $\mathcal{D}$ is considered to be slightly deviated from the borehole axis $\mathcal{B}$ (due to deflection of the BHA piping with respect to the borehole axis).

10. The vector function $\vec{r}(s, L)$ describes the position of the BHA axis $\mathcal{D}$ as a function of s and the current length of the borehole L.

11. The basis associated to the BHA $(\vec{i}_1, \vec{i}_2, \vec{i}_3)$ is obtained in a similar fashion as the borehole basis, such that $\vec{i}_1$ is the tangent unit vector to $\mathcal{D}$ and $\vec{i}_3 \cdot \vec{e}_y = 0$ (parallel) and $\vec{i}_1 \times \vec{i}_2 = \vec{i}_3$ (perpendicular) and defining the system as right-handed.

12. It is important to notice that in general the borehole and BHA axes are not coaxial, meaning that the bit does not drill in the same direction as the tangent of the borehole axis due to lateral forces on the bit generating lateral and angular penetration, so in general $\vec{I}_1 \neq \vec{i}_1$.

13. The BHA inclination θ is the angle between $\vec{e}_z$ and $\vec{i}_1$ as a function of the curvilinear coordinate s.

14. The BHA azimuth ϕ is the angle between $\vec{e}_x$ and the projection of $\vec{i}_1$ to the plane spanned by $\vec{e}_x$ and $\vec{e}_y$.

15. To simplify notation, a hat ($\hat{}$) is used for variables and bases evaluated at the bit, i.e., $\hat{\Theta} = \Theta(L)$ and $\hat{\Phi} = \Phi(L)$ in the case of the borehole; and $\hat{\theta} = \theta(L, 0)$ and $\hat{\phi} = \phi(L, 0)$ in the case of orientation of the bit itself.

16. The differences between the orientation of the bit and the borehole, called the tilt angles, are given by:

$$\begin{aligned} \psi_2 &= \hat{\theta} - \hat{\Theta}, \\ \psi_3 &= (\hat{\phi} - \hat{\Phi}) \sin \hat{\Theta}, \end{aligned} \tag{2-1}$$

see Figure 2-1. Since it is considered that the predominant element in the borehole evolution is the BHA, the model considers the effects at the upper part of the drillstring as a mere boundary condition (in terms of the axial force transmitted from the drill-string to the BHA).

The model of the directional drilling system is obtained from the interaction between three key model elements:

- kinematic relationships,
- the BHA model,
- bit/rock interface law.

The way these elements relate to each other is depicted in Figure 2-2. Furthermore, the vibrational effects in the BHA are ignored due to the fact that they take place at a much faster time scale than the time scales relevant for borehole propagation. This is why the forces and penetrations are averaged over several revolutions of the bit. An important consideration is that the stabilizers are assumed to always be in contact with the borehole wall, which in general is not always the case in practice [27].

The model is scaled at the BHA by introducing two characteristic quantities:

$$L_* := \ell_1, \qquad F_* := \frac{3E_y I}{\ell_1^2}, \tag{2-2}$$

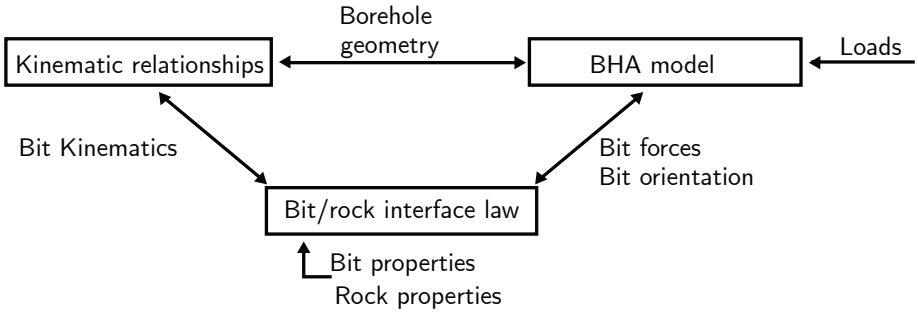

Figure 2-2: Interaction between the elements of the model.

where ℓ_1 is the distance between the bit and the first stabilizer (defining the characteristic length L_*), see Figure 2-3, and the product of the Young's module E_y with the area moment of inertia I represents the bending stiffness. The BHA is modeled as an Euler-Bernoulli beam, since deformations are presumed to be small because the radius of curvature of the borehole is typically large compared to ℓ_1. The reason for F_* being defined as shown is that this is the reaction force induced at the end of a simply supported beam of length ℓ_1 and stiffness E_yI in response to a unit inclination angle imposed at the end. The characteristic length L_* is used to scale the distance drilled L into a dimensionless distance drilled ξ:

$$\xi = \frac{L}{L_*}. \tag{2-3}$$

BHA model. Figure 2-3 shows the elements for a deflected BHA inside a borehole. The configuration is described by the position of the stabilizers and the RSS. Their location is given as $s = s_i$ where s_i is the s coordinate of the i-th stablizer and $\Lambda\ell_1$ is the location of the RSS where $\Lambda \in [0, 1]$. The distance between stabilizer i and $i-1$ is given by ℓ_i for $i = 2, ..., n$ and ℓ_1 defined as the distance between the bit and the first stabilizer again. Herein, n represents the number of stabilizers.

The external loads acting on the BHA are the distributed weight $\vec{w}$, the RSS force $\vec{F}_{rss}$, as well as the forces acting on the upper and lower boundaries of the BHA. The RSS force has two components on the direction of the $\vec{I}_2$ and $\vec{I}_3$ axes. These components and the distributed weight are scaled using the characteristic force F_* as follows:

$$\Upsilon = \frac{wL_*}{F_*}, \qquad \Gamma_2 = \frac{F_{rss,2}}{F_*}, \qquad \Gamma_3 = \frac{F_{rss,3}}{F_*}. \tag{2-4}$$

where Υ, Γ_2 and Γ_3 are the scaled versions of the distributed weight, the RSS force applied along axis $\vec{I}_2$ and $\vec{I}_3$, respectively. In further derivations, uniform bending stiffness E_yI and distributed weight w for the BHA are assumed; it is also assumed that the relative direction of the distributed weight with respect to the BHA is being aligned with the chord $\mathcal{C}_1$ which links the bit and the first stabilizer, see Figure 2-3.

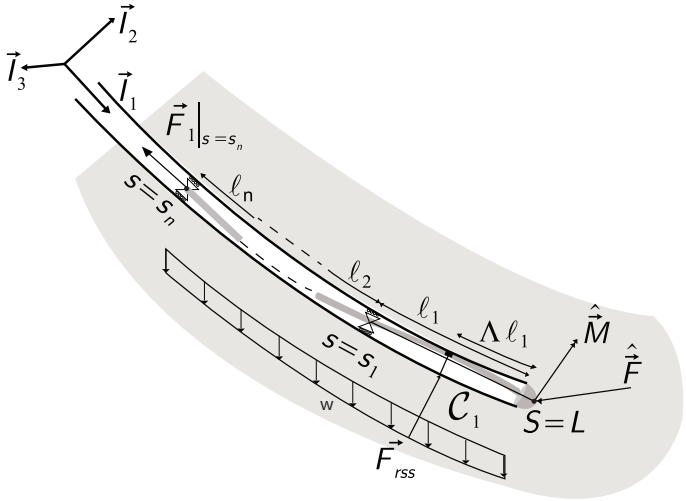

Figure 2-3: Deflected BHA.

The governing equations for the transverse deflection of the BHA as an Euler-Bernoulli beam are given by:

$$E_y I \frac{\partial^3 \theta_i}{\partial s^3} = w \sin \langle \theta \rangle_1, \qquad E_y I \sin \langle \theta \rangle_1 \frac{\partial^3 \phi_i}{\partial s^3} = 0, \tag{2-5}$$

where $\langle \theta \rangle_1$ is the average inclination of the BHA between the bit and the first stabilizer. The BHA is divided in $n+1$ (with n being the number of stabilizers) beams connected by ideal stabilizers. Each section between stabilizers is modeled as a beam and the section between the bit and the first stabilizer is separated into two parts, one corresponding to the section from the bit to the RSS and the other from the RSS to the first stabilizer, modeling both as beams as well. Using the following notation,

$$\begin{aligned}
&\theta(\xi,s) = \theta_i(\xi,s), \qquad \phi(\xi,s) = \phi_i(\xi,s), \qquad \text{for } s \in [s_{i-1}, s_i] \text{ for } i \in [2,...,n],\\
&\theta(\xi,s) = \theta_1(\xi,s), \qquad \phi(\xi,s) = \phi_1(\xi,s), \qquad \text{for } s \in [\Lambda\ell_1, s_1],\\
&\theta(\xi,s) = \theta_0(\xi,s), \qquad \phi(\xi,s) = \phi_0(\xi,s), \qquad \text{for } s \in [0, \Lambda\ell_1],
\end{aligned} \tag{2-6}$$

the general solution of Equation (2-5) is given by:

$$\begin{aligned}
\theta_i(\xi,s) &= \mathcal{A}_{i3}\left(\frac{s}{\ell_1}\right)^3 + \mathcal{A}_{i2}\left(\frac{s}{\ell_1}\right)^2 + \mathcal{A}_{i1}\left(\frac{s}{\ell_1}\right) + \mathcal{A}_{i0},\\
\phi_i(\xi,s) &= \mathcal{B}_{i2}\left(\frac{s}{\ell_1}\right)^2 + \mathcal{B}_{i1}\left(\frac{s}{\ell_1}\right) + \mathcal{B}_{i0}.
\end{aligned} \tag{2-7}$$

where $\mathcal{A}_{ij}$, for $j = 0, 1, 2, 3$, and $\mathcal{B}_{ik}$, for $k = 0, 1, 2$, are coefficients corresponding to the integration constants resulting from the solution of (2-5). To obtain the coefficients in (2-7), a set of $6(n+1)$ constraints needs to be imposed depending on factors related to the previously mentioned assumptions of the model. Firstly, the inclination and azimuth angles of the BHA are continuous at the boundary between adjacent segments; this results in the first set of n constraints depending on the number of stabilizers. A second set of constraints comes from the fact that the moment at all stabilizers is continuous. The third set of constraints is related to the coincidence of the borehole axis and the BHA axis at the stabilizers. These three sets of constraints constitute $3n$ constraints and are all related to the stabilizers. One of the other three remaining constraints is related to assumptions such as zero moment at the last stabilizer. This assumption is valid if a sufficient number of stabilizers is considered, since the amount of stabilizers is inversely proportional to the moment at the bit (as shown in Appendix B of [3]). The other two assumptions are related to the force balance between the RSS force and the BHA force at the segment between the bit and the RSS location, and the fact that $\theta_0 = \hat{\theta}$ and $\phi_0 = \hat{\phi}$ at the bit coming from the bit rock interaction. For the complete derivation of these constraints in the case of the 2D model see Appendix B of [23]. These constraints can also be extended to the 3D case since the expressions for the inclination and the azimuth are the same, considering that the gravity has no influence on the azimuth, and that the RSS force is given by $\frac{\Gamma_3}{\sin\Theta}$ instead of Γ_2 (see Appendix A-1). These constraints and coefficients $\mathcal{A}_{ij}$ and $\mathcal{B}_{ik}$ for the two stabilizer case are given in Appendix A-1 of this thesis. It has been proven that studying the two stabilizer case is sufficient, since the first two stabilizers dominate the dynamics of the directional drilling process [17]. Finally, the expressions for shear forces and bending moments acting on the bit expressed in the bit basis are obtained as follows:

$$
\begin{aligned}
\frac{\hat{F}_2}{F_*} &= \mathcal{F}_b\left(\hat{\theta} - \langle\Theta\rangle_1\right) + \mathcal{F}_w\Upsilon\sin\langle\Theta\rangle_1 + \mathcal{F}_r\Gamma_2 + \sum_{i=1}^{n-1}\mathcal{F}_i\left(\langle\Theta\rangle_i - \langle\Theta\rangle_{i+1}\right),\\
\frac{\hat{M}_3}{F_*\ell_1} &= \mathcal{M}_b\left(\hat{\theta} - \langle\Theta\rangle_1\right) + \mathcal{M}_w\Upsilon\sin\langle\Theta\rangle_1 + \mathcal{M}_r\Gamma_2 + \sum_{i=1}^{n-1}\mathcal{M}_i\left(\langle\Theta\rangle_i - \langle\Theta\rangle_{i+1}\right),\\
\frac{\hat{F}_3}{F_*} &= \mathcal{F}_b\left(\hat{\phi} - \langle\Phi\rangle_1\right)\sin\langle\Theta\rangle_1 + \mathcal{F}_r\Gamma_3 + \sum_{i=1}^{n-1}\mathcal{F}_i\left(\langle\Phi\rangle_{\mathrm{i}} - \langle\Phi\rangle_{\mathrm{i+1}}\right)\sin\langle\Theta\rangle_1,\\
\frac{\hat{M}_2}{F_*\ell_1} &= -\mathcal{M}_b\left(\hat{\phi} - \langle\Phi\rangle_1\right)\sin\langle\Theta\rangle_1 - \mathcal{M}_r\Gamma_3 - \sum_{i=1}^{n-1}\mathcal{M}_i\left(\langle\Phi\rangle_i - \langle\Phi\rangle_{i+1}\right)\sin\langle\Theta\rangle_1,
\end{aligned}
\tag{2-8}
$$

where $\mathcal{F}_b$, $\mathcal{F}_r$, $\mathcal{F}_w$, $\mathcal{F}_i$, $\mathcal{M}_b$, $\mathcal{M}_r$, $\mathcal{M}_w$, $\mathcal{M}_i$ are constant coefficients for a given BHA configuration which can be found in Appendix A-2 for the two stabilizer case. The average borehole inclination and azimuth at the i-th stabilizer $\langle\Theta\rangle_i$ and $\langle\Phi\rangle_i$ in (2-8) are given by

$$
\langle\Theta\rangle_i := \frac{1}{\varkappa_i}\int_{\xi_i}^{\xi_{i-1}}\Theta(\sigma)d\sigma, \qquad \langle\Phi\rangle_i := \frac{1}{\varkappa_i}\int_{\xi_i}^{\xi_{i-1}}\Phi(\sigma)d\sigma, \tag{2-9}
$$

where $\varkappa_i$ is the dimensionless length of the i-th BHA section given by $\varkappa_i = \frac{\ell_i}{\ell_1}$ and ξ_i is the dimensionless position of stabilizer i given by $\xi_i = \xi - \sum_{j=1}^{i}\varkappa_i$ for $i = 1, 2, ..., n$.

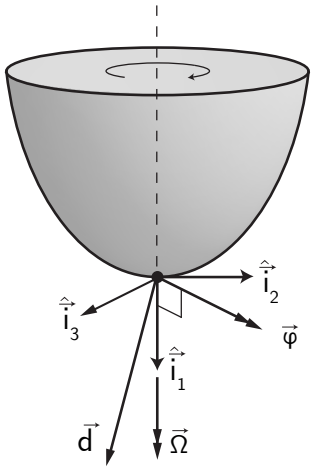

Figure 2-4: Definition of the penetration vector $\vec{d}$, the angular penetration vector $\vec{\varphi}$ and the angular velocity vector $\vec{\Omega}$ [3].

Kinematic relationships. The motion of the bit is described by the linear velocity vector $\vec{v}$, the spin vector $\vec{\omega}$ and the angular velocity $\vec{\Omega}$. The bit is rotating around $\vec{i}_1$ with angular velocity $\vec{\Omega}$. Using this we can define the two main penetration variables:

$$\vec{d} := \frac{2\pi\vec{v}}{|\vec{\Omega}|}, \qquad \vec{\varphi} := \frac{2\pi\vec{\omega}}{|\vec{\Omega}|}, \tag{2-10}$$

where $\vec{d}$ and $\vec{\varphi}$ are the linear and angular penetration, respectively. These variables are depicted in Figure 2-4. The linear penetration is the increment of the borehole over one revolution, which is expressed by using the operator $\delta(.) = |\vec{d}|\frac{d(.)}{dL}$. With this definition, the magnitude of the linear penetration $d = |\vec{d}|$ is equal to the increment of the borehole length δL.

The two vector penetration variables are decomposed in five scalar quantities corresponding to $\vec{d} = d_1\hat{\vec{i}}_1 + d_2\hat{\vec{i}}_2 + d_3\hat{\vec{i}}_3$, as well as φ_2 and φ_3 as the rotations around vectors $\hat{\vec{i}}_2$ and $\hat{\vec{i}}_3$, respectively. It is assumed that $d_1 \approx |\vec{d}|$ because components d_2 and d_3 depend on the tilt angles ψ_2 and ψ_3 (see Figure 2-5) which are generally small under normal drilling conditions and defined by:

$$\begin{aligned} d_2 &= -\psi_2 d_1, \\ d_3 &= -\psi_3 d_1. \end{aligned} \tag{2-11}$$

In addition, the expressions for φ_2 and φ_3 are given as:

$$\begin{aligned} \varphi_2 &= -\frac{d_1}{\ell_1}\frac{d\hat{\phi}}{d\xi}\sin\hat{\theta}, \\ \varphi_3 &= \frac{d_1}{\ell_1}\frac{d\hat{\theta}}{d\xi}, \end{aligned} \tag{2-12}$$

where these expressions are obtained by projecting the cross product $\hat{\vec{i}}_1 \times \delta\hat{\vec{i}}_1$ onto the bit basis [3].

Bit/rock interface law. This element of the model represents the interaction between the kinematics of the bit (defined by the set of penetration variables $\mathcal{P} = \{d_1, d_2, d_3, \varphi_2, \varphi_3\}$), and the forces and moments reacting on the bit (defined by $\mathcal{F} = \{\hat{F}_1, \hat{F}_2, \hat{F}_3, \hat{M}_2, \hat{M}_3\}$), due to the properties of the bit and the drilled rock.

A common type of bit used in directional drilling systems is the PDC bit (see Figure 1-5), and the interface law is derived for this kind of bit. There are three assumptions to be considered for this interface model. Firstly, the forces $\mathcal{F}$ and kinematic quantities $\mathcal{P}$ can be averaged over at least one revolution, since the time scale of the borehole evolution is much larger than the period of a revolution. Secondly, the interface law is rate-independent, based on single cutter experiments, which show independence of the torque on bit with the rotary speed. Hence, the model does not depend on the bit angular velocity Ω. Finally, the global relationship between forces and penetrations is assumed to be reduced to a point [28].

In addition to the previous three key assumptions, the rock is assumed to be isotropic and homogeneous, which means that the rock is uniform in all directions. Based on this assumptions and on single cutter experiments [29], the following linear relationship between the penetration variables $\mathcal{P}$ and the generalized forces and moments $\mathcal{F}$ is proposed:

$$\begin{bmatrix} \hat{F}_1 \\ \hat{F}_2 \\ \hat{F}_3 \\ \hat{M}_2 \\ \hat{M}_3 \end{bmatrix} = - \begin{bmatrix} G_1 \\ 0 \\ 0 \\ 0 \\ 0 \end{bmatrix} - \begin{bmatrix} H_1 & 0 & 0 & 0 & 0 \\ 0 & H_2 & H_3 & 0 & 0 \\ 0 & -H_3 & H_2 & 0 & 0 \\ 0 & 0 & 0 & H_0 & 0 \\ 0 & 0 & 0 & 0 & H_0 \end{bmatrix} \begin{bmatrix} d_1 \\ d_2 \\ d_3 \\ \varphi_2 \\ \varphi_3 \end{bmatrix}. \tag{2-13}$$

In (2-13), coefficient G_1 measures the axial force transmitted to the equivalent single cutter wear-flats, due to an increase of bluntness of the bit. For a perfectly sharp bit, G_1 is equal to zero. The first row of Equation (2-13) corresponds to the axial forces at the bit. The applied weight on bit (defined as $W_{app} = -\hat{F}_1$) is affected by the frictional forces denoted by coefficient G_1. The actual force applied in the axial direction is defined as the active weight on bit W_{act} and can be expressed as $W_{act} = W_{app} - G_1$. Furthermore, the active weight on bit can be scaled in the same way as the external loads of the BHA in (2-4) to a dimensionless parameter Π as follows:

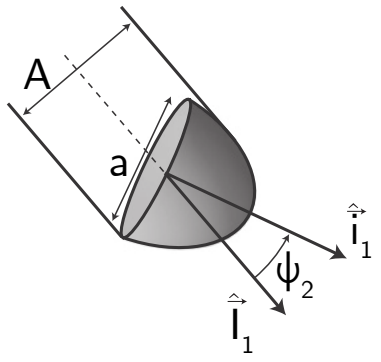

Figure 2-5: Borehole over-gauging caused by the bit tilt angle ψ_2 [4].

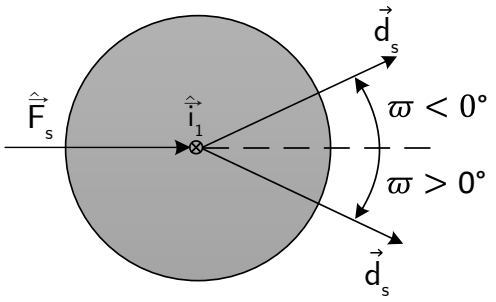

Figure 2-6: The bit walk angle ϖ is the angle between the lateral $\hat{\vec{F}}_s = \hat{F}_1\hat{\vec{i}}_1 + \hat{F}_2\hat{\vec{i}}_2$ and the lateral penetration $\vec{d}_s = d_2\hat{\vec{i}}_2 + d_3\hat{\vec{i}}_3$ (view at the front of the bit)[5].

$$\Pi = \frac{W_{act}}{F^*} \tag{2-14}$$

The coefficients H_0, H_1, H_2, H_3 depend on the bit geometry (such as cutting structure and gauge length) and the rock properties. These coefficients along with G_1 describe the relation between the penetration variables and the forces. Using these coefficients, the lateral and angular steering resistance can be defined as:

$$\eta = \frac{\sqrt{{H_2}^2 + {H_3}^2}}{H_1}, \qquad \chi = \frac{H_0}{{\ell_1}^2 H_1}. \tag{2-15}$$

These two parameters, η and χ, measure the opposition to impose lateral and angular penetration to the bit relative to the axial penetration, respectively. Another property of the system that is derived from the bit/rock interaction, is the bit walk tendency, which is the natural tendency of the bit to drift in a lateral direction while drilling. Bit walk takes place when the lateral forces at the bit are not coaxial with the lateral penetration vectors of the bit, and it can be quantified by measuring the angle between the lateral force and the lateral penetration (see Figure 2-6), obtained as follows:

$$\varpi = \arctan\frac{H_3}{H_2}. \tag{2-16}$$

It is important to stress, that the lateral and angular steering resistance η and χ come from inherent properties of the rock and the cutter geometry. In the case of the scaled active weight on bit Π, its value can change along the process due to variations in the applied hook-load, the interaction of the drillstring with the borehole and a reduction of the sharpness of the bit. Finally, the bit walk angle ϖ can be dependent on factors such as the rotation of the bit and over-gauging and it can also vary while drilling [5]. This is why, the active weight on bit Π and the bit walk angle ϖ are generally considered as uncertain parameters.

Making use of the expressions for Π, η, χ and ϖ, and using the fact that $\hat{F}_1 = -G_1 - H_1 d_1$; coefficients H_0, H_1, H_2 and H_3 can be substituted in the bit/rock interface law given in (2-13).

The complete derivation of this interaction law is given in [3], which arrives to the following dimensionless expression in the three-dimensional case:

$$\begin{bmatrix} \frac{\hat{F}_2}{F_*} \\ \frac{\hat{F}_3}{F_*} \\ \frac{\hat{M}_2}{F_*\ell_1} \\ \frac{\hat{M}_3}{F_*\ell_1} \end{bmatrix} = \begin{bmatrix} \eta\Pi\cos\varpi & \eta\Pi\sin\varpi & 0 & 0 \\ -\eta\Pi\sin\varpi & \eta\Pi\cos\varpi & 0 & 0 \\ 0 & 0 & -\frac{\chi\Pi\ell_1}{d_1} & 0 \\ 0 & 0 & 0 & -\frac{\chi\Pi\ell_1}{d_1} \end{bmatrix} \begin{bmatrix} \frac{d_2}{d_1} \\ \frac{d_3}{d_1} \\ \varphi_2 \\ \varphi_3 \end{bmatrix}. \tag{2-17}$$

This interface law, relates the penetration variables at the bit with the forces and moments at the bit as well.

Borehole evolution equations. By combining the BHA model Equations (2-8), the kinematic relationships (2-11) and (2-12) and the bit/rock interface law (2-17), the borehole evolution equations are derived as follows:

$$\eta\Pi\Big((\theta-\Theta)\cos\varpi+\sin\Theta\sin\varpi\,(\phi-\Phi)\Big)=\mathcal{F}_b\left(\theta-\langle\Theta\rangle_1\right)+\mathcal{F}_w\Upsilon\sin\langle\Theta\rangle_1+\mathcal{F}_r\Gamma_2 + \sum_{i=1}^{n-1}\mathcal{F}_i\left(\langle\Theta\rangle_i-\langle\Theta\rangle_{i+1}\right), \tag{2-18}$$

$$-\chi\Pi\theta'=\mathcal{M}_b\left(\theta-\langle\Theta\rangle_1\right)+\mathcal{M}_w\Upsilon\sin\langle\Theta\rangle_1+\mathcal{M}_r\Gamma_2+\sum_{i=1}^{n-1}\mathcal{M}_i\left(\langle\Theta\rangle_i-\langle\Theta\rangle_{i+1}\right), \tag{2-19}$$

$$\eta\Pi\Big(-(\theta-\Theta)\sin\varpi+\cos\varpi\sin\Theta\,(\phi-\Phi)\Big)=\mathcal{F}_b\left(\phi-\langle\Phi\rangle_1\right)\sin\langle\Theta\rangle_1+\mathcal{F}_r\Gamma_3 + \sum_{i=1}^{n-1}\mathcal{F}_i\left(\langle\Phi\rangle_i-\langle\Phi\rangle_{i+1}\right)\sin\langle\Theta\rangle_1, \tag{2-20}$$

$$-\chi\Pi\phi'\sin\theta=\mathcal{M}_b\left(\phi-\langle\Phi\rangle_1\right)\sin\langle\Theta\rangle_1+\mathcal{M}_r\Gamma_3+\sum_{i=1}^{n-1}\mathcal{M}_i\left(\langle\Phi\rangle_i-\langle\Phi\rangle_{i+1}\right)\sin\langle\Theta\rangle_1. \tag{2-21}$$

Herein, the ($\hat{}$) character has been omitted for notational clarity and we emphasize that in these equations all variables are evaluated at the bit. Moreover, the derivatives of the inclination and the azimuth of the BHA with respect to the dimensionless length (i.e, $\frac{d\theta}{d\xi}$ and $\frac{d\phi}{d\xi}$) are replaced by θ' and ϕ', respectively. This set of equations represents the way the borehole will evolve along the independent variable ξ in terms of the borehole and BHA inclination and azimuth. It is important to notice, that the final goal is to be able to describe how the borehole will change along the process; this means that it would be more convenient to express the BHA orientation variables θ and ϕ in terms of the borehole variables Θ and Φ and input variables Γ_2 and Γ_3 (which represent the RSS force), i.e, we seek a model in the form:

$$\begin{aligned} \Theta'(\xi) &= f_\Theta(\Theta_\xi,\Phi_\xi,\Gamma_2,\Gamma_3,{\Gamma_2}',{\Gamma_3}'), \\ \Phi'(\xi) &= f_\Phi(\Theta_\xi,\Phi_\xi,\Gamma_2,\Gamma_3,{\Gamma_2}',{\Gamma_3}'), \end{aligned} \tag{2-22}$$

using the following notational convention:

$$\Theta_\xi(\sigma):=\Theta(\xi+\sigma),\qquad \Phi_\xi(\sigma):=\Phi(\xi+\sigma).$$

This can be achieved by solving Equations (2-18) and (2-20) for θ and ϕ, respectively. Prior to doing this, the borehole evolution equations (2-18)-(2-21) can be simplified by making use of the following approximation:

$$\sin\theta \approx \sin\langle\Theta\rangle_1 \approx \sin\Theta. \tag{2-23}$$

This approximation is valid under the assumption that the bit tilt angles (the difference between borehole and BHA orientation) are small, which is usually the case under normal drilling conditions. It has to be noticed, that this approximation does not imply that one can neglect the difference between θ, Θ and $\langle\Theta\rangle_1$, since the explicit difference between these angles is one of the main elements of the borehole evolution, since it is part of the kinematic relationships that relate the BHA model with the bit/rock interaction. This approximation was implemented in [5]. The derivation of the model in the form of Equations (2-22) was done as well without making use of the approximation, and it is given as additional material included in Appendix B of the same publication.

After applying the approximation in (2-23), the borehole evolution equations are reduced to:

$$\eta\Pi\Big((\theta-\Theta)\cos\varpi+\sin\Theta\sin\varpi\,(\phi-\Phi)\Big)=\mathcal{F}_b\left(\theta-\langle\Theta\rangle_1\right)+\mathcal{F}_w\Upsilon\sin\langle\Theta\rangle_1+\mathcal{F}_r\Gamma_2 + \sum_{i=1}^{n-1}\mathcal{F}_i\left(\langle\Theta\rangle_i-\langle\Theta\rangle_{i+1}\right), \tag{2-24}$$

$$-\chi\Pi\theta'=\mathcal{M}_b\left(\theta-\langle\Theta\rangle_1\right)+\mathcal{M}_w\Upsilon\sin\langle\Theta\rangle_1+\mathcal{M}_r\Gamma_2+\sum_{i=1}^{n-1}\mathcal{M}_i\left(\langle\Theta\rangle_i-\langle\Theta\rangle_{i+1}\right), \tag{2-25}$$

$$\eta\Pi\left(-\frac{(\theta-\Theta)\sin\varpi}{\sin\Theta}+\cos\varpi\,(\phi-\Phi)\right)=\mathcal{F}_b\left(\phi-\langle\Phi\rangle_1\right)+\mathcal{F}_r\frac{\Gamma_3}{\sin\Theta}+\sum_{i=1}^{n-1}\mathcal{F}_i\left(\langle\Phi\rangle_i-\langle\Phi\rangle_{i+1}\right), \tag{2-26}$$

$$-\chi\Pi\phi'=\mathcal{M}_b\left(\phi-\langle\Phi\rangle_1\right)+\mathcal{M}_r\frac{\Gamma_3}{\sin\Theta}+\sum_{i=1}^{n-1}\mathcal{M}_i\left(\langle\Phi\rangle_i-\langle\Phi\rangle_{i+1}\right). \tag{2-27}$$

From Equations (2-24) and (2-26), expressions for θ and ϕ can be obtained as follows:

$$\theta = a_1 + a_2\phi, \tag{2-28}$$

$$\phi = a_3 + a_4\theta, \tag{2-29}$$

where the auxiliary variables a_i, for $i = 1, ..., 4$, are given by:

$$a_0 := \frac{1}{\eta\Pi\cos\varpi - \mathcal{F}_b},$$

$$\begin{aligned}
a_1(\xi) :=& a_0\Big(\eta\Pi\cos\varpi\Theta + \eta\Pi\sin\Theta\sin\varpi\Phi - \mathcal{F}_b\langle\Theta\rangle_1 + \mathcal{F}_w\Upsilon\sin\langle\Theta\rangle_1 + \mathcal{F}_r\Gamma_2 + \\
& \sum_{i=1}^{n-1}\mathcal{F}_i\left(\langle\Theta\rangle_i - \langle\Theta\rangle_{i+1}\right)\Big),\\
a_2(\xi) :=& -a_0\eta\Pi\sin\Theta\sin\varpi,\\
a_3(\xi) :=& a_0\Big(-\mathcal{F}_b\langle\Phi\rangle_1 + \mathcal{F}_r\frac{\Gamma_3}{\sin\Theta} + \sum_{i=1}^{n-1}\mathcal{F}_i(\langle\Phi\rangle_i - \langle\Phi\rangle_{i+1}) - \frac{\eta\Pi\Theta\sin\varpi}{\sin\Theta} + \eta\Pi\cos\varpi\Phi\Big),\\
a_4(\xi) :=& a_0\frac{\eta\Pi\sin\varpi}{\sin\Theta}.
\end{aligned}$$

One can then obtain expressions of θ and ϕ in terms of Θ, Φ, Γ_2 and Γ_3 (since all the auxiliary variables only depend on these variables) resulting in:

$$\theta = \frac{a_1 + a_2a_3}{1 - a_2a_4}, \qquad \phi = \frac{a_3 + a_1a_4}{1 - a_2a_4}. \tag{2-30}$$

After this, the derivatives of the BHA orientation at the bit with respect to ξ are obtained and substituted in (2-25) and (2-27) as follows:

$$\theta' = \frac{1}{1 - a_2a_4}\left(a_1' + \left(a_3 + \frac{a_4(a_1 + a_2a_3)}{1 - a_2a_4}\right)a_2' + a_2a_3' + \frac{a_2(a_1 + a_2a_3)}{1 - a_2a_4}a_4'\right), \tag{2-31}$$

$$\phi' = \frac{1}{1 - a_2a_4}\left(a_4a_1' + \frac{a_4(a_3 + a_4a_1)}{1 - a_2a_4}a_2' + a_3' + \left(a_1 + \frac{a_2(a_3 + a_1a_4)}{1 - a_2a_4}\right)a_4'\right), \tag{2-32}$$

where the derivatives of the auxiliary variables a_1-a_4 are given by:

$$a_1' = b_1\Theta' + b_2\Phi' + b_3, \tag{2-33}$$

$$a_2' = b_4\Theta', \tag{2-34}$$

$$a_3' = b_5\Theta' + b_6\Phi' + b_7, \tag{2-35}$$

$$a_4' = b_8\Theta', \tag{2-36}$$

with the new auxiliary variables b_i, for $i = 1, ..., 8$, defined as follows:

$$\begin{aligned}
b_0 :=& \frac{1}{\eta\Pi\cos\varpi - \mathcal{F}_b},\\
b_1(\xi) :=& b_0(\eta\Pi\cos\varpi + \eta\Pi\Phi\sin\varpi\cos\Theta),\\
b_2(\xi) :=& b_0\eta\Pi\sin\Theta\sin\varpi,\\
b_3(\xi) :=& b_0\Big(- \mathcal{F}_b\left(\Theta - \Theta_1\right) + \mathcal{F}_w\Upsilon\cos\langle\Theta\rangle_1\left(\Theta - \Theta_1\right) + \mathcal{F}_r\Gamma_2^{'}\\
&+ \sum_{i=1}^{n-1}\mathcal{F}_i\left(\frac{\Theta_{i-1} - \Theta_i}{\varkappa_i} - \frac{\Theta_i - \Theta_{i+1}}{\varkappa_{i+1}}\right)\Big),\\
b_4(\xi) :=& - b_0\eta\Pi\cos\Theta\sin\varpi,\\
b_5(\xi) :=& - \frac{b_0}{(\sin\Theta)^2}(\eta\Pi\sin\varpi\left(\sin\Theta - \Theta\cos\Theta\right) + \mathcal{F}_r\Gamma_3\cos\Theta),\\
b_6(\xi) :=& b_0\eta\Pi\cos\varpi,\\
b_7(\xi) :=& b_0\Big(- \mathcal{F}_b\left(\Phi - \Phi_1\right) + \mathcal{F}_r\frac{\Gamma_3^{'}}{\sin\Theta} + \sum_{i=1}^{n-1}\mathcal{F}_i\left(\frac{\Theta_{i-1} - \Theta_i}{\varkappa_i} - \frac{\Theta_i - \Theta_{i+1}}{\varkappa_{i+1}}\right)\Big),\\
b_8(\xi) :=& - \frac{b_0}{(\sin\Theta)^2}\eta\Pi\sin\varpi\cos\Theta.
\end{aligned}$$

It has to be noticed that in order to obtain the derivatives of the a_i auxiliary variables, the derivatives of the average states given in Equation (2-9) have to be obtained (this will be also helpful in order to formulate a state-space representation of the system). These derivatives are given by:

$$\langle\Theta\rangle_i^{'} = \frac{1}{\varkappa_i}\left(\Theta_{i-1} - \Theta_i\right), \qquad \langle\Phi\rangle_i^{'} = \frac{1}{\varkappa_i}\left(\Phi_{i-1} - \Phi_i\right), \tag{2-37}$$

where $\Theta_i = \Theta(\xi_i)$ and $\Phi_i = \Phi(\xi_i)$ with ξ_i being the location of the i-th stabilizer of the BHA. Finally, one can give the explicit expressions for the evolution of the borehole inclination and azimuth as follows:

$$\mathcal{E}\begin{bmatrix}\Theta'\\ \Phi'\end{bmatrix} = \begin{bmatrix}
-\frac{1}{\chi\Pi}\Big(\mathcal{M}_b\left(\frac{a_1 + a_2a_3}{1 - a_2a_4} - \langle\Theta\rangle_1\right) + \mathcal{M}_w\Upsilon\sin\langle\Theta\rangle_1 + \mathcal{M}_r\Gamma_2 + ... \\
\qquad + \sum_{i=1}^{n-1}\mathcal{M}_i\left(\langle\Theta\rangle_i - \langle\Theta\rangle_{i+1}\right)\Big) - \frac{b_3 + a_2b_7}{1 - a_2a_4}\\
-\frac{1}{\chi\Pi}\Big(\mathcal{M}_b\left(\frac{a_3 + a_4a_1}{1 - a_4a_2} - \langle\Phi\rangle_1\right) + \mathcal{M}_r\frac{\Gamma_3}{\sin\Theta} + ... \\
\qquad + \sum_{i=1}^{n-1}\mathcal{M}_i\left(\langle\Phi\rangle_i - \langle\Phi\rangle_{i+1}\right)\Big) - \frac{a_4b_3 + b_7}{1 - a_2a_4}
\end{bmatrix}, \tag{2-38}$$

where $\mathcal{E}$ is given by:

$$\mathcal{E} = \frac{1}{1 - a_2a_4}\begin{bmatrix} b_1 + a_3b_4 + a_2b_5 + \frac{(a_1 + a_2a_3)(a_4b_4 + a_2b_8)}{1 - a_2a_4} & b_2 + a_2b_6\\ a_4b_1 + b_5 + a_1b_8 + \frac{(a_3 + a_4a_1)(a_4b_4 + a_2b_8)}{1 - a_2a_4} & a_4b_2 + b_6\end{bmatrix}. \tag{2-39}$$

This representation of the evolution equations was a contribution of [5], and it represents the model explicitly in the form of nonlinear second order delay differential equations. The delay

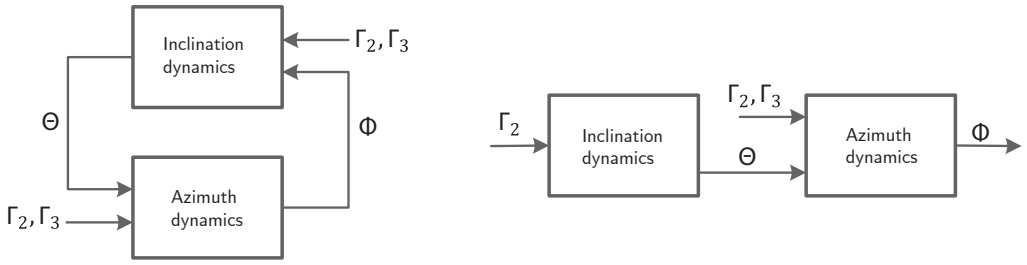

Figure 2-7: Interaction of Θ and Φ for non-neutral (left) and neutral (right) bit walk models [5].

nature of the system arises from the presence of terms Θ_i, $\langle\Theta\rangle_i$, Φ_i and $\langle\Phi\rangle_i$ for $i = 1, ..., n$. Furthermore the delay terms Θ_i and Φ_i can be defined as point-wise delays, and the terms $\langle\Theta\rangle_i$ and $\langle\Phi\rangle_i$ as distributed delays (due to the fact that they make use of integrals, defining them continuously along whole function segments).

These system dynamics present significant challenges for controller design. Firstly, since there is presence of delay effects in the dynamics, there exists an infinite number of poles, which provides difficulties for stability analysis and renders some controller design strategies (for example, pole-placement for finite-dimensional Linear Time Invariant (LTI) systems) unfeasible to implement. Additionally, the nonlinear effects present in the dynamics related to the bit walk angle ϖ and the average inclination $\langle\Theta\rangle_1$ discard (a priori) the possibility to exploit well-known linear control strategies. Furthermore, the presence of uncertainty on the active weight on bit Π and the bit walk angle ϖ has to be considered, since they could affect stability and performance. The model also describes the borehole evolution in terms of the borehole inclination and azimuth, but in reality these variables are not directly measurable, since only measurements of the orientation of the BHA at specific locations are available. Finally, the system is a Multiple Input Multiple Output (MIMO) system with bilateral coupling between the inclination and the azimuth dynamics. Nevertheless, it can be noticed that for the specific case where there is no bit walk angle present in the process ($\varpi = 0°$), this coupling is only present from the inclination to the azimuth. These two situations are depicted in Figure 2-7. The neutral bit walk model (i.e., for zero bit walk angle) is used as a first approach in order to simplify the controller design process. The derivation of the equations for $\varpi = 0°$ is performed in Section 2-1-1, with the corresponding output equations.

2-1-1 Derivation of the neutral bit walk model

As a starting point for the derivation of the model for zero bit walk angle, Equation (2-38) describing the generic dynamic for non-zero bit walk is considered. If then, as stated, the bit walk angle is set to be $\varpi = 0°$, then the borehole evolution equations for the neutral bit walk model read as follows:

$$
\begin{aligned}
\chi\Pi\Theta' =& -\mathcal{M}_b(\Theta - \langle\Theta\rangle_1) - \frac{\mathcal{M}_b F_1 + \mathcal{M}_1\left(\eta\Pi - \mathcal{F}_b\right)}{\eta\Pi}\left(\langle\Theta\rangle_1 - \langle\Theta\rangle_2\right) \\
&+ \frac{\chi}{\eta}\mathcal{F}_b\left(\Theta - \Theta_1\right) - \frac{\chi}{\eta}\mathcal{F}_1\left(\Theta - \Theta_1 - \frac{\Theta_1 - \Theta_2}{\varkappa_2}\right) \\
&- \frac{\mathcal{M}_b\mathcal{F}_r + (\eta\Pi - F_b)\mathcal{M}_r}{\eta\Pi}\Gamma_\Theta - \frac{\chi}{\eta}\mathcal{F}_r\Gamma'_\Theta + W, \\
\chi\Pi\Phi' =& -\mathcal{M}_b\left(\Phi - \langle\Phi\rangle_1\right) - \frac{\mathcal{M}_b F_1 + \mathcal{M}_1\left(\eta\Pi - F_b\right)}{\eta\Pi}\left(\langle\Phi\rangle_1 - \langle\Phi\rangle_2\right) \\
&+ \frac{\chi}{\eta}\mathcal{F}_b\left(\Phi - \Phi_1\right) - \frac{\chi}{\eta}\mathcal{F}_1\left(\Phi - \Phi_1 - \frac{\Phi_1 - \Phi_2}{\varkappa_2}\right) \\
&+ \left(\frac{\chi}{\eta}\frac{\mathcal{F}_r\Theta'\cos\Theta}{(\sin\Theta)^2} - \frac{\mathcal{M}_b\mathcal{F}_r + \mathcal{M}_r\left(\eta\Pi - \mathcal{F}_b\right)}{\eta\Pi\sin\Theta}\right)\Gamma_\Phi - \frac{\chi}{\eta}\frac{\mathcal{F}_r}{\sin\Theta}\Gamma'_\Phi,
\end{aligned}
\tag{2-40}
$$

where the term related to the weight of the BHA is included in the first equation and is given by $W := -\frac{\mathcal{M}_b\mathcal{F}_w + (\eta\Pi - \mathcal{F}_b)\mathcal{M}_w}{\eta\Pi}\Upsilon\sin\langle\Theta\rangle_1 - \frac{\chi}{\eta}\mathcal{F}_w(\Theta - \Theta_1)\Upsilon\cos\langle\Theta\rangle_1$ and Υ is the normalized distributed weight of the BHA. Moreover, the RSS forces Γ_2 and Γ_3 have been replaced by Γ_Θ and Γ_Φ, to make explicit that these inputs are related to the inclination and azimuth dynamics, respectively.

From Equation (2-40), the states of the system can be defined as:

$$
x_\Theta = \begin{bmatrix} \Theta \\ \langle\Theta\rangle_1 \\ \langle\Theta\rangle_2 \end{bmatrix}, \qquad x_\Phi = \begin{bmatrix} \Phi \\ \langle\Phi\rangle_1 \\ \langle\Phi\rangle_2 \end{bmatrix}. \tag{2-41}
$$

Output equations. As it has been mentioned before, measurements of the orientation of the borehole at the bit are not directly available. Instead, inclination and azimuth are measured at specific locations on the BHA. For a two stabilizer directional drilling system (which is the case that it is being analyzed here), a common location for the orientation sensors is: one placed between the RSS and the bit (i.e., the sensor location within the BHA satisfies $s_{m,1} \in [0, \Lambda\ell_1]$) and a second one located between the first and the second stabilizer (i.e., $s_{m,2} \in [\ell_1, \ell_1 + \ell_2]$).

In order to have a reliable representation of the location of these sensors, the system's output equations should be given in the following way:

$$
y_\theta = \left[\theta_0(\xi, s_{m,1}),\ \theta_2(\xi, s_{m,2})\right]^T \tag{2-42}
$$

$$
y_\phi = \left[\phi_0(\xi, s_{m,1}),\ \phi_2(\xi, s_{m,2})\right]^T. \tag{2-43}
$$

In order to obtain explicit output equations, we can refer back to the general solution of the BHA model equation, given by (2-6) and (2-7), which can be rewritten in the following way to have constant coefficients in terms of sensor location and BHA configuration:

$$
\theta_i(\xi, s) = \mathcal{C}_{i1}(s)\hat{\theta} + \mathcal{C}_{i2}(s)\Gamma_2 + \mathcal{C}_{i3}(s)\langle\Theta\rangle_1 + \mathcal{C}_{i4}(s)\langle\Theta\rangle_2 + \mathcal{C}_{i5}(s)\Upsilon\sin\langle\Theta\rangle_1, \tag{2-44}
$$

$$
\phi_i(\xi, s) = \mathcal{D}_{i1}(s)\hat{\phi} + \mathcal{D}_{i2}(s)\frac{\Gamma_3}{\sin\Theta} + \mathcal{D}_{i3}(s)\langle\Phi\rangle_1 + \mathcal{D}_{i4}(s)\langle\Phi\rangle_2, \tag{2-45}
$$

where $\mathcal{C}_{ij}$, $j = 1, 2, ..., 5$, and $\mathcal{D}_{ik}$, $k = 1, 2, ..., 4$, are the previously mentioned constant coefficients. It can be noticed that the BHA inclination and azimuth at the bit are present in (2-44) and (2-45) (here the ($\hat{}$) character is explicitly shown again). These bit orientations can be replaced using Equations (2-30), while evaluating these at $\varpi = 0°$; this results in the following constraint equations:

$$\hat{\theta} = \frac{1}{\eta\Pi - \mathcal{F}_b}\Big(\eta\Pi\Theta - \mathcal{F}_b\langle\Theta\rangle_1 + \mathcal{F}_w\Upsilon\sin\langle\Theta\rangle_1 + \mathcal{F}_r\Gamma_2 + \sum_{i=1}^{n-1}\mathcal{F}_i\left(\langle\Theta\rangle_i - \langle\Theta\rangle_{i+1}\right)\Big), \tag{2-46}$$

$$\hat{\phi} = \frac{1}{\eta\Pi - \mathcal{F}_b}\Big(\eta\Pi\Phi - \mathcal{F}_b\langle\Phi\rangle_1 + \mathcal{F}_r\frac{\Gamma_3}{\sin\Theta} + \sum_{i=1}^{n-1}\mathcal{F}_i(\langle\Phi\rangle_i - \langle\Phi\rangle_{i+1})\Big). \tag{2-47}$$

Next, Equations (2-46) and (2-47) are substituted in (2-44) and (2-45) and as a result the output equations of the system can be given by:

$$y_\Theta = C_\Theta x_\Theta + D_\Theta\Gamma_\Theta + E\Upsilon\sin\langle\Theta\rangle_1, \tag{2-48}$$

$$y_\Phi = C_\Phi x_\Phi + D_\Phi\frac{\Gamma_\Phi}{\sin\Theta}. \tag{2-49}$$

If it is assumed that both the inclination and the azimuth sensors are at the same location then $C_\Theta = C_\Phi$ and $D_\Theta = D_\Phi$. Explicit expressions for the coefficients in (2-48) and (2-49) are given in [5].

2-2 Benchmark system definition

In order to perform simulations of the system, some parameters have to be chosen to represent a real directional drilling system. Without loss of generality, it can be assumed that a two stabilizer system captures the key dynamics of the process, according to [17]. In previous works ([5], [23]), the geometric characteristics and the steering resistance properties were selected according to [3].

The BHA is considered to be made of pipes of steel. The key properties to be able to perform simulations of the system are the Young's Modulus (E_y), density (ρ), inner (I_r) and outer (O_r) radii of the BHA pipes, their cross section surface area ($A = \pi(O_r^2 - I_r^2)$) and the second moment of inertia ($I = \frac{\pi}{4}(O_r^4 - I_r^4)$), the distance of the bit to the first stabilizer (ℓ_1), the distance of the second stabilizer with respect to the first (ℓ_2) and the distance of the RSS actuator from the bit, expressed as a fraction of ℓ_1 ($\Lambda\ell_1$). The chosen parameters are shown in Tables 2-1 and 2-2.

Table 2-1: Geometric properties of the benchmark system.

$I_r[m]$	$O_r[m]$	$A[m^2]$	$I[m^4]$	$\ell_1[m]$	$\ell_2[m]$	$\Lambda\ell_1[m]$
0.0533	0.0857	0.0141	3.6×10^{-5}	3.66	6.10	0.61

Table 2-2: Material properties of the benchmark system.

$E_y[N/m^2]$	$\rho[kg/m^3]$
2×10^{11}	7800

Using this set of parameters, the distributed weight of the BHA can be computed as $w = 9.81\pi\rho(O_r^2 - I_r^2) = 1.08 \times 10^3 N/m$. The model makes use of several dimensionless quantities (which are for the two stabilizer case $\varkappa_1$, $\varkappa_2$, Λ, χ, η, Υ, Π, Γ_2, Γ_3). The dimensionless location the i-th stabilizer is defined as $\varkappa_i = \frac{\ell_i}{\ell_1}$, for $i = 1, 2$. The angular and lateral steering resistance χ and η are defined as (2-15). Regarding this bit/rock interaction parameters, the chosen values for η and χ correspond to a bit with a rather long passive gauge. Finally, the scaled force related quantities Υ, Γ_2, Γ_3 and Π, are defined as in (2-4) and (2-14), respectively. The active weight on bit Π and the bit walk angle ϖ are not given values since they are considered uncertain (the effect of these parameters is analyzed in further sections), although for Π a "nominal" value of $\bar{\Pi} = \frac{14000[N]}{F^*}$ is used for controller design. Table 2-3 shows the values for the dimensionless parameters used for simulation.

Table 2-3: Dimensionless parameters of the benchmark system.

$\varkappa_1$	$\varkappa_2$	Λ	χ	η
1	1.67	0.167	0.1	30

This set of parameters can be considered to be reliable, as they can be compared to the quantities shown in [17], as part of a series of analysis for different types of directional drilling systems. The use of this parameter set will also simplify the comparison between the strategies developed in this research with the previous works in [5] and [23].

2-3 Open-loop dynamics

Extensive evaluation of the open-loop dynamics has been performed in [5]. It was determined that for the derived model, the performance using constant RSS forces Γ_2 and Γ_3, is not desired, amongst others, due to the fact that oscillations in the borehole trajectory can occur under certain conditions. This behavior in the response is the so-called borehole spiraling phenomenon. In this study, also the effect of uncertain parameters active weight on bit Π and bit walk angle ϖ was investigated. It draws the conclusion that, as the value of Π decreases the system response starts to move closer to instability (i.e., the poles of the system move closer to the right-hand side of the complex plane). The same effect of instability is shown for increments in the absolute value of ϖ.

One of the main goals of this thesis is to provide a control strategy that displays robustness properties against the aforementioned parameters. In this section we focus in showing the presence of the negative effects and their relation to the uncertain parameters in the open-loop response of the system, by means of simulation.

The initial conditions for these simulations are set to be $\Theta = 20°$ and $\Phi = 0°$. The behavior of the system for several values of active weight on bit Π is tested, considering $\varpi = 0°$. This simulation is performed using the parameters defined in Section 2-2. It can be seen in Figure 2-8 that as the value of Π decreases, as mentioned before, the system begins to oscillate. The main reason for this to happen, is that the open-loop poles of the system depend on the composite parameter $\eta\Pi$ and, as it is shown in [24], as the value of the active weight on bit decreases, the open-loop poles are moved towards the right-half complex plane. For the benchmark system under analysis in this research, the value of Π for which the right-most

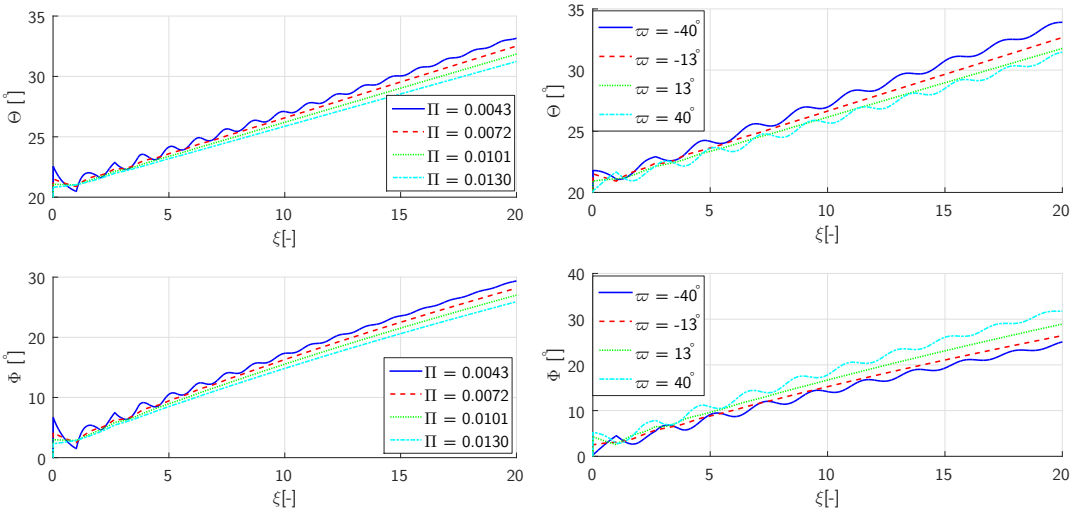

Figure 2-8: Open-loop response of the Θ and the Φ for different values of weight on bit Π and $\varpi = 0°$ (left) and bit walk angle ϖ and $\Pi = \bar{\Pi} = 0.0087$ (right).

pole (pair) crosses the imaginary axis is $\Pi = 0.0037$ [5]. Furthermore, for high values of Π, the system exhibits a non-minimum phase response, and this effect is studied in [24]. The physical explanation of this behavior, is that for high values of $\eta\Pi$, the penetration direction of the bit is mainly affected by the forces originated due to the deformation of the BHA and not the lateral cutting action of the bit [3]. It is not the purpose of this research to design a control strategy for systems that show a non-minimum phase behavior, for which this effect is not taken into account in the open-loop simulations. Finally, one drawback that has been dealt with in previous publications ([5], [23]) is the sudden change in inclination and azimuth due to the fast variation of the applied RSS actuator force (which can be seen at $\xi = 0$ in Figure 2-8). This produces a kink in the borehole, which has been denoted as a negative effect in the borehole in Chapter 1, and it was counteracted by means of a low-pass filter. The results of this simulation with constant RSS actuator force $\Gamma_2 = \Gamma_3 = 0.0074$ are shown in Figure 2-8.

Secondly, evaluating the effect of changing the bit walk angle it is clear that having $\varpi \neq 0°$ has much more harmful consequences to the performance of the system. This is due to the fact that it is related to nonlinear coupling terms in the model. The same kink present when the RSS force is applied in the previous simulations appears, followed by a spiraling behavior. When the bit walk angle is not severe, after some oscillations, the inclination and azimuth starts to grow linearly (i.e., constant curvature is generated). As mentioned before, as the absolute value of ϖ increases, the response becomes more oscillating, and in the severe case of $\varpi = \pm 40°$, close to instability. It can be seen that there is a symmetric behavior, since all the terms in which the bit walk angle is present are sine or cosine functions. This could be insightful for the robust controller design to reduce the range of parameters for which a robust controller strategy could be designed.

Finally, a simulation where the combined effect of these two parameters is shown. In this case, the extreme situations (in terms of low weight-on-bit and large bit walk angle) shown in the previous simulations are considered (i.e., $\Pi = 0.0043$ and $\varpi = -40°$), see Figure 2-9. It can be seen that not only the system shows undamped oscillations caused by the presence

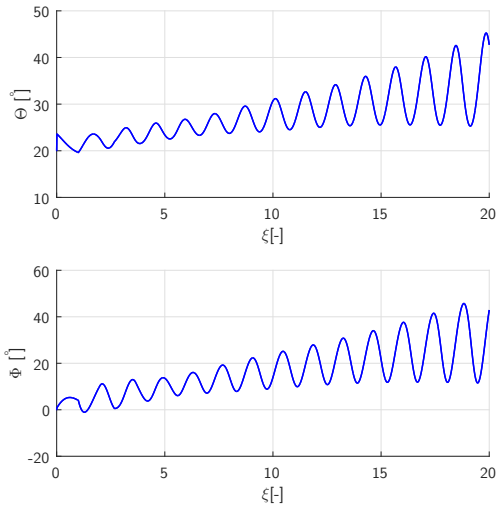

Figure 2-9: Open-loop simulation for $\Pi = 0.0043$ and $\varpi = -40°$.

of a pole at zero [24], but it is also unstable since the response starts growing unbounded, which can lead to the conclusion that there is a pole in the right-half of the complex plane.

These results highlight the need to develop a strategy, that is able to cope with the variation of these two parameters along the process. A decrease of the active weight on bit Π may shift the poles of the system to the right-half of the complex plane, generating higher levels of oscillations and potentially instability. On the other hand, a small increase in the absolute value of the bit walk angle ϖ already generates negative effects on the response, due to the fact that this parameter is the cause of the nonlinear bidirectional coupling between the inclination and the azimuth. Borehole spiraling and rippling may become present while drilling, and in extreme cases dangerous instability may occur.

2-4 Discussion

In this chapter, the model to be used for controller design was described. The interaction between the main three elements of the description (BHA model, bit/rock interaction and kinematic relationships between the bit trajectory and the borehole geometry) was introduced in order to construct the borehole evolution equations, which describe the way the inclination Θ and the azimuth Φ change with respect to the dimensionless lenght of the borehole ξ.

The resulting MIMO system constitutes a set of nonlinear delay differential equations with distributed delays. The model contains parameter uncertainty related to what is called the active weight on bit (Π) and the bit walk angle (ϖ). The system shows bidirectional coupling between the inclination and the azimuth, due to the presence of terms related to ϖ. It was explained that if $\varpi = 0$, the coupling is only present from the inclination to azimuth dynamics. This insight, related to the coupling, will be used later to address the controller design problem in a simpler manner.

Next, a benchmark BHA configuration was described and the parameters that describe the geometric and dynamic properties of the system were explained. This set of parameters

reliably represent a real directional drilling system, and will be used later in order to perform simulations, stability analysis and controller design and tuning.

Finally, this chapter ends with the open-loop simulations of the model. The results corroborate the negative effects present when only constant RSS actuator force is used. First of all, a decrease on the active weight on bit Π produces oscillations in the response, and can potentially lead the system to instability. It was also mentioned that high values of this parameter can generate a non-minimum phase response, although this type of phenomenon will not be investigated. On the other hand, it was shown that the bit walk angle ϖ has as well a negative influence with respect to the desired response of the system. As the absolute value of this parameter increases, a higher level of oscillations was observed. Also it was seen that there is a similar behavior between positive and negative values of ϖ. Also, kinking is present since a sudden change in the RSS force causes that a rapid variation of the inclination and azimuth in the system. It was shown, that the changes in this parameters produce many undesired effects, and on extreme cases may even cause instability of the system.

Chapter 3

Controller design

In this and the following chapter lies the core of this thesis. This chapter is intended to explain in detail the control strategies to overcome the negative effects present in directional drilling processes, such as borehole spiraling, rippling and kinking, which were shown to be present in certain scenarios when only constant RSS actuator force is applied. Section 3-1 aims to define the specific control objectives of the system (stability, reference tracking, robustness, disturbance rejection) in order to start developing a strategy. In this section, the problem is stated in such a way that the overall goal of the developed controller design is to solve a tracking problem, while relying on measurements of the inclination and azimuth of the BHA close to the bit only and being able to maintain stability despite uncertainties in the system parameters.

Section 3-2 describes the elements present in the proposed control structure for the system. The input decoupling transformation implemented in [5] is applied here as well, but making the explicit difference between real and estimated states. This process already implies the inclusion of an observer. A control strategy for this case is proposed, followed by the derivation of the closed-loop error dynamics. The system is linearized with the purpose of stability analysis of the closed-loop system and to perform controller synthesis. The stability analysis leads to a strategy that makes use of the cascaded structure of the sytem dynamics in the case of zero bit walk. After synthesizing the controller, its effectiveness is tested via simulation.

3-1 Control problem and approach

To start solving the controller design problem, one needs to specify it by means of specific measurable quantities. In this case, it has been mentioned that the goal is to be able to drill boreholes with complex geometries, while avoiding undesired effects such as borehole spiraling, rippling and kinking. This has to be translated into a specific control objective.

This can be stated as a reference tracking problem. Firstly, the trajectory to be tracked has to be designed, due to the fact that a smooth continuous geometry is needed. This is because of several reasons; one reason is that if the trajectory is designed with sudden changes of

inclination or azimuth, this can diminish the quality of the casting process in the borehole. The trajectory in terms of Θ and Φ is designed to be continuously differentiable with respect to ξ. We then consider in this study generic trajectories (continuously differentiable) that potentially go through an entire range of $\Theta \in (0, \frac{\pi}{2}]$ (due to a singularity in the model $\Theta = 0$ can not be properly described) in inclination and $\Phi \in [0, \pi]$. An specific example of this trajectory is used in Section 3-5. The controller should be able to solve the tracking problem such that the designed path is an asymptotically stable trajectory of the closed-loop system. Thereby, instability leading to steady-state borehole spiraling is avoided, while also avoiding transient oscillations in the borehole geometry.

Regarding the robustness properties of the system, the objectives for the neutral bit walk model differ from the ones of the non-neutral bit walk model. In both cases, it is desired that the system remains stable and avoids undesired behavior, despite the uncertainties in the active weight on bit Π.

Formally stating this, after considering the results of several data analyses performed in [17], it is considered that a reasonable window of values for the system to be stable is $\Pi \in [0.5\bar{\Pi}, 1.5\bar{\Pi}]$, where $\bar{\Pi}$ represents the nominal weight on bit of the system. Since in the neutral bit walk case the bit walk angle is equal to zero, robustness against this parameter is considered only for the non-neutral bit walk case, where we consider the objective for the system to remain stable and avoid undesired effects for $\varpi \in [-40°, 40°]$, where $\varpi = \pm 40°$ represents a rather extreme scenario. The robust stability analysis of the system is considered in Chapter 4.

After defining the control objectives of the system, the controller design and synthesis is derived in the following sections of this chapter.

3-2 Controller design

As mentioned before, this section aims to develop a strategy for the neutral bit walk model. The reason to start the analysis for this case, is that the system only presents coupling from inclination to the azimuth, contrary to the case when $\varpi \neq 0$, where nonlinear coupling terms appear as well from the azimuth to the inclination. The strategy should rely only on local measurements of the BHA inclination and azimuth. One should realize that the purpose of the control strategy is the stabilization of a desired trajectory in terms of the inclination and azimuth of the borehole, not that of the BHA. Indeed the inclination and azimuth of the BHA at the bit differ from those of the borehole due to the deflection of the BHA caused by the RSS force and gravity. Moreover, the inclination and azimuth of the BHA can not even be measured at the bit but only at some distance behind the bit. In order to cope with these sensor constraints, we aim to design an observer that estimates the inclination and azimuth of the borehole based on (the model) and measurements of the inclination and azimuth of the BHA at some distance behind the bit.

Next, a combined feedforward and feedback control strategy is developed, that employs the state estimates provided by the observer and asymptotically stabilizes the desired trajectory.

Figure 3-1 depicts the proposed control strategy for the system. Along with the already mentioned elements of the structure (feedforward, feedback and observer), the strategy makes use of an input filter in order to deal with the presence of terms related to the derivatives of the inputs in Equations (2-40). The strategy also proposes the use of a nonlinear decoupling

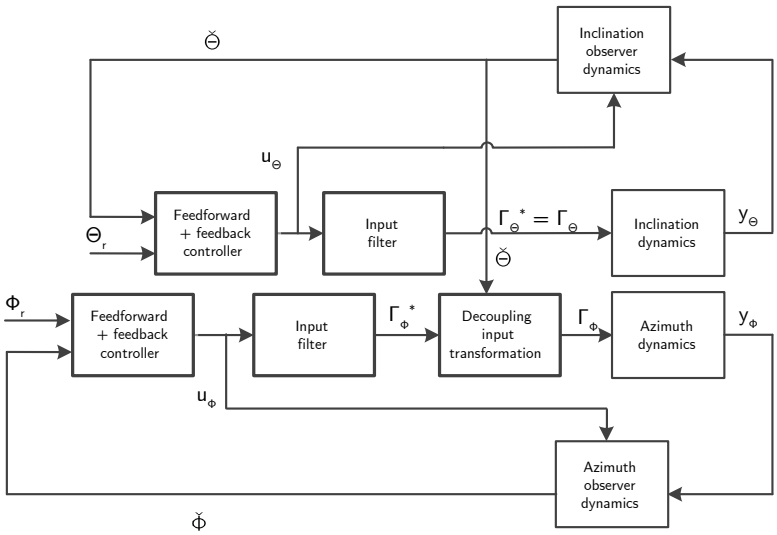

Figure 3-1: Control strategy.

transformation in order to be able to design the controllers for the inclination and azimuth with a certain degree of independence. A high degree of complexity in the equations of the closed-loop dynamics is expected, especially because of the fact that the terms related to the derivatives of the inclination and its estimate are affecting the azimuth dynamics. This is mainly due to the difference between the inclination Θ and its estimate denoted $\check{\Theta}$. For the zero bit walk case (as considered here), this complexity vanishes when $\check{\Theta} = \Theta$. Assuming that we will be able to design an observer that indeed provides (asymptotically) such correct estimate of the inclination, the structure of the controller will be designed for the case when this condition is met. We proceed to explain the elements that build the proposed control strategy.

Input decoupling transformation. The input transformation in Equation (3-1) is proposed in order to achieve decoupling of the system between the inclination and azimuth dynamics:

$$\begin{bmatrix} \Gamma_\Theta^* \\ \Gamma_\Phi^* \end{bmatrix} := \begin{bmatrix} 1 & 0 \\ 0 & \frac{1}{\sin\check{\Theta}} \end{bmatrix} \begin{bmatrix} \Gamma_\Theta \\ \Gamma_\Phi \end{bmatrix}, \qquad \text{for } \Theta \in (0,\ \pi). \tag{3-1}$$

We denote the estimate of a state using the character ($\check{}$). Herein, $\check{\Theta}$ denotes the estimate of the inclination Θ of the borehole at the bit, which will be provided by an observer to be designed later (N.B.: Θ can not be measured).

Note that if $\check{\Theta} = \Theta$ (a perfect estimate), then (3-1) indeed fully decouples the azimuth dynamics from the inclination dynamics, which simplifies the design of the structure of the controller and observer. However, in general $\check{\Theta} \neq \Theta$ (at least in transients of the observer) and the mismatch between Θ and $\check{\Theta}$ affects the decoupling transformation. Since the input transformation does not change the structure of the first equation in (2-40), only the second

equation in (2-40) (the azimuth dynamics) is shown and is given by:

$$\begin{aligned}\chi\Pi\Phi' = &-\mathcal{M}_b\left(\Phi - \langle\Phi\rangle_1\right) - \frac{\mathcal{M}_b F_1 + \mathcal{M}_1\left(\eta\Pi - F_b\right)}{\eta\Pi}\left(\langle\Phi\rangle_1 - \langle\Phi\rangle_2\right)\\ &+ \frac{\chi}{\eta}\mathcal{F}_b\left(\Phi - \Phi_1\right) - \frac{\chi}{\eta}\mathcal{F}_1\left(\Phi - \Phi_1 - \frac{\Phi_1 - \Phi_2}{\varkappa_2}\right)\\ &+ \left(\frac{\chi}{\eta}\frac{\mathcal{F}_r\Theta'\cos\Theta\sin\check{\Theta}}{\left(\sin\Theta\right)^2} - \frac{\left(\mathcal{M}_b\mathcal{F}_r + \mathcal{M}_r\left(\eta\Pi - \mathcal{F}_b\right)\right)\sin\check{\Theta}}{\eta\Pi\sin\Theta} - \frac{\chi}{\eta}\frac{\mathcal{F}_r\check{\Theta}'\cos\check{\Theta}}{\left(\sin\Theta\right)}\right)\Gamma^*_\Phi\\ &- \frac{\chi}{\eta}\frac{\mathcal{F}_r\sin\check{\Theta}}{\sin\Theta}\Gamma^{*\prime}_\Phi,\end{aligned} \tag{3-2}$$

in terms of the states defined in (2-41), the system dynamics after the decoupling input transformation can be written as:

$$\begin{aligned}\begin{bmatrix}x'_\Theta\\ x'_\Phi\end{bmatrix} = &\begin{bmatrix}A_0 & 0\\ 0 & A_0\end{bmatrix}\begin{bmatrix}x_\Theta(\xi)\\ x_\Phi(\xi)\end{bmatrix} + \begin{bmatrix}A_1 & 0\\ 0 & A_1\end{bmatrix}\begin{bmatrix}x_\Theta(\xi_1)\\ x_\Phi(\xi_1)\end{bmatrix} + \begin{bmatrix}A_2 & 0\\ 0 & A_2\end{bmatrix}\begin{bmatrix}x_\Theta(\xi_2)\\ x_\Phi(\xi_2)\end{bmatrix}\\ &+ \begin{bmatrix}B_{0\Theta} & 0\\ 0 & B_{0\Phi}\end{bmatrix}\begin{bmatrix}\Gamma^*_\Theta\\ \Gamma^*_\Phi\end{bmatrix} + \begin{bmatrix}B_{1\Theta} & 0\\ 0 & B_{1\Phi}\end{bmatrix}\begin{bmatrix}\Gamma^{*\prime}_\Theta\\ \Gamma^{*\prime}_\Phi\end{bmatrix} + \begin{bmatrix}BW\\ 0\end{bmatrix},\end{aligned} \tag{3-3}$$

where the matrices and vectors A_0, A_1, A_2, B, B_{0i}, B_{1i}, are given by:

$$A_0 = \frac{1}{\chi\Pi}\begin{bmatrix}-\mathcal{M}_b + \frac{\chi}{\eta}(\mathcal{F}_b - \mathcal{F}_1) & \mathcal{M}_b - \mathcal{M}_1 + \frac{\mathcal{F}_b\mathcal{M}_1 - \mathcal{F}_1\mathcal{M}_b}{\eta\Pi} & \mathcal{M}_1 + \frac{(-\mathcal{F}_b\mathcal{M}_1 + \mathcal{F}_1\mathcal{M}_b)}{\eta\Pi}\\ \chi\Pi & 0 & 0\\ 0 & 0 & 0\end{bmatrix},$$

$$A_1 = \frac{1}{\chi\Pi}\begin{bmatrix}\frac{\chi}{\eta}(\mathcal{F}_1 + \frac{\mathcal{F}_1}{\varkappa_2} - \mathcal{F}_b) & 0 & 0\\ -\chi\Pi & 0 & 0\\ \frac{\chi\Pi}{\varkappa_2} & 0 & 0\end{bmatrix}, \qquad A_2 = \frac{1}{\chi\Pi}\begin{bmatrix}-\frac{\chi\mathcal{F}_1}{\eta\varkappa_2} & 0 & 0\\ 0 & 0 & 0\\ -\frac{\chi\Pi}{\varkappa_2} & 0 & 0\end{bmatrix},$$

$$B_{0\Theta} = \frac{1}{\chi\Pi}\left[-\frac{\mathcal{M}_b\mathcal{F}_r + (\eta\Pi - F_b)\mathcal{M}_r}{\eta\Pi}, \quad 0, \quad 0\right]^T, \qquad B_{1\Theta} = \frac{1}{\chi\Pi}\left[-\frac{\chi}{\eta}\mathcal{F}_r, \quad 0, \quad 0\right]^T,$$

$$B_{0\Phi} = \frac{1}{\chi\Pi}\left[\frac{\chi}{\eta}\frac{\mathcal{F}_r\Theta'\cos\Theta\sin\check{\Theta}}{(\sin\Theta)^2} - \frac{(\mathcal{M}_b\mathcal{F}_r + \mathcal{M}_r(\eta\Pi - \mathcal{F}_b))\sin\check{\Theta}}{\eta\Pi\sin\Theta} - \frac{\chi}{\eta}\frac{\mathcal{F}_r\check{\Theta}'\cos\check{\Theta}}{(\sin\Theta)}, \quad 0, \quad 0\right]^T$$

$$B_{1\Phi} = \frac{1}{\chi\Pi}\left[-\frac{\chi}{\eta}\mathcal{F}_r\frac{\sin\check{\Theta}}{\sin\Theta}, \quad 0, \quad 0\right]^T, \qquad B = \begin{bmatrix}1 & 0 & 0\end{bmatrix}^T.$$

After the input transformation, the output equations in (2-48) and (2-49) are given by:

$$y_\Theta = C_\Theta x_\Theta + D_\Theta\Gamma^*_\Theta + EW_y, \tag{3-4}$$

$$y_\Phi = C_\Phi x_\Phi + D_\Phi\Gamma^*_\Phi\frac{\sin\check{\Theta}}{\sin\Theta}, \tag{3-5}$$

where the gravity related term in y_Θ has been renamed to EW_y, with $W_y := \Upsilon\sin\langle\Theta\rangle_1$ to simplify notation. We emphasize again that we consider W and W_y as quasi-constant disturbances.

Input filter design. As a next step, we note that in (3-3) both the (transformed) RSS forces and their derivatives appear. In order to combine the (transformed) RSS force inputs Γ_i^* for $i = \Theta, \Phi$ and their derivatives, the following transformation is proposed:

$$Bu_i = B_{0i}\Gamma_i^* + B_{1i}\Gamma_i^{*'}, \tag{3-6}$$

where $B = \begin{bmatrix}1 & 0 & 0\end{bmatrix}^T$ and vectors B_{0i} and B_{1i} correspond to the 3 by 1 vectors related to the inputs of the azimuth and the inclination defined above.

This would fully replace the terms related to Γ_i^*, for $i = \Theta, \Phi$, and their derivatives in the dynamics given by (3-3) with Bu_i. However, it is not possible to use the input filter as in (3-6) here, since vectors $B_{0\Phi}$ and $B_{1\Phi}$ depend on Θ, which is not known to the controller, since it can not be measured. To overcome this, the design of this input filter will be done for the ideal case when $\breve{\Theta} = \Theta$, i.e.,

$$\Gamma_i^{*'} = -\frac{\mathcal{M}_b\mathcal{F}_r + (\eta\Pi - \mathcal{F}_b)\mathcal{M}_r}{\chi\Pi\mathcal{F}_r}\Gamma_i^* - \frac{\eta\Pi}{\mathcal{F}_r}u_i. \tag{3-7}$$

Herein, u_i is a new control input, comprised of the sum of the feedforward and feedback inputs (which are defined below in this section) given by

$$u_i = v_i + u_{ri}. \tag{3-8}$$

The stability of the filters in (3-7) is guaranteed as long as $\frac{B_{0i}}{B_{1i}} > 0$. It can be seen that considering only uncertainty for the weight on bit, this condition is met up to a certain value of $\Pi = \Pi_{nmp}$. It was proven in [23] that if indeed $\Pi < \Pi_{nmp}$ corresponds to the situation where the system is minimum-phase. From now on, we will only consider the case that this minimum-phase condition is met. In (3-8), the feedforward input u_{ri} is defined based on the inverse dynamics of the system for a reference trajectory x_{ri}, for $i = \Theta, \Phi$:

$$u_{ri} = B^T(x_{ri}'(\xi) - A_0x_{ri}(\xi) - A_1x_{ri}(\xi_1) - A_2x_{ri}(\xi_2)). \tag{3-9}$$

It is important to mention that the gravity-related term in the inclination dynamics (W in (3-3)), is omitted from the feedforward design since it can be considered as a quasi-constant (unknown) disturbance, which can be dealt with by implementing integral action in the control structure. Furthermore, this feedforward is designed again for the case when $\breve{\Theta} = \Theta$. Due to this simplification of the feedforward design, a (transient) feedforward error is introduced to the system, which will be taken into account explicitly in the resulting error dynamics later.

If the input filters in (3-7) are substituted in Equation (3-3), then the system dynamics are given by:

$$\begin{bmatrix}x_\Theta' \\ x_\Phi'\end{bmatrix} = \begin{bmatrix}A_0 & 0 \\ 0 & A_0\end{bmatrix}\begin{bmatrix}x_\Theta(\xi) \\ x_\Phi(\xi)\end{bmatrix} + \begin{bmatrix}A_1 & 0 \\ 0 & A_1\end{bmatrix}\begin{bmatrix}x_\Theta(\xi_1) \\ x_\Phi(\xi_1)\end{bmatrix} + \begin{bmatrix}A_2 & 0 \\ 0 & A_2\end{bmatrix}\begin{bmatrix}x_\Theta(\xi_2) \\ x_\Phi(\xi_2)\end{bmatrix}$$
$$+ \begin{bmatrix}0 & 0 \\ 0 & B\frac{\mathcal{F}_r}{\eta\Pi\sin\Theta}\left(\frac{\Theta'\cos\Theta\sin\breve{\Theta}}{\sin\Theta} - \breve{\Theta}'\cos\breve{\Theta}\right)\end{bmatrix}\begin{bmatrix}\Gamma_\Theta^* \\ \Gamma_\Phi^*\end{bmatrix} + \begin{bmatrix}B & 0 \\ 0 & B\frac{\sin\breve{\Theta}}{\sin\Theta}\end{bmatrix}\begin{bmatrix}u_\Theta \\ u_\Phi\end{bmatrix} + \begin{bmatrix}BW \\ 0\end{bmatrix}. \tag{3-10}$$

In the case of the inclination dynamics, the input filter successfully makes the terms related to Γ_Θ^* disappear from the equation. On the other hand, in the equation related to the azimuth

dynamics, one term related to Γ^*_Φ remains due to the mismatch between $\check{\Theta}$ and Θ. Moreover, in (3-10) there is a nonlinear factor multiplied by input u_Φ. If the input filters in (3-7) are included in the state-space model, the system dynamics can be rewritten as follows:

$$\begin{bmatrix} x'_\Theta \\ \Gamma^{*'}_\Theta \\ x'_\Phi \\ \Gamma^{*'}_\Phi \end{bmatrix} = \begin{bmatrix} A_0 & 0 & 0 & 0 \\ 0 & -b_0 & 0 & 0 \\ 0 & 0 & A_0 & B\alpha(\Theta,\check{\Theta},\Theta',\check{\Theta}') \\ 0 & 0 & 0 & -b_0 \end{bmatrix} \begin{bmatrix} x_\Theta(\xi) \\ \Gamma^*_\Theta(\xi) \\ x_\Phi(\xi) \\ \Gamma^*_\Phi(\xi) \end{bmatrix} + \begin{bmatrix} A_1 & 0 & 0 & 0 \\ 0 & 0 & 0 & 0 \\ 0 & 0 & A_1 & 0 \\ 0 & 0 & 0 & 0 \end{bmatrix} \begin{bmatrix} x_\Theta(\xi_1) \\ \Gamma^*_\Theta(\xi_1) \\ x_\Phi(\xi_1) \\ \Gamma^*_\Phi(\xi_1) \end{bmatrix}$$
$$+ \begin{bmatrix} A_2 & 0 & 0 & 0 \\ 0 & 0 & 0 & 0 \\ 0 & 0 & A_2 & 0 \\ 0 & 0 & 0 & 0 \end{bmatrix} \begin{bmatrix} x_\Theta(\xi_2) \\ \Gamma^*_\Theta(\xi_2) \\ x_\Phi(\xi_2) \\ \Gamma^*_\Phi(\xi_2) \end{bmatrix} + \begin{bmatrix} B & 0 \\ -b_1 & 0 \\ 0 & B\frac{\sin\check{\Theta}}{\sin\Theta} \\ 0 & -b_1 \end{bmatrix} \begin{bmatrix} u_\Theta \\ u_\Phi \end{bmatrix} + \begin{bmatrix} BW \\ 0 \\ 0 \\ 0 \end{bmatrix}, \tag{3-11}$$

where:

$$b_0 = \frac{\mathcal{M}_b\mathcal{F}_r + (\eta\Pi - \mathcal{F}_b)\mathcal{M}_r}{\chi\Pi\mathcal{F}_r}, \quad b_1 = \frac{\eta\Pi}{\mathcal{F}_r},$$
$$\alpha(\Theta,\check{\Theta},\Theta',\check{\Theta}') = \frac{\mathcal{F}_r}{\eta\Pi\sin\Theta}\left(\frac{\Theta'\cos\Theta\sin\check{\Theta}}{\sin\Theta} - \check{\Theta}'\cos\check{\Theta}\right). \tag{3-12}$$

It has to be noticed that α depends on the states Θ and $\check{\Theta}$, and their derivatives. To simplify notation, we will write α instead of $\alpha(\Theta,\check{\Theta},\Theta',\check{\Theta}')$.

State-feedback controller. We define the state feedback controller corresponding to the input v_i as:

$$z'_{1i} = \zeta \begin{bmatrix} k_{1i} & 0 & 0 \end{bmatrix} e_i \tag{3-13}$$
$$z'_{2i} = -\gamma z_{2i} + \gamma(z_{1i} + K_i e_i) \tag{3-14}$$
$$v_i = z_{2i}. \tag{3-15}$$

This controller consists of a static state (in fact, tracking error $e_i = x_i - x_{ri}$) feedback part, a low-pass filter and integral action. The low-pass filter is used in order to prevent fast changes in the response of the system, since these produce what is called kinking. The purpose of the integral action, is to reject the influence of the gravity related terms in the inclination dynamics (as they are considered as a quasi-constant disturbance). This feedback controller is based on the works of [5].

Observer design. Considering the fact that the states can not be measured directly, an observer needs to be designed in order to support the implementation of the controller in (3-13)-(3-15). Since the weight of the BHA is taken into account as a quasi-constant disturbance, integral action is also added to the observer design. The integral action of the observer is embedded through the integral filter:

$$q'_i = \zeta[l_1, l_2](y_i - \check{y}_i), \qquad \text{for } i = \Theta, \Phi. \tag{3-16}$$

The observer consists of a model-based (predictor) part and an output-injection part. The predictor part of the observer is designed by again considering the model under the condition where $\Theta = \check{\Theta}$. In total, the dynamics of the observer with integral action are given by:

$$\begin{bmatrix} \check{x}'_\Theta \\ q'_\Theta \\ \check{x}'_\Phi \\ q'_\Phi \end{bmatrix} = \begin{bmatrix} A_0 & 0 & 0 & 0 \\ 0 & 0 & 0 & 0 \\ 0 & 0 & A_0 & 0 \\ 0 & 0 & 0 & 0 \end{bmatrix} \begin{bmatrix} \check{x}_\Theta(\xi) \\ q_\Theta(\xi) \\ \check{x}_\Phi(\xi) \\ q_\Phi(\xi) \end{bmatrix} + \begin{bmatrix} A_1 & 0 & 0 & 0 \\ 0 & 0 & 0 & 0 \\ 0 & 0 & A_1 & 0 \\ 0 & 0 & 0 & 0 \end{bmatrix} \begin{bmatrix} \check{x}_\Theta(\xi_1) \\ q_\Theta(\xi_1) \\ \check{x}_\Phi(\xi_1) \\ q_\Phi(\xi_1) \end{bmatrix}$$
$$+ \begin{bmatrix} A_2 & 0 & 0 & 0 \\ 0 & 0 & 0 & 0 \\ 0 & 0 & A_2 & 0 \\ 0 & 0 & 0 & 0 \end{bmatrix} \begin{bmatrix} \check{x}_\Theta(\xi_2) \\ q_\Theta(\xi_2) \\ \check{x}_\Phi(\xi_2) \\ q_\Phi(\xi_2) \end{bmatrix} + \begin{bmatrix} L_\Theta(y_\Theta - \check{y}_\Theta) \\ \zeta[l_{1\Theta}, l_{2\Theta}](y_\Theta - \check{y}_\Theta) \\ L_\Phi(y_\Phi - \check{y}_\Phi) \\ \zeta[l_{1\Phi}, l_{2\Phi}](y_\Phi - \check{y}_\Phi) \end{bmatrix} + \begin{bmatrix} Bq_\Theta \\ 0 \\ Bq_\Phi \\ 0 \end{bmatrix} + \begin{bmatrix} B(u_{r\Theta} + v_\Theta) \\ 0 \\ B(u_{r\Phi} + v_\Phi) \\ 0 \end{bmatrix}, \tag{3-17}$$

where L_i is defined as:

$$L_i = \begin{bmatrix} l_{1i} & l_{2i} \\ 0 & 0 \\ 0 & 0 \end{bmatrix}, \tag{3-18}$$

and with the output observer equations (taking into account the ideal input decoupling transformation) given by:

$$\check{y}_\Theta = C_\Theta \check{x}_\Theta + D_\Theta \Gamma^*_\Theta \tag{3-19}$$
$$\check{y}_\Phi = C_\Phi \check{x}_\Phi + D_\Phi \Gamma^*_\Phi. \tag{3-20}$$

In the next section, the elements of this control strategy are used to derive the closed-loop error dynamics of the system.

3-3 Closed-loop error dynamics

In this section, the complete derivation of the closed-loop error dynamics is provided. The previously presented elements that build up the proposed control strategy are analyzed and used to derive the tracking error and observer error dynamics of the system.

Making use of equation (3-11), the error dynamics of the system (with the tracking errors defined as $e_i = x_i - x_{ri}$) are obtained in (3-21), using for the feedforward the expression given

in (3-9) and the control input decomposition $u_i = u_{ri} + v_i$:

$$\begin{bmatrix} e'_\Theta \\ \Gamma^{*'}_\Theta \\ e'_\Phi \\ \Gamma^{*'}_\Phi \end{bmatrix} = \begin{bmatrix} A_0 & 0 & 0 & 0 \\ 0 & -b_0 & 0 & 0 \\ 0 & 0 & A_0 & B\alpha \\ 0 & 0 & 0 & -b_0 \end{bmatrix} \begin{bmatrix} e_\Theta(\xi) \\ \Gamma^*_\Theta(\xi) \\ e_\Phi(\xi) \\ \Gamma^*_\Phi(\xi) \end{bmatrix} + \begin{bmatrix} A_1 & 0 & 0 & 0 \\ 0 & 0 & 0 & 0 \\ 0 & 0 & A_1 & 0 \\ 0 & 0 & 0 & 0 \end{bmatrix} \begin{bmatrix} e_\Theta(\xi_1) \\ \Gamma^*_\Theta(\xi_1) \\ e_\Phi(\xi_1) \\ \Gamma^*_\Phi(\xi_1) \end{bmatrix}$$
$$+ \begin{bmatrix} A_2 & 0 & 0 & 0 \\ 0 & 0 & 0 & 0 \\ 0 & 0 & A_2 & 0 \\ 0 & 0 & 0 & 0 \end{bmatrix} \begin{bmatrix} e_\Theta(\xi_2) \\ \Gamma^*_\Theta(\xi_2) \\ e_\Phi(\xi_2) \\ \Gamma^*_\Phi(\xi_2) \end{bmatrix} + \begin{bmatrix} B & 0 \\ -b_1 & 0 \\ 0 & B\left(\frac{\sin\check{\Theta}}{\sin\Theta}\right) \\ 0 & -b_1 \end{bmatrix} \begin{bmatrix} v_\Theta \\ v_\Phi \end{bmatrix} + \begin{bmatrix} 0 \\ -b_1 u_{r\Theta} \\ B\left(\frac{\sin\check{\Theta}}{\sin\Theta} - 1\right) u_{r\Phi} \\ -b_1 u_{r\Phi} \end{bmatrix}$$
$$+ \begin{bmatrix} BW \\ 0 \\ 0 \\ 0 \end{bmatrix}. \tag{3-21}$$

As a next step, we will introduce also error coordinates for the transformed RSS force inputs. In order to do so, an input filter as in equation (3-7) is designed based on the feedforward input

$$\Gamma^{*'}_{id} = -\frac{\mathcal{M}_b \mathcal{F}_r + (\eta\Pi - \mathcal{F}_b)}{\chi\Pi\mathcal{F}_r}\Gamma^*_{id} - \frac{\eta\Pi}{\mathcal{F}_r}u_{ri}, \tag{3-22}$$

where Γ^*_{id} is a desired input of the RSS corresponding to the feedforward input. Then, an error coordinate for the transformed input Γ^*_i can be defined as $\Delta\Gamma^*_i = \Gamma^*_i - \Gamma^*_{id}$. Then equation (3-21) can be rewritten as:

$$\begin{bmatrix} e'_\Theta \\ \Delta\Gamma^{*'}_\Theta \\ e'_\Phi \\ \Delta\Gamma^{*'}_\Phi \end{bmatrix} = \begin{bmatrix} A_0 & 0 & 0 & 0 \\ 0 & -b_0 & 0 & 0 \\ 0 & 0 & A_0 & B\alpha \\ 0 & 0 & 0 & -b_0 \end{bmatrix} \begin{bmatrix} e_\Theta(\xi) \\ \Delta\Gamma^*_\Theta(\xi) \\ e_\Phi(\xi) \\ \Delta\Gamma^*_\Phi(\xi) \end{bmatrix} + \begin{bmatrix} A_1 & 0 & 0 & 0 \\ 0 & 0 & 0 & 0 \\ 0 & 0 & A_1 & 0 \\ 0 & 0 & 0 & 0 \end{bmatrix} \begin{bmatrix} e_\Theta(\xi_1) \\ \Delta\Gamma^*_\Theta(\xi_1) \\ e_\Phi(\xi_1) \\ \Delta\Gamma^*_\Phi(\xi_1) \end{bmatrix}$$
$$+ \begin{bmatrix} A_2 & 0 & 0 & 0 \\ 0 & 0 & 0 & 0 \\ 0 & 0 & A_2 & 0 \\ 0 & 0 & 0 & 0 \end{bmatrix} \begin{bmatrix} e_\Theta(\xi_2) \\ \Delta\Gamma^*_\Theta(\xi_2) \\ e_\Phi(\xi_2) \\ \Delta\Gamma^*_\Phi(\xi_2) \end{bmatrix} + \begin{bmatrix} B & 0 \\ -b_1 & 0 \\ 0 & B\left(\frac{\sin\check{\Theta}}{\sin\Theta}\right) \\ 0 & -b_1 \end{bmatrix} \begin{bmatrix} v_\Theta \\ v_\Phi \end{bmatrix} + \begin{bmatrix} 0 \\ 0 \\ B\left(\frac{\sin\check{\Theta}}{\sin\Theta} - 1\right) u_{r\Phi} \\ 0 \end{bmatrix}$$
$$+ \begin{bmatrix} BW \\ 0 \\ B\alpha\Gamma^*_{\Phi d} \\ 0 \end{bmatrix}. \tag{3-23}$$

Using the observer shown in Equation (3-17), we can compute the observer error dynamics (with the observer errors defined as $\delta_i = x_i - \check{x}_i$, for $i = \Theta, \Phi$) and including the integral

action results in the following equations:

$$\begin{bmatrix}\delta'_\Theta\\ q'_\Theta\\ \delta'_\Phi\\ q'_\Phi\end{bmatrix} = \begin{bmatrix} A_0 - L_\Theta C_\Theta & -B & 0 & 0\\ \zeta[l_{1\Theta}, l_{2\Theta}]C_\Theta & 0 & 0 & 0\\ 0 & 0 & A_0 - L_\Phi C_\Phi & -B\\ 0 & 0 & \zeta[l_{1\Phi}, l_{2\Phi}]C_\Phi & 0\end{bmatrix}\begin{bmatrix}\delta_\Theta(\xi)\\ q_\Theta(\xi)\\ \delta_\Phi(\xi)\\ q_\Phi(\xi)\end{bmatrix} + \begin{bmatrix} A_1 & 0 & 0 & 0\\ 0 & 0 & 0 & 0\\ 0 & 0 & A_1 & 0\\ 0 & 0 & 0 & 0\end{bmatrix}\begin{bmatrix}\delta_\Theta(\xi_1)\\ q_\Theta(\xi_1)\\ \delta_\Phi(\xi_1)\\ q_\Phi(\xi_1)\end{bmatrix}$$
$$+ \begin{bmatrix} A_2 & 0 & 0 & 0\\ 0 & 0 & 0 & 0\\ 0 & 0 & A_2 & 0\\ 0 & 0 & 0 & 0\end{bmatrix}\begin{bmatrix}\delta_\Theta(\xi_2)\\ q_\Theta(\xi_2)\\ \delta_\Phi(\xi_2)\\ q_\Phi(\xi_2)\end{bmatrix} + \begin{bmatrix} 0\\ 0\\ B(u_{r\Phi} + v_\Phi)(\frac{\sin\check{\Theta}}{\sin\Theta} - 1)\\ 0\end{bmatrix}$$
$$+ \begin{bmatrix} BW - L_\Theta E W_y\\ \zeta[l_{1\Theta}, l_{2\Theta}]E W_y\\ (B\alpha - L_\Phi D_\Phi(\frac{\sin\check{\Theta}}{\sin\Theta} - 1))\Gamma^*_\Phi\\ \zeta[l_{1\Phi}, l_{2\Phi}]D_\Phi(\frac{\sin\check{\Theta}}{\sin\Theta} - 1)\Gamma^*_\Phi\end{bmatrix}. \tag{3-24}$$

If now, the observer is combined with the state-feedback controller, the error dynamics can be obtained, first applying the controller in the following observer-based feedback form:

$$z'_{1i} = \zeta\begin{bmatrix}k_{1i} & 0 & 0\end{bmatrix}(\check{x}_i - x_{ri}) \tag{3-25}$$
$$z'_{2i} = -\gamma z_{2i} + \gamma(z_{1i} + K_i(\check{x}_i - x_{ri})) \tag{3-26}$$
$$v_i = z_{2i}, \tag{3-27}$$

and using the fact that $\check{x}_i - x_{ri} = e_i - \delta_i$ and $\Gamma^*_i = \Delta\Gamma^*_i + \Gamma^*_{id}$, the total error dynamics corresponding to the state vector:

$$X(\xi) = \begin{bmatrix}e^T_\Theta(\xi)\ \Delta\Gamma^*_\Theta(\xi)\ z_{1\Theta}(\xi)\ z_{2\Theta}(\xi)\ \delta^T_\Theta(\xi)\ q_\Theta(\xi)\ e^T_\Phi(\xi)\ \Delta\Gamma^*_\Phi(\xi)\ z_{1\Phi}(\xi)\ z_{2\Phi}(\xi)\ \delta^T_\Phi(\xi)\ q_\Phi(\xi)\end{bmatrix}^T,$$

are given by:

$$X'(\xi) = A_{0cl}X(\xi) + A_{1cl}X(\xi_1) + A_{2cl}X(\xi_2) + P_{cl}(u_{r\Phi}, \Gamma^*_{\Phi d}, \alpha, \Theta, \check{\Theta}, W), \tag{3-28}$$

where matrices A_{0cl}, A_{1cl}, A_{2cl} are given by

$$A_{0cl} = \begin{bmatrix}A_{0\Theta} & 0\\ 0 & A_{0\Phi}\end{bmatrix}, \qquad A_{1cl} = \begin{bmatrix}A_{1\Theta} & 0\\ 0 & A_{1\Phi}\end{bmatrix}, \qquad A_{2cl} = \begin{bmatrix}A_{2\Theta} & 0\\ 0 & A_{2\Phi}\end{bmatrix}, \tag{3-29}$$

where the system matrices in (3-29) and the vector P_{cl} are given by:

$$A_{0\Theta} = \left[\begin{array}{cccc:cc} A_0 & 0 & 0 & B & 0 & 0 \\ 0 & -b_0 & 0 & -b_1 & 0 & 0 \\ \zeta\left[k_{1\Theta},0,0\right] & 0 & 0 & 0 & -\zeta\left[k_{1\Theta},0,0\right] & 0 \\ \gamma K_\Theta & 0 & \gamma & -\gamma & -\gamma K_\Theta & 0 \\ \hdashline 0 & 0 & 0 & 0 & A_0 - L_\Theta C_\Theta & -B \\ 0 & 0 & 0 & 0 & \zeta\left[l_{1\Theta},l_{2\Theta}\right] C_\Theta & 0 \end{array}\right],$$

$$A_{0\Phi} = \left[\begin{array}{cccc:cc} A_0 & B\alpha & 0 & B\left(\frac{\sin\breve{\Theta}}{\sin\Theta}\right) & 0 & 0 \\ 0 & -b_0 & 0 & -b_1 & 0 & 0 \\ \zeta\left[k_{1\Phi},0,0\right] & 0 & 0 & 0 & -\zeta\left[k_{1\Phi},0,0\right] & 0 \\ \gamma K_\Phi & 0 & \gamma & -\gamma & -\gamma K_\Phi & 0 \\ \hdashline 0 & B\alpha - L_\Phi D_\Phi\left(\frac{\sin\breve{\Theta}}{\sin\Theta}-1\right) & 0 & B(\frac{\sin\breve{\Theta}}{\sin\Theta}-1) & A_0 - L_\Phi C_\Phi & -B \\ 0 & \zeta\left[l_{1\Phi},l_{2\Phi}\right] D_\Phi\left(\frac{\sin\breve{\Theta}}{\sin\Theta}-1\right) & 0 & 0 & \zeta\left[l_{1\Phi},l_{2\Phi}\right] C_\Phi & 0 \end{array}\right],$$

$$A_{1i} = \left[\begin{array}{cccc:cc} A_1 & 0 & 0 & 0 & 0 & 0 \\ 0 & 0 & 0 & 0 & 0 & 0 \\ 0 & 0 & 0 & 0 & 0 & 0 \\ 0 & 0 & 0 & 0 & 0 & 0 \\ \hdashline 0 & 0 & 0 & 0 & A_1 & 0 \\ 0 & 0 & 0 & 0 & 0 & 0 \end{array}\right], \quad A_{2i} = \left[\begin{array}{cccc:cc} A_2 & 0 & 0 & 0 & 0 & 0 \\ 0 & 0 & 0 & 0 & 0 & 0 \\ 0 & 0 & 0 & 0 & 0 & 0 \\ 0 & 0 & 0 & 0 & 0 & 0 \\ \hdashline 0 & 0 & 0 & 0 & A_2 & 0 \\ 0 & 0 & 0 & 0 & 0 & 0 \end{array}\right],$$

$$P_{cl}(u_{r\Phi},\Gamma^*_{\Phi d},\alpha,\Theta,\breve{\Theta},W) = \left[\begin{array}{c} BW \\ 0 \\ 0 \\ 0 \\ \hdashline BW - L_\Theta E W_y \\ \zeta[l_{1\Theta},l_{2\Theta}]EW_y \\ \hdashline B\left(\frac{\sin\breve{\Theta}}{\sin\Theta}-1\right)u_{r\Phi} + B\alpha\Gamma^*_{\Phi d} \\ 0 \\ 0 \\ 0 \\ \hdashline B\left(\frac{\sin\breve{\Theta}}{\sin\Theta}-1\right)u_{r\Phi} + B\alpha\Gamma^*_{\Phi d} - LD\left(\frac{\sin\breve{\Theta}}{\sin\Theta}-1\right)\Gamma^*_{\Phi d} \\ \zeta\left[l_{1\Phi},l_{2\Phi}\right] D_\Phi\left(\frac{\sin\breve{\Theta}}{\sin\Theta}-1\right)\Gamma^*_{\Phi d} \end{array}\right].$$

It can be seen that the vector P_{cl} contains the gravity-related terms, which were not included in the feedforward design. This terms in P_{cl}, can be rejected by dedicated integral action. As well, the other perturbation terms in P_{cl} vanish if $\check{\Theta} = \Theta$ (i.e., if the inclination observer error is zero).

3-3-1 Linearization of the error dynamics

The error dynamics in (3-28) will be linearized around an equilibrium point corresponding to zero tracking and observer errors, i.e., $e_i = 0$ and $\delta_i = 0$, for $i = \Theta, \Phi$. Recall that the inclination-related errors have been defined as follows:

$$e_\Theta = \begin{bmatrix} e_{\Theta_0} \\ e_{\langle\Theta\rangle_1} \\ e_{\langle\Theta\rangle_2} \end{bmatrix} := \begin{bmatrix} \Theta - \Theta_d \\ \langle\Theta\rangle_1 - \langle\Theta\rangle_{1d} \\ \langle\Theta\rangle_2 - \langle\Theta\rangle_{2d} \end{bmatrix}. \tag{3-30}$$

From this expression, Θ, $\langle\Theta\rangle_1$ and $\langle\Theta\rangle_2$ can be obtained as:

$$\Theta = e_{\Theta_0} + \Theta_d, \quad \langle\Theta\rangle_1 = e_{\langle\Theta\rangle_1} + \langle\Theta\rangle_{1d}, \quad \langle\Theta\rangle_2 = e_{\langle\Theta\rangle_2} + \langle\Theta\rangle_{2d}. \tag{3-31}$$

In a similar fashion, the observer errors related to the inclination have been defined as:

$$\delta_\Theta = \begin{bmatrix} \delta_{\Theta_0} \\ \delta_{\langle\Theta\rangle_1} \\ \delta_{\langle\Theta\rangle_2} \end{bmatrix} := \begin{bmatrix} \Theta - \check{\Theta} \\ \langle\Theta\rangle_1 - \langle\check{\Theta}\rangle_1 \\ \langle\Theta\rangle_2 - \langle\check{\Theta}\rangle_2 \end{bmatrix}. \tag{3-32}$$

Then $\check{\Theta}$, $\langle\check{\Theta}\rangle_1$ and $\langle\check{\Theta}\rangle_2$ can be obtained as:

$$\check{\Theta} = e_{\Theta_0} + \Theta_d - \delta_{\Theta_0}, \quad \langle\check{\Theta}\rangle_1 = e_{\langle\Theta\rangle_1} + \langle\Theta\rangle_{1d} - \delta_{\langle\Theta\rangle_1}, \quad \langle\check{\Theta}\rangle_2 = e_{\langle\Theta\rangle_2} + \langle\Theta\rangle_{2d} - \delta_{\langle\Theta\rangle_2}. \tag{3-33}$$

In order to obtain the nominal values for the rest of the states, the values of $e_i = 0$ and $\delta_i = 0$ are substituted into Equation (3-28). It has to be noticed that the gravity-related term in the output Equation (3-4) has been omitted from the equilibrium equations. The reasoning behind this, is that if the influence of this term is considered, the solution of the equilibrium equations would lead to a point where $\delta_\Theta \neq 0$, which is clearly not desired. Furthermore, in [24], it has been noted that the influence of this gravity-related term on the measured output is generally very small. For this reason the gravity-related term W_y appearing in Equation (3-28) is not considered for controller and observer design system and its effect will be assessed by means of simulation. When the observer errors δ_i are zero, the condition $\check{\Theta} = \Theta$ is met, and by subsequently setting the derivatives to zero we obtain the following set of equilibrium equations:

$$\begin{aligned} 0 &= BW + Bz_{2\Theta}, \\ 0 &= -b_0\Delta\Gamma^*_\Theta - b_1 z_{2\Theta}, \\ 0 &= -\gamma z_{2\Theta} + \gamma z_{1\Theta}, \\ 0 &= BW - Bq_\theta, \\ 0 &= Bz_{2\Phi}, \\ 0 &= -b_0\Delta\Gamma^*_\Phi - b_1 z_{2\Phi}, \\ 0 &= -\gamma z_{2\Phi} + \gamma z_{1\Phi}, \\ 0 &= -Bq_\Phi. \end{aligned} \tag{3-34}$$

From the set of equations (3-34), the nominal values for z_{1i}, z_{2i}, $\Delta\Gamma_i^*$ and q_i can be obtained. With these remarks, the equilibrium values for all the states are given by:

$$\begin{aligned} e_i &= 0, \\ \delta_i &= 0, \\ z_{1\Theta} &= -W, \\ z_{2\Theta} &= -W, \\ q_\Theta &= W, \\ z_{1\Phi} &= 0, \\ z_{2\Phi} &= 0, \\ q_\Phi &= 0, \\ \Delta\Gamma_\Theta^* &= \frac{b_1}{b_0} W \\ \Delta\Gamma_\Phi^* &= 0. \end{aligned} \tag{3-35}$$

We can then introduce the perturbed versions of the states where the equilibrium is not at a value of zero as follows:

$$\begin{aligned} \Delta z_{1\Theta} &= z_{1\Theta} - (-W) \\ \Delta z_{2\Theta} &= z_{2\Theta} - (-W) \\ \Delta q_\Theta &= q_\Theta - W \\ \Delta\bar{\Gamma}_\Theta^* &= \Delta\Gamma_\Theta^* - \frac{b_1}{b_0} W \end{aligned} \tag{3-36}$$

In order to perform the linearization, the equations are expressed in terms of the error dynamics and the observer error dynamics. Furthermore, the terms related to Θ' and $\check{\Theta}'$ in α as defined in (3-12), were substituted by the dynamics in (2-40). Due to the complexity of the computations involved this was done using the Symbolic Math Toolbox of MATLAB® [30] according to the following equation:

$$\bar{X}'(\xi) = \left.\frac{\partial X'(\xi)}{\partial X(\xi)}\right|_N \bar{X}(\xi) + \left.\frac{\partial X'(\xi)}{\partial X(\xi_1)}\right|_N \bar{X}(\xi_1) + \left.\frac{\partial X'(\xi)}{\partial X(\xi_2)}\right|_N \bar{X}(\xi_2), \tag{3-37}$$

where the perturbation state vector $\bar{X}(\xi)$ given by:

$$\bar{X}(\xi) = \left[e_\Theta^T(\xi)\ \Delta\bar{\Gamma}_\Theta^*(\xi)\ \Delta z_{1\Theta}(\xi)\ \Delta z_{2\Theta}(\xi)\ \delta_\Theta^T(\xi)\ \Delta q_\Theta(\xi)\ e_\Phi^T(\xi)\ \Delta\Gamma_\Phi^*(\xi)\ z_{1\Phi}(\xi)\ z_{2\Phi}(\xi)\ \delta_\Phi^T(\xi)\ q_\Phi(\xi)\right]^T,$$

After linearizing, the system equations are:

$$\bar{X}'(\xi) = \bar{A}_{0cl}\bar{X}(\xi) + \bar{A}_{1cl}\bar{X}(\xi_1) + \bar{A}_{2cl}\bar{X}(\xi_2), \tag{3-38}$$

where the linearized matrices $\bar{A}_{0cl}$, $\bar{A}_{1cl}$ and $\bar{A}_{2cl}$, are given by:

$$\bar{A}_{0cl} = \begin{bmatrix} \bar{A}_{0\Theta} & 0 \\ \bar{A}_{0c} & \bar{A}_{0\Phi} \end{bmatrix}, \qquad \bar{A}_{1cl} = \begin{bmatrix} \bar{A}_{1\Theta} & 0 \\ \bar{A}_{1c} & \bar{A}_{1\Phi} \end{bmatrix}, \qquad \bar{A}_{2cl} = \begin{bmatrix} \bar{A}_{2\Theta} & 0 \\ \bar{A}_{2c} & \bar{A}_{2\Phi} \end{bmatrix}, \tag{3-39}$$

and sub-matrices defined as:

$$\bar{A}_{0i} = \left[\begin{array}{ccccc|cc} A_0 & 0 & 0 & B & 0 & 0 \\ 0 & -b_0 & 0 & -b_1 & 0 & 0 \\ \zeta\left[k_{1i},0,0\right] & 0 & 0 & 0 & -\zeta\left[k_{1i},0,0\right] & 0 \\ \gamma K_i & 0 & \gamma & -\gamma & -\gamma K_i & 0 \\ \hline 0 & 0 & 0 & 0 & A_0 - L_i C_i & -B \\ 0 & 0 & 0 & 0 & \zeta\left[l_{1i}, l_{2i}\right] C_i & 0 \end{array}\right],$$

$$\bar{A}_{0c} = \left[\begin{array}{cccc|cc} 0 & 0 & 0 & 0 & p_{0e1}(\xi) & p_{0e2}(\xi) \\ 0 & 0 & 0 & 0 & 0 & 0 \\ 0 & 0 & 0 & 0 & 0 & 0 \\ 0 & 0 & 0 & 0 & 0 & 0 \\ \hline 0 & 0 & 0 & 0 & p_{0\delta 1}(\xi) & p_{0\delta 2}(\xi) \\ 0 & 0 & 0 & 0 & p_{0q}(\xi) & 0 \end{array}\right],$$

$$\bar{A}_{1i} = \left[\begin{array}{cccc|cc} A_1 & 0 & 0 & 0 & 0 & 0 \\ 0 & 0 & 0 & 0 & 0 & 0 \\ 0 & 0 & 0 & 0 & 0 & 0 \\ 0 & 0 & 0 & 0 & 0 & 0 \\ \hline 0 & 0 & 0 & 0 & A_1 & 0 \\ 0 & 0 & 0 & 0 & 0 & 0 \end{array}\right], \qquad \bar{A}_{1c} = \left[\begin{array}{cccc|cc} 0 & 0 & 0 & 0 & p_{1e}(\xi) & 0 \\ 0 & 0 & 0 & 0 & 0 & 0 \\ 0 & 0 & 0 & 0 & 0 & 0 \\ 0 & 0 & 0 & 0 & 0 & 0 \\ \hline 0 & 0 & 0 & 0 & p_{1\delta}(\xi) & 0 \\ 0 & 0 & 0 & 0 & 0 & 0 \end{array}\right],$$

$$\bar{A}_{2i} = \left[\begin{array}{cccc|cc} A_2 & 0 & 0 & 0 & 0 & 0 \\ 0 & 0 & 0 & 0 & 0 & 0 \\ 0 & 0 & 0 & 0 & 0 & 0 \\ 0 & 0 & 0 & 0 & 0 & 0 \\ \hline 0 & 0 & 0 & 0 & A_2 & 0 \\ 0 & 0 & 0 & 0 & 0 & 0 \end{array}\right], \qquad \bar{A}_{2c} = \left[\begin{array}{cccc|cc} 0 & 0 & 0 & 0 & p_{2e}(\xi) & 0 \\ 0 & 0 & 0 & 0 & 0 & 0 \\ 0 & 0 & 0 & 0 & 0 & 0 \\ 0 & 0 & 0 & 0 & 0 & 0 \\ \hline 0 & 0 & 0 & 0 & p_{2\delta}(\xi) & 0 \\ 0 & 0 & 0 & 0 & 0 & 0 \end{array}\right],$$

and with coefficients given by:

$$p_{0e1}(\xi) = -B\frac{\mathcal{F}_r\Gamma^*_{\Phi d}}{\eta\Pi\sin\Theta_d}\begin{bmatrix}\beta_1\Theta_d+\beta_2\langle\Theta\rangle_{1d}+\beta_3\langle\Theta\rangle_{2d}+\beta_4\Theta_{1d}+\beta_5\Theta_{2d}\left(\frac{1}{\sin\Theta_d}\right)+... \\ (-\beta_1+\beta_2\langle\Theta\rangle_{1d}+\beta_3\langle\Theta\rangle_{2d}+\beta_4\Theta_{1d}+\beta_5\Theta_{2d})\cos\Theta_d \\ -\beta_2\cos\Theta_d \\ -\beta_3\cos\Theta_d\end{bmatrix}^T - B\begin{bmatrix}\frac{\cos\Theta_d}{\sin\Theta_d}u_{r\Phi}\\ \\ 0\\0\end{bmatrix}^T,$$

$$p_{0e2}(\xi) = -B\frac{\mathcal{F}_r\Gamma^*_{\Phi d}}{\eta\Pi\sin\Theta_d}\cos\Theta_d,$$

$$p_{0\delta1}(\xi) = -B\frac{\mathcal{F}_r\Gamma^*_{\Phi d}}{\eta\Pi\sin\Theta_d}\begin{bmatrix}\beta_1\Theta_d+\beta_2\langle\Theta\rangle_{1d}+\beta_3\langle\Theta\rangle_{2d}+\beta_4\Theta_{1d}+\beta_5\Theta_{2d}\left(\frac{1}{\sin\Theta_d}\right)+... \\ (-\beta_1+\beta_2\langle\Theta\rangle_{1d}+\beta_3\langle\Theta\rangle_{2d}+\beta_4\Theta_{1d}+\beta_5\Theta_{2d})\cos\Theta_d \\ -\beta_2\cos\Theta_d \\ -\beta_3\cos\Theta_d\end{bmatrix}^T - B\begin{bmatrix}\frac{\cos\Theta_d}{\sin\Theta_d}u_{r\Phi}\\ \\ 0\\0\end{bmatrix}^T + L_\Phi D_\Phi\begin{bmatrix}\Gamma^*_{\Phi d}\frac{\cos\Theta_d}{\sin\Theta_d}\\ \\ 0\\0\end{bmatrix}^T,$$

$$p_{0\delta2}(\xi) = -B\frac{\mathcal{F}_r\Gamma^*_{\Phi d}}{\eta\Pi\sin\Theta_d}\cos\Theta_d, \quad p_{0q}(\xi) = -\zeta\Gamma^*_{\Phi d}[l_{1\Phi}, l_{2\Phi}]D_\Phi\frac{\cos\Theta_d}{\sin\Theta_d},$$

$$p_{1e}(\xi) = B\frac{\mathcal{F}_r\Gamma^*_{\Phi d}\cos\Theta_d}{\eta\Pi\sin\Theta_d}\begin{bmatrix}\beta_4 & 0 & 0\end{bmatrix}, \qquad p_{1\delta}(\xi) = B\frac{\mathcal{F}_r\Gamma^*_{\Phi d}\cos\Theta_d}{\eta\Pi\sin\Theta_d}\begin{bmatrix}\beta_4 & 0 & 0\end{bmatrix},$$

$$p_{2e}(\xi) = B\frac{\mathcal{F}_r\Gamma^*_{\Phi d}\cos\Theta_d}{\eta\Pi\sin\Theta_d}\begin{bmatrix}\beta_5 & 0 & 0\end{bmatrix}, \quad p_{2\delta}(\xi) = B\frac{\mathcal{F}_r\Gamma^*_{\Phi d}\cos\Theta_d}{\eta\Pi\sin\Theta_d}\begin{bmatrix}\beta_5 & 0 & 0\end{bmatrix},$$

where elements β_j, for $j \in \{1, 2..., 5\}$, correspond to the following elements of the matrices A_0, A_1 and A_2:

$$\beta_1 = A_0(1,1), \quad \beta_2 = A_0(1,2), \quad \beta_3 = A_0(1,3), \quad \beta_4 = A_1(1,1), \quad \beta_5 = A_2(1,1). \tag{3-40}$$

Note that, after the linearization the nonlinear perturbation vector P_{cl} vanishes. The nonlinear elements in this vector depend on Θ and $\dot{\Theta}$. As a result of expressing these two states in terms of e_i and δ_i, for $i = \Theta, \Phi$, after linearizing these terms affect the $\bar{A}_{0c}$, $\bar{A}_{1c}$ and $\bar{A}_{2c}$ matrices. Moreover, the partial derivatives of these terms with respect to e_Θ are zero, so only coefficients in these matrices corresponding to the state δ_Θ appear in the equation.

3-4 Optimization-based controller and observer tuning

In this section, the controller and observer gains will be synthesized using an optimization-based, supported by the analysis of the structure of the error dynamics of the system.

3-4-1 Analysis of the structure of the error dynamics

In order to propose an output-based controller design for the system, the structure of the matrices of equation (3-38) is analyzed in more detail.

First, we note that the main diagonals of $\bar{A}_{ocl}$, $\bar{A}_{1cl}$ and $\bar{A}_{2cl}$ in (3-38) have the same structure for both the inclination and the azimuth dynamics. The matrices $\bar{A}_{0c}$, $\bar{A}_{1c}$ and $\bar{A}_{2c}$ couple the azimuth dynamics with the inclination dynamics, but this coupling is only present in terms of the inclination observer error and the integral action of the inclination observer. This fact can be used advantageously, since the inclination observer error dynamics does not depend on the azimuth dynamics. Figure 3-2 depicts a cascaded structure showing how the error dynamics and the observer error dynamics are interconnected.

As mentioned before, the inclination dynamics are independent from the azimuth dynamics. It is important to stress this fact since this unilateral coupling is the key element for the stability analysis in the neutral bit walk case. Considering the inclination-related dynamics (see top part of Figure 3-2), the error and the observer error dynamics are in a series interconnection, and this interconnection involves constant (ξ-independent) gain-terms (see the matrix $\bar{A}_{0\Theta}$ in (3-39)), allowing to design controller and observer for the inclination error dynamics separately due to its linear time-invariant nature, complying with the separation principle.

It is important to analyze the evolution of the signal δ_Θ, since it perturbs the rest of the (azimuth) error dynamics, as depicted in Figure 3-2. As stated before, the design for the observer gain L_Θ for the inclination observer can be done independently and the related inclination observer error dynamics are guaranteed to be asymptotically stable if the poles of the inclination observer error dynamics are located in the open left-hand side of the complex plane. On the other hand, the way this signal is interconnected with the blocks related to the δ_Φ-dynamics and the e_Φ-dynamics is through ξ-dependent terms (namely, the "$p(\xi)$" terms in Equation (3-39)). This may render controller design challenging, since these coefficients

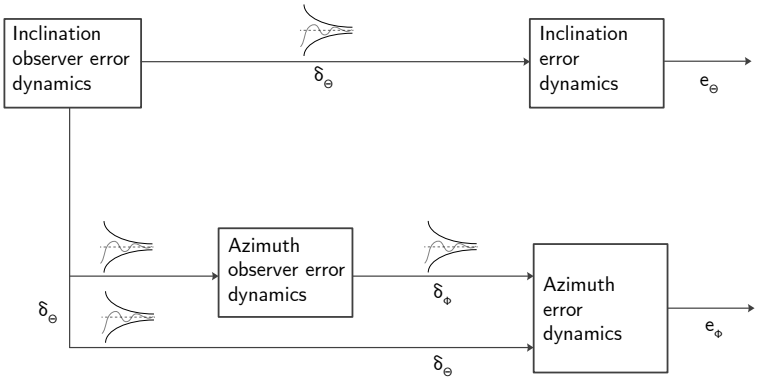

Figure 3-2: Cascaded structure of the error dynamics.

change along the trajectory, which would not allow to take an eigenvalue-based approach towards stability analysis or as a basis for designing the gains of the azimuth observer and controller. Despite this fact, the ξ-dependent terms in (3-39) are entirely related to the designed reference trajectory, meaning that these terms remain bounded according to the bounded reference trajectory.

If then the combination (product) of the signal coming from the δ_Θ-dynamics and the ξ-dependent terms is considered, we use the fact that the δ_Θ-dynamics are asymptotically stable (in fact, δ_Θ eventually converges to zero exponentially) and that the "$p(\xi)$" terms are bounded, making the perturbation signals exciting the δ_Φ-dynamics and the e_Φ-dynamics bounded and converging to zero in an exponential fashion. Another remark is that there is also coupling (through a ξ-dependent gain term) towards the δ_Φ-dynamics and the e_Φ-dynamics related to the state q_Θ, for which the same argument of, firstly, it being asymptotically stable (since it corresponds to the observer integral action of the inclination, which also converges exponentially by design of the inclination observer) and, secondly, the boundedness of the related coupling term also holds.

In order to guarantee stability of the whole system, it only remains to check the internal stability of the δ_Φ-dynamics and the e_Φ-dynamics in Figure 3-2. Considering that the perturbation signals are converging to zero exponentially, the stability of these error and observer error dynamics can be analysed without considering these perturbation terms. This leads to the same series interconnection found from the δ_Θ-dynamics to the e_Θ-dynamics, allowing to design once again, controller and observer gains of the azimuth dynamics separately, without compromising stability of the whole system. An important observation as well, is that the stability of the linearized system is independent from the actual desired trajectory, as this only influences the interconnection terms.

After this analysis, it can be concluded that the controller synthesis of gains K_i and L_i, for $i = \Theta, \Phi$ can be done using an eigenvalue approach as in [23] and [5], for the following isolated partial error system dynamics:

1. the isolated inclination tracking error dynamics:

$$\begin{bmatrix} e'_\Theta(\xi) \\ \Delta\bar{\Gamma}^{*\prime}_\Theta(\xi) \\ \Delta z'_{1\Theta}(\xi) \\ \Delta z'_{2\Theta}(\xi) \end{bmatrix} = \begin{bmatrix} A_0 & 0 & 0 & B \\ 0 & -b_0 & 0 & -b_1 \\ \zeta\begin{bmatrix} k_{1\Theta}, 0, 0 \end{bmatrix} & 0 & 0 & 0 \\ \gamma K_\Theta & 0 & \gamma & -\gamma \end{bmatrix} \begin{bmatrix} e_\Theta(\xi) \\ \Delta\bar{\Gamma}^*_\Theta(\xi) \\ \Delta z_{1\Theta}(\xi) \\ \Delta z_{2\Theta}(\xi) \end{bmatrix} + \begin{bmatrix} A_1 & 0 & 0 & 0 \\ 0 & 0 & 0 & 0 \\ 0 & 0 & 0 & 0 \\ 0 & 0 & 0 & 0 \end{bmatrix} \begin{bmatrix} e_\Theta(\xi_1) \\ \Delta\bar{\Gamma}^*_\Theta(\xi_1) \\ \Delta z_{1\Theta}(\xi_1) \\ \Delta z_{2\Theta}(\xi_1) \end{bmatrix} + \begin{bmatrix} A_2 & 0 & 0 & 0 \\ 0 & 0 & 0 & 0 \\ 0 & 0 & 0 & 0 \\ 0 & 0 & 0 & 0 \end{bmatrix} \begin{bmatrix} e_\Theta(\xi_2) \\ \Delta\bar{\Gamma}^*_\Theta(\xi_2) \\ \Delta z_{1\Theta}(\xi_2) \\ \Delta z_{2\Theta}(\xi_2) \end{bmatrix}, \tag{3-41}$$

2. the isolated azimuth tracking error dynamics:

$$\begin{bmatrix} e'_{\Phi}(\xi) \\ \Delta\Gamma^{*\prime}_{\Phi}(\xi) \\ z'_{1\Phi}(\xi) \\ z'_{2\Phi}(\xi) \end{bmatrix} = \begin{bmatrix} A_0 & 0 & 0 & B \\ 0 & -b_0 & 0 & -b_1 \\ \zeta \begin{bmatrix} k_{1\Phi}, 0, 0 \end{bmatrix} & 0 & 0 & 0 \\ \gamma K_{\Phi} & 0 & \gamma & -\gamma \end{bmatrix} \begin{bmatrix} e_{\Phi}(\xi) \\ \Delta\Gamma^{*}_{\Phi}(\xi) \\ z_{1\Phi}(\xi) \\ z_{2\Phi}(\xi) \end{bmatrix} + \begin{bmatrix} A_1 & 0 & 0 & 0 \\ 0 & 0 & 0 & 0 \\ 0 & 0 & 0 & 0 \\ 0 & 0 & 0 & 0 \end{bmatrix} \begin{bmatrix} e_{\Phi}(\xi_1) \\ \Delta\Gamma^{*}_{\Phi}(\xi_1) \\ z_{1\Phi}(\xi_1) \\ z_{2\Phi}(\xi_1) \end{bmatrix} + \begin{bmatrix} A_2 & 0 & 0 & 0 \\ 0 & 0 & 0 & 0 \\ 0 & 0 & 0 & 0 \\ 0 & 0 & 0 & 0 \end{bmatrix} \begin{bmatrix} e_{\Phi}(\xi_2) \\ \Delta\Gamma^{*}_{\Phi}(\xi_2) \\ z_{1\Phi}(\xi_2) \\ z_{2\Phi}(\xi_2) \end{bmatrix}, \tag{3-42}$$

3. the isolated inclination observer error dynamics:

$$\begin{bmatrix} \delta'_{\Theta}(\xi) \\ \Delta q'_{\Theta}(\xi) \end{bmatrix} = \begin{bmatrix} A_0 - L_{\Theta}C_{\Theta} & -B \\ \zeta \begin{bmatrix} l_{1\Theta}, l_{2\Theta} \end{bmatrix} C_{\Theta} & 0 \end{bmatrix} \begin{bmatrix} \delta_{\Theta}(\xi) \\ \Delta q_{\Theta}(\xi) \end{bmatrix} + \begin{bmatrix} A_1 & 0 \\ 0 & 0 \end{bmatrix} \begin{bmatrix} \delta_{\Theta}(\xi_1) \\ \Delta q_{\Theta}(\xi_1) \end{bmatrix} + \begin{bmatrix} A_2 & 0 \\ 0 & 0 \end{bmatrix} \begin{bmatrix} \delta_{\Theta}(\xi_2) \\ \Delta q_{\Theta}(\xi_2) \end{bmatrix}, \tag{3-43}$$

4. the isolated azimuth tracking error dynamics:

$$\begin{bmatrix} \delta'_{\Phi}(\xi) \\ q'_{\Phi}(\xi) \end{bmatrix} = \begin{bmatrix} A_0 - L_{\Phi}C_{\Phi} & -B \\ \zeta \begin{bmatrix} l_{1\Phi}, l_{2\Phi} \end{bmatrix} C_{\Phi} & 0 \end{bmatrix} \begin{bmatrix} \delta_{\Phi}(\xi) \\ q_{\Phi}(\xi) \end{bmatrix} + \begin{bmatrix} A_1 & 0 \\ 0 & 0 \end{bmatrix} \begin{bmatrix} \delta_{\Phi}(\xi_1) \\ q_{\Phi}(\xi_1) \end{bmatrix} + \begin{bmatrix} A_2 & 0 \\ 0 & 0 \end{bmatrix} \begin{bmatrix} \delta_{\Phi}(\xi_2) \\ q_{\Phi}(\xi_2) \end{bmatrix}. \tag{3-44}$$

Asymptotic stability can be achieved if gains K_i and L_i, for $i = \Theta, \Phi$ are chosen in such way that the poles of (3-41), (3-42), (3-43) and (3-44) are in the open left-half of the complex plane. If only stability is considered as a requirement, one could use the same design and tuning procedure for the controller and observer gains of the azimuth and inclination dynamics. Despite the fact that asymptotic stability can be ensured this way, the transient performance of the system could not be adequate, since the initial observer errors could cause a high level of transient oscillations in the tracking errors (causing transient borehole spiraling).

In order to cope with this initial estimation error in a way favorable for transient performance, it is proposed to use the available measurements of the BHA orientation close to the bit as initial values for the observer dynamics. These measurements are given by the output equations in (2-48) and (2-49). Additionally, in order to avoid undesired transients, the controller and observer gains (for both the inclination and azimuth dynamics) are designed differently, making sure that the observer dynamics converge faster than the tracking error dynamics.

3-4-2 Controller synthesis

Although the structure of the controller has already been designed, it remains to design the parameters of the controller, observer, integral-action and low-pass filter gains. The asymptotic stability of the linearized system is guaranteed as long as the closed-loop poles are located in the open left-hand side of the imaginary axis in the complex plane. In other

words, for the system to be asymptotically stable, the following conditions have to be met (for corresponding isolated error systems (3-41), (3-42), (3-43) and (3-44)):

$$\max_{j\in[1,2,\ldots,\infty]}\{\mathfrak{Re}(\lambda_{jK\Theta}(K_\Theta,\zeta,\gamma))\}<0, \tag{3-45}$$

$$\max_{j\in[1,2,\ldots,\infty]}\{\mathfrak{Re}(\lambda_{jK\Phi}(K_\Phi,\zeta,\gamma))\}<0, \tag{3-46}$$

$$\max_{j\in[1,2,\ldots,\infty]}\{\mathfrak{Re}(\lambda_{jL\Theta}(L_\Theta,\zeta))\}<0, \tag{3-47}$$

$$\max_{j\in[1,2,\ldots,\infty]}\{\mathfrak{Re}(\lambda_{jL\Phi}(L_\Phi,\zeta))\}<0, \tag{3-48}$$

where $\lambda_{jKi}(K_i,\zeta,\gamma)$ and $\lambda_{jLi}(L_i,\zeta)$ for $i=\Theta,\Phi$ represent the j-th closed-loop pole of the isolated error systems corresponding to the controller and observer dynamics, respectively. Furthermore, the transient response of the isolated system becomes faster if the poles are located further to the left in the complex plane. In order to obtain specific values for the controller and observer gains, based on the conditions given by (3-45), (3-46), (3-47) and (3-48), we can formulate an optimization problem consisting on minimizing the following objective functions:

$$J_1=\max_{j\in[1,2,\ldots,\infty]}\{\mathfrak{Re}(\lambda_{jK\Theta}(K_\Theta,\zeta,\gamma))\}, \tag{3-49}$$

$$J_2=\max_{j\in[1,2,\ldots,\infty]}\{\mathfrak{Re}(\lambda_{jK\Phi}(K_\Phi,\zeta,\gamma))\}, \tag{3-50}$$

$$J_3=\max_{j\in[1,2,\ldots,\infty]}\{\mathfrak{Re}(\lambda_{jL\Theta}(L_\Theta,\zeta))\}, \tag{3-51}$$

$$J_4=\max_{j\in[1,2,\ldots,\infty]}\{\mathfrak{Re}(\lambda_{jL\Phi}(L_\Phi,\zeta))\}, \tag{3-52}$$

corresponding to isolated systems (3-41), (3-42), (3-43) and (3-44), respectively. These four independent non-smooth optimization problems can be solved using a gradient-sampling algorithm [23]. This algorithm can be implemented via the MATLAB® toolbox given in [31], which also allows to optimize the location of the real part of the right-most pole. Despite this fact, the evaluation of the objective functions in (3-49), (3-50), (3-51) and (3-52) can be computationally expensive. In order to reduce the effort, the gains of the integral action ζ and the low-pass filter γ are fixed for each iteration. This can be done since the control objectives that these gains pursue are on a different "length" scale than those of the state-feedback and observer gains [5]. Specifically, in the case of the integral action, its purpose is to counteract the effects of gravity (which is being considered as a quasi-constant disturbance) in both the error and the observer error dynamics, implying that its influence varies slowly with respect to the borehole evolution along the length. On the other hand, the low-pass filter pursues the objective to avoid aggressive responses against initial errors, preventing borehole kinking. The selection of these gains will be done in an iterative process until the desired performance is reached.

It has to be kept in mind that, since the inclination observer dynamics have to converge faster than the rest of the dynamics of the system, the location of its right-most pole has to

be chosen further into the left-half complex plane than for the rest of the rest of the dynamics of the system; this will be explained in more detail in the next section.

The stopping criterion for the optimization routine will be the location of the right-most pole of each of the isolated error systems (3-41), (3-42), (3-43) and (3-44). In order to propose the values of these right-most poles for the optimization problem to compute the corresponding controller and observer gains, a time ('length') scale for the convergence of δ_i and e_i for $i = [\Theta, \Phi]$, based on the cascaded structure of Figure 3-2 is introduced. The determining dynamics of the cascaded structure are given by the δ_Θ block. Because of this, it has been decided to set these dynamics as the $fast$ converging dynamics. As long as the rest of the elements in the structure have a slower convergence, the inclination observer will not lead to large transients in the other dynamics (regarding δ_Φ, e_Θ and e_Φ) which would invalidate the assumptions motivating the stability analysis based on linearization. On the other hand, δ_Φ has to be faster than e_Φ, so it is placed in a *medium* length scale. For the error dynamics e_Θ and e_Φ, the choice can be made to set e_Θ in the same *medium* length scale as δ_Φ and to set e_Φ in a *slow* time scale (since inclination does not depend on the azimuth). It has been decided to keep e_Θ and e_Φ on the same *slow* length scale to have a similar behavior for both Θ and Φ.

3-5 Simulation Results

Table 3-1 shows the values designed for the low-pass filter and integral part fixed for the optimization, as well as the value of the real part of the right-most pole and its corresponding feedback and observer gains designed using the optimization-based approach discussed above.

Table 3-1: Parameters for controller gains.

Gain	Objective right-most pole location	Feedback values	γ	ζ
e_Θ	-0.6	$K_\Theta = \begin{bmatrix} -6310 & -2571 & 1288 \end{bmatrix}$	0.8	0.5
δ_Θ	-0.9	$L_\Theta = \begin{bmatrix} 1014 & 3299 \\ 0 & 0 \\ 0 & 0 \end{bmatrix}$	0	0.5
e_Φ	-0.6	$K_\Phi = \begin{bmatrix} -2146 & -1050 & 524 \end{bmatrix}$	0.8	0
δ_Φ	-0.7	$L_\Phi = \begin{bmatrix} -48.5 & 2555 \\ 0 & 0 \\ 0 & 0 \end{bmatrix}$	0	0.3

The most critical values to be designed are the ones corresponding to the inclination observer error δ_Θ, since all of the dynamics are in a series interconnection with its states. It can be seen that the real part of the right-most pole is chosen to be the furthest from the imaginary axis (at real -0.9), in order to have a faster convergence. It has to be considered as well, that if the poles are pushed too much to the left, this could result in high observer gains,

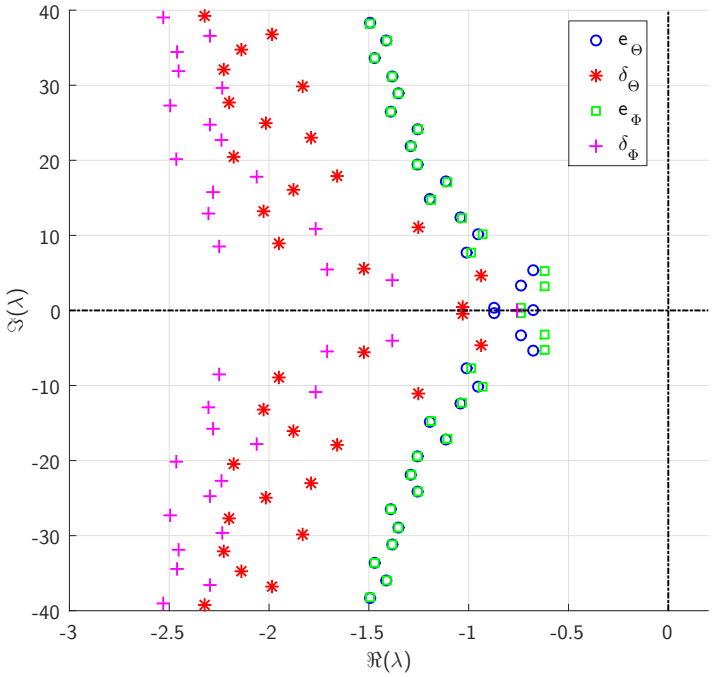

Figure 3-3: Closed-loop poles of the four different isolated error systems for the neutral bit walk system for $\eta\Pi = 0.261$.

which could potentially amplify the effect of disturbances such as noise or model uncertainty. The integrator value for the observer is chosen to be the same as the one for the tracking controller, since it is also counteracting the effect of gravity related terms. It has been chosen to not implement a low-pass filter in both observers, since its function is to avoid fast changes in the response, which is not a problem in the estimation error. The low-pass filter gains are kept the same for both the inclination and azimuth tracking error dynamics. As for the integral part of the azimuth error e_Φ, it has been decided to take the parameter ζ of the tracking error dynamics as zero, since there are no gravity terms affecting these dynamics and implementing it would only slow down the response of the controller, potentially generating a bigger overshoot. On the other hand, due to initial estimation error (despite the fact that available measurements are used), the observer error δ_Φ could be disturbed by the observer error of the inclination δ_Θ. To account for this effect, the integral action is kept for the azimuth observer, in order to slow down the influence of this perturbation. This is implemented in both the controller an observer of the azimuth, although with a smaller value, since the disturbance to be rejected is of a different type.

Figure 3-3 shows the union of the closed-loop poles of the isolated systems (3-41), (3-42), (3-43) and (3-44) after implementing the controller gains of Table 3-1. The right-most pole (poles at the origin are not considered since they are introduced by the state description [23]) is at -0.6195, which is indeed below the chosen maximum value for the right-most poles of the error dynamics.

As mentioned in Section 3-1, the objective of this controller is to be able to track a desired trajectory. The proposed reference trajectory is the same as in [5], since it is considered to represent a real desired borehole geometry, and as long as the trajectory possesses the

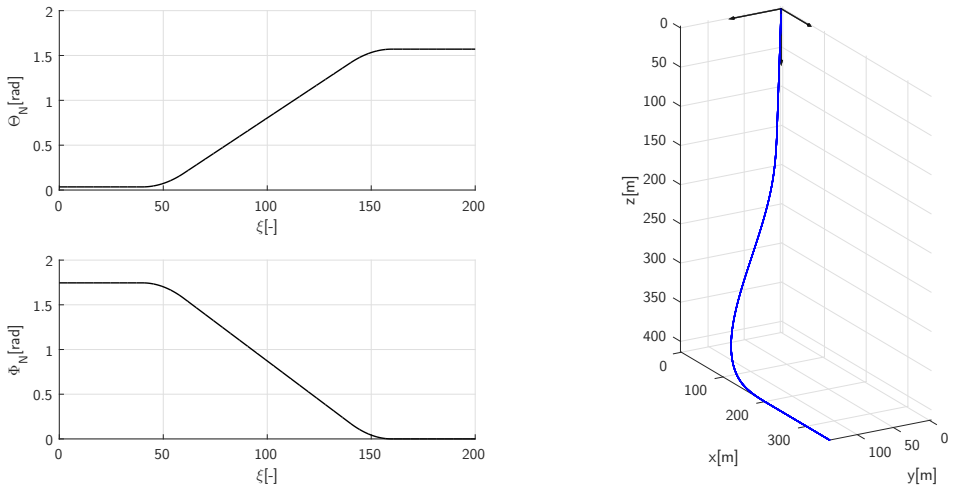

Figure 3-4: Desired borehole geometry and trajectory to be tracked.

properties mentioned in Section 3-1, there will be no loss of generality since the proposed control strategy should be able to solve the reference tracking for any path. The desired trajectory is given by

$$\begin{aligned}
&\Theta_r(\xi) = 0.0349, && \Phi_r(\xi) = 1.75, && \xi \in [0, 40],\\
&\Theta_r(\xi) = 0.649 - 0.0307\xi + 3.8 \cdot 10^{-4}\xi^2, && \Phi_r(\xi) = 1.05 + 0.0349\xi - 4.4 \cdot 10^{-4}\xi^2, && \xi \in [40, 60],\\
&\Theta_r(\xi) = -0.733 + 0.0154\xi, && \Phi_r(\xi) = 2.62 - 0.0175\xi, && \xi \in [60, 140],\\
&\Theta_r(\xi) = -8.26 + 0.123\xi - 3.8 \cdot 10^{-4}\xi^2, && \Phi_r(\xi) = 11.2 - 0.140\xi + 4.4 \cdot 10^{-4}\xi^2, && \xi \in [140, 160],\\
&\Theta_r(\xi) = 1.57, && \Phi_r(\xi) = 0, && \xi \in [160, 200].
\end{aligned} \tag{3-53}$$

This corresponds to the geometry described in Figure 3-4. The inclination trajectory starts at $\Theta = 1°$, this represents an angle close to the vertical (due to a singularity in the model at $\Theta = 0°$ straight vertical boreholes can not be properly described using this angle parametrization of rotation). It is followed by a linearly increasing reference in Θ, until $\xi = 150$, where it becomes a constant inclination of $90°$. The azimuth starts from a constant reference, followed by a linearly increasing trajectory, and finally reaching $\Phi = 0°$. This could represent a typical three-dimensional borehole geometry, since there are changes of direction in the two planes that correspond to the azimuth and inclination dynamics and a full transition from a (near) vertical borehole to a horizontal borehole are represented.

The controller will be tested for several initial conditions, since its behavior could be sensitive to initial errors in the observer. The first measurements of the (inclination and azimuth) sensors measuring the orientation of the BHA some distance back from the bit, are taken into account to improve the transient response. This is done by first simulating the system for one time step (with sampling length $\xi_s = 0.0005$), and obtaining the first entry of the output vectors given by Equations (2-48) and (2-49), which are used as initial conditions for the observer dynamics. The system will be tested for the initial conditions $\Theta(0) = \{1°, 10°, 20°\}$ and $\Phi(0) = \{100°, 90°, 80°\}$. Additionally, the gravity-related terms are considered in simulation for the system dynamics and the output equations (i.e., W and W_y terms). Figure 3-5 shows the inclination and azimuth response for each set of initial conditions.

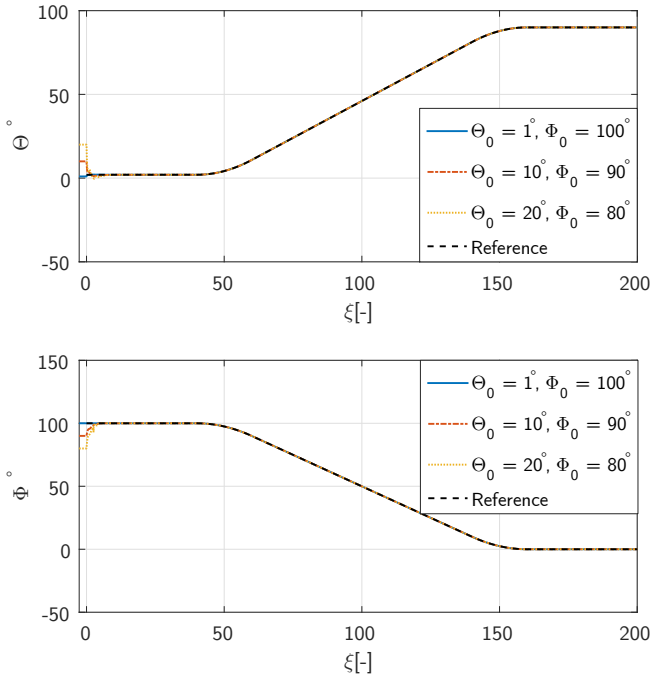

Figure 3-5: Inclination and azimuth responses of the system for $\eta\Pi = 0.261$.

Despite the fact that the initial condition does affect the transient at the beginning of the response, the controller is able to track the trajectory close to the reference. Also, the influence of the initial condition on the applied RSS force has to be considered, this is depicted in Figure 3-6.

The influence of the initial condition is clearly seen as well when the RSS begins to be applied, for both the inclination and the azimuth. This is related to the fact that although the initial conditions for the observers are taken from the measurements on the BHA orientations, as you start further away from the reference, the RSS has to apply more force in order to compensate for that initial error. Finally, the tracking and observer errors are shown in Figure 3-7, up to $\xi = 25$ since at that (dimensionless) distance the error already converged (close) to zero.

The error for both the inclination and the azimuth reaches steady state at approximately $\xi = 10$ (equivalent to 2.73 meters), this result complies with a fast enough response in order to drill a complex borehole geometry. The behavior of the observer is as expected in the case of the inclination. It can be noticed that there is an increment of the initial observer error as the initial condition starts further from the reference trajectory. This can be explained considering the location of the sensors. If we consider a completely straight (either vertical or horizontal) borehole, the orientation being read from the sensors will be the same as the orientation of the borehole. On the other hand, if a curved geometry of the borehole is considered, measurement errors will become present, since they are located in "delayed" locations from the bit and on the BHA. Particularly, the difference between the measurements coming from the output equations of y_Θ and y_Φ in (2-48) and (2-49) and the actual borehole inclination and azimuth Θ and Φ will increase if the curvature increases.

On the other hand, the observer error dynamics of the azimuth show a particular behavior. It can be seen, that in the case of the initial condition $\Theta_0 = 20°$ and $\Phi_0 = 80°$, the error is much

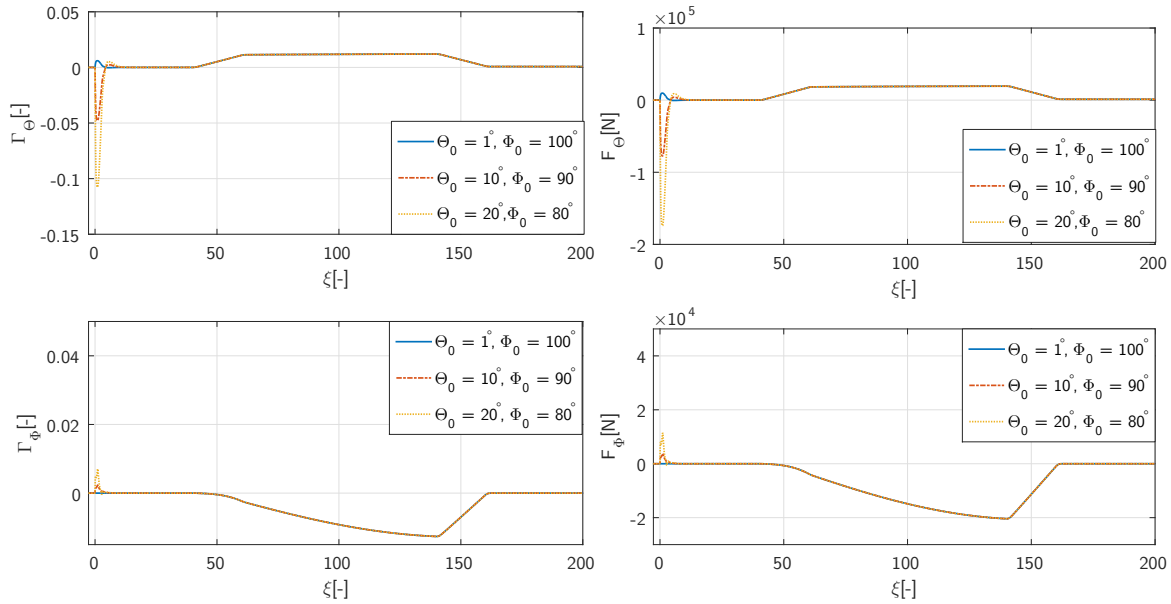

Figure 3-6: Scaled (left) and real (right) RSS applied to the system for $\eta\Pi = 0.261$.

bigger in comparison with the other two sets of initial conditions. This could be explained, since the system was linearized to work around $e_i = 0$ and $\delta_i = 0$, and the nonlinear terms were all related to the difference between Θ and $\breve{\Theta}$. If there is a big enough difference between these two variables, the linearized system will no longer be valid and this could generate estimation errors.

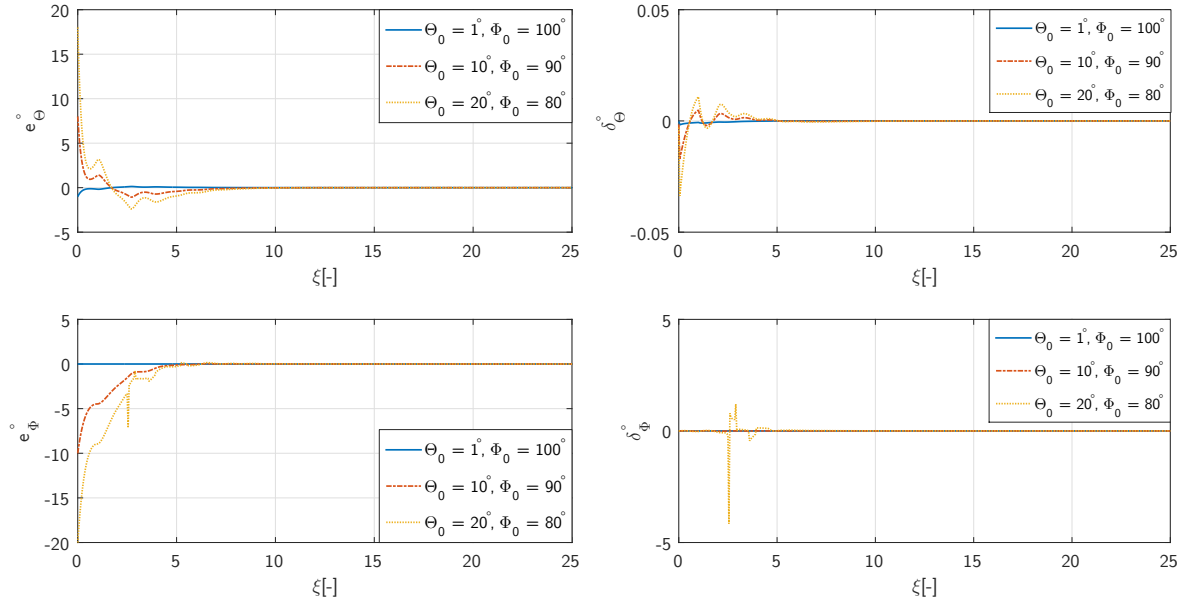

Figure 3-7: Tracking (left) and observer(right) error dynamics for different initial conditions.

Furthermore, besides having to deal with its own initial estimation error, the error in δ_Θ also affects the azimuth observer until it reaches zero as shown in the nonlinear dynamic equations (3-28). It can be seen as well, that there are initial fast transients in the observer error dynamics of the azimuth, which can also be explained with the fact that both the initial estimation errors of the inclination and the azimuth affect the dynamics of δ_Φ, and it can be seen that as the dynamics of δ_Θ approach steady state this transients become smaller and less aggressive.

3-6 Discussion

Several conclusions can be drawn from this chapter. After stating the nature of the reference tracking problem, the approach taken was to derive the closed-loop error dynamics, to subsequently linearize the system around an operation point corresponding to an equilibrium where the tracking errors and the observer errors were all equal to zero. This is a reasonable assumption, considering several facts. First of all the initial conditions can not be far from this condition, since it is set to drill based on a already designed trajectory. This means that the operators can orientate the bit close to the initial direction in the trajectory. In order to reduce initial estimation errors, we considered the first measurement of the BHA orientation in order to provide the initial condition of the observer. Furthermore, if appropriate state-feedback control gains are synthesized, the error will remain around the equilibrium point.

The linearized system was used to perform stability analysis and to subsequently propose a control strategy making use of a cascaded structure of the tracking and observer error dynamics that included the effects for both the inclination and azimuth dynamics, and their interconnections for the neutral bit walk case. This structure was used advantageously to perform controller synthesis, based on the spectral analysis of the location of the closed-loop poles of the linearized system in order to guarantee stability and provide a desired performance.

Ultimately, time domain simulations were performed in other to test the performance of the proposed strategy in a realistic scenario, corresponding to the benchmark system used in Chapter 2 for open-loop simulations. It was shown that the system is able to track a reference trajectory, while avoiding undesired effects such as borehole spiraling, rippling or kinking. Moreover, the strategy was tested for different initial conditions, where the implemented controller managed to fulfill the reference tracking objectives, even for extreme scenarios where the initial conditions are significantly far from the reference trajectory (i.e., $e_\Theta(0) = 19°$, $e_\Phi(0) = -20°$).

A control strategy which only makes use of local measurements of the BHA orientation, which is able to track complex borehole geometries while avoiding undesired behavior was developed. In the next chapter, this control strategy is extended to be able to cope with uncertainty in the active weight on bit Π.

Chapter 4

Robust stability analysis and controller design

An important aspect for controller design is the robustness of the control strategy against uncertainties in the parameters of the model. In the case of a directional drilling system, there are two main parameters that can be considered to be uncertain: the active weight on bit Π and the bit walk angle ϖ. In the case of Π, this uncertainty is related to different factors. In particular, changes in the applied hook-load, the uncertainty in the drag force interaction of the drillstring with the borehole, and the decrease of sharpness of the bit and the rock layer properties as the trajectory evolves are some of the factors that may affect the value of this parameter. It has to be mentioned that all of these changes are usually considered to influence the fluctuation of Π slowly (i.e., at a large length scale) with respect to the dominant length scale relevant to the closed-loop dynamics. Hence, Π can be considered uncertain, though constant. Regarding the bit walk angle ϖ: this parameter is present in the process due to its 3D nature, being one of the main factors that causes undesired behaviors such as borehole spiraling. This parameter is not based only on properties of the system, but it is also affected by the orientation of the bit (which is generally not known) and borehole over-gauging [32]. These effects may cause variation on this parameter as the borehole trajectory evolves, which is why it can be considered as uncertain. The effect of this parameter will be analyzed by means of simulation, since the terms related to this parameter add nonlinear effects and coupling to the already complex dynamics of the system. At first, the bit walk angle will be considered as constant and equal to zero, therefore the analysis in this section will first focus on the uncertainty in Π.

The controller design of Chapter 3 was based on a nominal value of weight on bit Π. To test if the designed strategy is able to cope with the uncertainty of this parameter, it will be considered as $\Pi = \bar{\Pi} + \delta\Pi$, where $\bar{\Pi}$ represents the nominal value of weight on bit, Π the actual weight on bit and $\delta\Pi$ the uncertainty on the weight on bit.

This chapter starts with the derivation of the closed-loop error dynamics accounting for the uncertainty on the active weight on bit Π and in the same manner as in the nominal case, we provide a linearization of the system for stability analysis and controller design. Secondly,

making use of the previous analysis, we go in detail about the robust controller design strategy that was implemented to the system and finally, we test the developed control strategy by means of simulation for two different scenarios: neutral and non-neutral bit walk tendency.

4-1 Error dynamics for robust stability analysis and controller design

The error dynamics of the system are derived once again, since the uncertainty of the parameter Π affects the error dynamics (since the real dynamics depend on Π, while in the controller/observer we can only employ knowledge on $\bar{\Pi}$). Recalling Equation (3-3), the dynamics of the system are given by

$$\begin{aligned}\begin{bmatrix} x'_\Theta \\ x'_\Phi \end{bmatrix} &= \begin{bmatrix} A_0 & 0 \\ 0 & A_0 \end{bmatrix} \begin{bmatrix} x_\Theta(\xi) \\ x_\Phi(\xi) \end{bmatrix} + \begin{bmatrix} A_1 & 0 \\ 0 & A_1 \end{bmatrix} \begin{bmatrix} x_\Theta(\xi_1) \\ x_\Phi(\xi_1) \end{bmatrix} + \begin{bmatrix} A_2 & 0 \\ 0 & A_2 \end{bmatrix} \begin{bmatrix} x_\Theta(\xi_2) \\ x_\Phi(\xi_2) \end{bmatrix} \\ &+ \begin{bmatrix} B_{0\Theta} & 0 \\ 0 & B_{0\Phi}(\Theta, \check{\Theta}, \Theta', \check{\Theta}') \end{bmatrix} \begin{bmatrix} \Gamma^*_\Theta \\ \Gamma^*_\Phi \end{bmatrix} + \begin{bmatrix} B_{1\Theta} & 0 \\ 0 & B_{1\Phi}(\Theta, \check{\Theta}) \end{bmatrix} \begin{bmatrix} \Gamma^{*\prime}_\Theta \\ \Gamma^{*\prime}_\Phi \end{bmatrix} + \begin{bmatrix} BW \\ 0 \end{bmatrix}, \end{aligned} \tag{4-1}$$

and with output equations given by:

$$y_\Theta = C_\Theta x_\Theta + D_\Theta \Gamma^*_\Theta + EW_y, \tag{4-2}$$

$$y_\Phi = C_\Phi x_\Phi + D_\Phi \Gamma^*_\Phi \frac{\sin \check{\Theta}}{\sin \Theta}. \tag{4-3}$$

Herein matrices A_0, A_1, A_2, B_{0i}, B_{1i}, C_i and D_i for $i = \Theta, \Phi$ defined the same as in (3-3), evaluated at $\Pi = \bar{\Pi} + \delta\Pi$. It has to be noted that matrices $B_{0\Phi}$ and $B_{1\Phi}$ are kept in the formulation of the dynamics in (4-1) (i.e., not introducing the α term) and have a dependency with respect to Θ, $\check{\Theta}$, Θ' and $\check{\Theta}'$. From here on, this dependency is not made explicit.

As before, an input filter is introduced as follows:

$$\Gamma^{*\prime}_i = -\bar{b}_0 \Gamma^*_i - \bar{b}_1 u_i, \tag{4-4}$$

where $\bar{b}_0$ and $\bar{b}_1$ are defined as in (3-12) and evaluated at $\bar{\Pi}$. An important remark is that this input filter will not be able to eliminate the Γ^*_i-related terms (not even in the case of the inclination dynamics), due to the difference between nominal matrices $\bar{B}_{0i}$ and $\bar{B}_{1i}$ and their real counterparts. The system dynamics can be derived (using the actual versions of the state matrices), by applying the input filter and including Γ^*_i as a state of the system as follows:

$$\begin{bmatrix} x'_\Theta \\ \Gamma^{*'}_\Theta \\ x'_\Phi \\ \Gamma^{*'}_\Phi \end{bmatrix} = \begin{bmatrix} A_0 & (B_{0\Theta} - B_{1\Theta}\bar{b}_0) & 0 & 0 \\ 0 & -\bar{b}_0 & 0 & 0 \\ 0 & 0 & A_0 & (B_{0\Phi} - B_{1\Phi}\bar{b}_0) \\ 0 & 0 & 0 & -\bar{b}_0 \end{bmatrix} \begin{bmatrix} x_\Theta(\xi) \\ \Gamma^*_\Theta(\xi) \\ x_\Phi(\xi) \\ \Gamma^*_\Phi(\xi) \end{bmatrix} + \begin{bmatrix} A_1 & 0 & 0 & 0 \\ 0 & 0 & 0 & 0 \\ 0 & 0 & A_1 & 0 \\ 0 & 0 & 0 & 0 \end{bmatrix} \begin{bmatrix} x_\Theta(\xi_1) \\ \Gamma^*_\Theta(\xi_1) \\ x_\Phi(\xi_1) \\ \Gamma^*_\Phi(\xi_1) \end{bmatrix}$$
$$+ \begin{bmatrix} A_2 & 0 & 0 & 0 \\ 0 & 0 & 0 & 0 \\ 0 & 0 & A_2 & 0 \\ 0 & 0 & 0 & 0 \end{bmatrix} \begin{bmatrix} x_\Theta(\xi_2) \\ \Gamma^*_\Theta(\xi_2) \\ x_\Phi(\xi_2) \\ \Gamma^*_\Phi(\xi_2) \end{bmatrix} + \begin{bmatrix} -B_{1\Theta}\bar{b}_1 & 0 \\ -\bar{b}_1 & 0 \\ 0 & -B_{1\Phi}\bar{b}_1 \\ 0 & -\bar{b}_1 \end{bmatrix} \begin{bmatrix} u_\Theta \\ u_\Phi \end{bmatrix} + \begin{bmatrix} BW \\ 0 \\ 0 \\ 0 \end{bmatrix}. \tag{4-5}$$

The feedforward input can be now defined as:

$$u_{ri} = B^T(x'_{ri}(\xi) - \bar{A}_0 x_{ri}(\xi) - \bar{A}_1 x_{ri}(\xi_1) - \bar{A}_2 x_{ri}(\xi_2)). \tag{4-6}$$

This feedforward input can be utilized to define once again a desired input Γ^*_{id} as in Equation (3-22) and to define an error coordinate $\Delta\Gamma^*_i$. Then, the error dynamics can be defined as in (4-7) below, using the fact that $x_i = e_i + x_{ri}$.

$$\begin{bmatrix} e'_\Theta \\ \Delta\Gamma^{*'}_\Theta \\ e'_\Phi \\ \Delta\Gamma^{*'}_\Phi \end{bmatrix} = \begin{bmatrix} A_0 & (B_{0\Theta} - B_{1\Theta}\bar{b}_0) & 0 & 0 \\ 0 & -b_0 & 0 & 0 \\ 0 & 0 & A_0 & (B_{0\Phi} - B_{1\Phi}\bar{b}_0) \\ 0 & 0 & 0 & -b_0 \end{bmatrix} \begin{bmatrix} e_\Theta(\xi) \\ \Delta\Gamma^*_\Theta(\xi) \\ e_\Phi(\xi) \\ \Delta\Gamma^*_\Phi(\xi) \end{bmatrix}$$
$$+ \begin{bmatrix} A_1 & 0 & 0 & 0 \\ 0 & 0 & 0 & 0 \\ 0 & 0 & A_1 & 0 \\ 0 & 0 & 0 & 0 \end{bmatrix} \begin{bmatrix} e_\Theta(\xi_1) \\ \Delta\Gamma^*_\Theta(\xi_1) \\ e_\Phi(\xi_1) \\ \Delta\Gamma^*_\Phi(\xi_1) \end{bmatrix} + \begin{bmatrix} A_2 & 0 & 0 & 0 \\ 0 & 0 & 0 & 0 \\ 0 & 0 & A_2 & 0 \\ 0 & 0 & 0 & 0 \end{bmatrix} \begin{bmatrix} e_\Theta(\xi_2) \\ \Delta\Gamma^*_\Theta(\xi_2) \\ e_\Phi(\xi_2) \\ \Delta\Gamma^*_\Phi(\xi_2) \end{bmatrix}$$
$$+ \begin{bmatrix} -B_{1\Theta}\bar{b}_1 & 0 \\ -\bar{b}_1 & 0 \\ 0 & -B_{1\Phi}\bar{b}_1 \\ 0 & -\bar{b}_1 \end{bmatrix} \begin{bmatrix} v_\Theta \\ v_\Phi \end{bmatrix} + \begin{bmatrix} (-B - B_{1\Theta}\bar{b}_1) \\ 0 \\ (-B - B_{1\Phi}\bar{b}_1) \\ 0 \end{bmatrix} \begin{bmatrix} u_{r\Theta} \\ u_{r\Phi} \end{bmatrix} + \begin{bmatrix} F_{p\Theta} \\ 0 \\ F_{p\Phi} \\ 0 \end{bmatrix}, \tag{4-7}$$

where the perturbation terms $F_{p\Theta}$ and $F_{p\Phi}$ are defined as:

$$F_{p\Theta} = (B_{0\Theta} - B_{1\Theta}\bar{b}_0)\Gamma^*_{\Theta d} + \Delta A_0 x_{r\Theta}(\xi) + \Delta A_1 x_{r\Theta}(\xi_1) + \Delta A_2 x_{r\Theta}(\xi_2) + BW, \tag{4-8}$$
$$F_{p\Phi} = (B_{0\Phi} - B_{1\Phi}\bar{b}_0)\Gamma^*_{\Phi d} + \Delta A_0 x_{r\Phi}(\xi) + \Delta A_1 x_{r\Phi}(\xi_1) + \Delta A_2 x_{r\Phi}(\xi_2), \tag{4-9}$$

and where $\Delta A_t = A_t - \bar{A}_t$ for $t = 0, 1, 2$. Then, the state feedback controller v_i is implemented in the same way as in (3-25), (3-26) and (3-27), i.e,

$$z'_{1i} = \zeta \begin{bmatrix} k_{1i} & 0 & 0 \end{bmatrix} (\check{x}_i - x_{ri}), \tag{4-10}$$
$$z'_{2i} = -\gamma z_{2i} + \gamma(z_{1i} + K_i(\check{x}_i - x_{ri})), \tag{4-11}$$
$$v_i = z_{2i}. \tag{4-12}$$

Accounting for the observer design, the same integral action will be included and defined as in (3-16), namely,

$$q_i' = \zeta[l_{1i}, l_{2i}](y_i - \check{y}_i).$$

Then, the observer dynamics can be defined as:

$$\begin{bmatrix} \check{x}_\Theta' \\ q_\Theta' \\ \check{x}_\Phi' \\ q_\Phi' \end{bmatrix} = \begin{bmatrix} \bar{A}_0 & 0 & 0 & 0 \\ 0 & 0 & 0 & 0 \\ 0 & 0 & \bar{A}_0 & 0 \\ 0 & 0 & 0 & 0 \end{bmatrix} \begin{bmatrix} \check{x}_\Theta(\xi) \\ q_\Theta(\xi) \\ \check{x}_\Phi(\xi) \\ q_\Phi(\xi) \end{bmatrix} + \begin{bmatrix} \bar{A}_1 & 0 & 0 & 0 \\ 0 & 0 & 0 & 0 \\ 0 & 0 & \bar{A}_1 & 0 \\ 0 & 0 & 0 & 0 \end{bmatrix} \begin{bmatrix} \check{x}_\Theta(\xi_1) \\ q_\Theta(\xi_1) \\ \check{x}_\Phi(\xi_1) \\ q_\Phi(\xi_1) \end{bmatrix} + \begin{bmatrix} \bar{A}_2 & 0 & 0 & 0 \\ 0 & 0 & 0 & 0 \\ 0 & 0 & \bar{A}_2 & 0 \\ 0 & 0 & 0 & 0 \end{bmatrix} \begin{bmatrix} \check{x}_\Theta(\xi_2) \\ q_\Theta(\xi_2) \\ \check{x}_\Phi(\xi_2) \\ q_\Phi(\xi_2) \end{bmatrix}$$
$$+ \begin{bmatrix} L_\Theta(y_\Theta - \check{y}_\Theta) \\ \zeta[l_{1\Theta}, l_{2\Theta}](y_\Theta - \check{y}_\Theta) \\ L_\Phi(y_\Phi - \check{y}_\Phi) \\ \zeta[l_{1\Phi}, l_{2\Phi}](y_\Phi - \check{y}_\Phi) \end{bmatrix} + \begin{bmatrix} Bq_\Theta \\ 0 \\ Bq_\Phi \\ 0 \end{bmatrix} + \begin{bmatrix} B(u_{r\Theta} + v_\Theta) \\ 0 \\ B(u_{r\Phi} + v_\Phi) \\ 0 \end{bmatrix}, \tag{4-13}$$

and with corresponding output equations

$$\check{y}_\Theta = \bar{C}_\Theta \check{x}_\Theta + \bar{D}_\Theta \Gamma_\Theta^*, \tag{4-14}$$
$$\check{y}_\Phi = \bar{C}_\Phi \check{x}_\Phi + \bar{D}_\Phi \Gamma_\Phi^*. \tag{4-15}$$

Since matrices C_i and D_i differ from their nominal versions ($\bar{C}_i$ and $\bar{D}_i$), the description for the derivatives of the states of the integral action for both inclination and azimuth are defined by (after substituting the output equations and considering the fact that $\check{x}_i = e_i + x_{ri} - \delta_i$):

$$q_\Theta' = \zeta[l_{1\Theta}, l_{2\Theta}](\Delta C_\Theta e_\Theta + \Delta C_\Theta x_{r\Theta} + \Delta D_\Theta \Delta\Gamma_\Theta^* + \Delta D_\Theta \Gamma_{\Theta d}^* + \bar{C}_\Theta \delta_\Theta + EW_y), \tag{4-16}$$

$$q_\Phi' = \zeta[l_{1\Phi}, l_{2\Phi}](\Delta C_\Phi e_\Phi + \Delta C_\Phi x_{r\Phi} + D_\Phi(\Delta\Gamma_\Phi + \Gamma_{\Phi d}^*)^* \frac{\sin\check{\Theta}}{\sin\Theta} - \bar{D}_\Phi(\Delta\Gamma_\Phi^* + \Gamma_{\Phi d}^*) + \bar{C}_\Phi \delta_\Phi), \tag{4-17}$$

where $\Delta D_i = D_i - \bar{D}_i$ and $\Delta C_i = C_i - \bar{C}_i$, for $i = \Theta, \Phi$. Now, the observer error dynamics can be obtained. The main difference is that, in this case, due to model uncertainty, the observer dynamics are not decoupled from the system dynamics (not even for the inclination dynamics). The complete system closed-loop error dynamics (for state vector $X(\xi)$ defined as in (3-28)) are given by

$$\begin{aligned} X'(\xi) =& A_{0cl}X(\xi) + A_{1cl}X(\xi_1) + A_{2cl}X(\xi_2) + \\ & P_{cl}(u_{r\Theta}, u_{r\Phi}, \Gamma_{\Theta d}^*, \Gamma_{\Phi d}^*, x_{r\Theta}(\xi), x_{r\Theta}(\xi_1), x_{r\Theta}(\xi_2), x_{r\Phi}(\xi), x_{r\Phi}(\xi_1), x_{r\Phi}(\xi_2), \Theta, \check{\Theta}, W, W_y), \end{aligned} \tag{4-18}$$

where:

$$A_{0cl} = \begin{bmatrix} A_{0\Theta} & 0 \\ 0 & A_{0\Phi} \end{bmatrix}, \qquad A_{1cl} = \begin{bmatrix} A_{1\Theta} & 0 \\ 0 & A_{1\Phi} \end{bmatrix}, \qquad A_{2cl} = \begin{bmatrix} A_{2\Theta} & 0 \\ 0 & A_{2\Phi} \end{bmatrix}, \tag{4-19}$$

where the system matrices in (4-19) and the vector $P_{cl}(\xi, \xi_1, \xi_2, \Theta, \breve{\Theta}, W, W_y)$ (where all the dependencies on terms related to desired trajectory have been expressed by dependencies on ξ, ξ_1 and ξ_2) are given by

$$A_{0\Theta} = \left[\begin{array}{cccc:cc} A_0 & (B_{0\Theta} - B_{1\Theta}\bar{b}_0) & 0 & -B_{1\Theta}\bar{b}_1 & 0 & 0 \\ 0 & -\bar{b}_0 & 0 & -\bar{b}_1 & 0 & 0 \\ \zeta\left[k_{1\Theta}, 0, 0\right] & 0 & 0 & 0 & -\zeta\left[k_{1\Theta}, 0, 0\right] & 0 \\ \gamma K_\Theta & 0 & \gamma & -\gamma & -\gamma K_\Theta & 0 \\ \hdashline (\Delta A_0 - L_\Theta \Delta C_\Theta) & (B_{0\Theta} - B_{1\Theta}\bar{b}_0 - L_\Theta \Delta D_\Theta) & 0 & (-B - B_{1\Theta}\bar{b}_1) & \bar{A}_0 - L_\Theta \bar{C}_\Theta & -B \\ \zeta\left[l_{1\Theta}, l_{2\Theta}\right]\Delta C_\Theta & \zeta\left[l_{1\Theta}, l_{2\Theta}\right]\Delta D_\Theta & 0 & 0 & \zeta\left[l_{1\Theta}, l_{2\Theta}\right]\bar{C}_\Theta & 0 \end{array}\right],$$

$$A_{0\Phi} = \left[\begin{array}{cccc:cc} A_0 & (B_{0\Phi} - B_{1\Phi}\bar{b}_0) & 0 & -B_{1\Phi}\bar{b}_1 & 0 & 0 \\ 0 & -\bar{b}_0 & 0 & -\bar{b}_1 & 0 & 0 \\ \zeta\left[k_{1\Phi}, 0, 0\right] & 0 & 0 & 0 & -\zeta\left[k_{1\Phi}, 0, 0\right] & 0 \\ \gamma K_\Phi & 0 & \gamma & -\gamma & -\gamma K_\Phi & 0 \\ \hdashline (\Delta A_0 - L_\Phi \Delta C_\Phi) & (B_{0\Phi} - B_{1\Phi}\bar{b}_0 - L_\Phi(D_\Phi \frac{\sin\breve{\Theta}}{\sin\Theta} - \bar{D}_\Phi)) & 0 & (-B - B_{1\Phi}\bar{b}_1) & \bar{A}_0 - L_\Phi \bar{C}_\Phi & -B \\ \zeta\left[l_{1\Phi}, l_{2\Phi}\right]\Delta C_\Phi & \zeta\left[l_{1\Phi}, l_{2\Phi}\right](D_\Phi \frac{\sin\breve{\Theta}}{\sin\Theta} - \bar{D}_\Phi) & 0 & 0 & \zeta\left[l_{1\Phi}, l_{2\Phi}\right]\bar{C}_\Phi & 0 \end{array}\right],$$

$$A_{1i} = \left[\begin{array}{cccc:cc} A_1 & 0 & 0 & 0 & 0 & 0 \\ 0 & 0 & 0 & 0 & 0 & 0 \\ 0 & 0 & 0 & 0 & 0 & 0 \\ 0 & 0 & 0 & 0 & 0 & 0 \\ \hdashline \Delta A_1 & 0 & 0 & 0 & \bar{A}_1 & 0 \\ 0 & 0 & 0 & 0 & 0 & 0 \end{array}\right], \quad A_{2i} = \left[\begin{array}{cccc:cc} A_2 & 0 & 0 & 0 & 0 & 0 \\ 0 & 0 & 0 & 0 & 0 & 0 \\ 0 & 0 & 0 & 0 & 0 & 0 \\ 0 & 0 & 0 & 0 & 0 & 0 \\ \hdashline \Delta A_2 & 0 & 0 & 0 & \bar{A}_2 & 0 \\ 0 & 0 & 0 & 0 & 0 & 0 \end{array}\right],$$

$$P_{cl}(\xi,\xi_1,\xi_2,\Theta,\check{\Theta},W,W_y) = \left[\begin{array}{c} F_{p\Theta} + (-B - B_{1\Theta}\bar{b}_1)u_{r\Theta} \\ 0 \\ 0 \\ 0 \\ \hline F_{r\Theta} + (-B - B_{1\Theta}\bar{b}_1)u_{r\Theta} \\ \zeta\left[l_{1\Theta}, l_{2\Theta}\right](\Delta C_\Theta x_{r\Theta} + \Delta D_\Theta \Gamma^*_{\Theta d} + EW_y) \\ \hline F_{p\Phi} + (-B - B_{1\Phi}\bar{b}_1)u_{r\Phi} \\ 0 \\ 0 \\ 0 \\ \hline F_{r\Phi} + (-B - B_{1\Phi}\bar{b}_1)u_{r\Phi} \\ \zeta\left[l_{1\Phi}, l_{2\Phi}\right](\Delta C_\Phi x_{r\Phi} + (D_\Phi \frac{\sin\check{\Theta}}{\sin\Theta} - \bar{D}_\Phi)\Gamma^*_{\Phi d}) \end{array}\right].$$

The expressions for F_{ri}, for $i = \Theta, \Phi$ are given by

$$\begin{aligned} F_{r\Theta} =& (B_{0\Theta} - B_{1\Theta}\bar{b}_0 - L_\Theta \Delta D_\Theta)\Gamma^*_{\Theta d} + (\Delta A_0 - L_\Theta \Delta C_\Theta)x_{r\Theta}(\xi) + \Delta A_1 x_{r\Theta}(\xi_1) \\ &+ \Delta A_2 x_{r\Theta}(\xi_2) + BW - L_\Theta E W_y, \end{aligned} \tag{4-20}$$

$$\begin{aligned} F_{r\Phi} =& \left(B_{0\Phi} - B_{1\Phi}\bar{b}_0 - L_\Phi\left(D_\Phi \frac{\sin\check{\Theta}}{\sin\Theta} - \bar{D}_\Phi\right)\right)\Gamma^*_{\Phi d} + (\Delta A_0 - L_\Phi \Delta C_\Phi)x_{r\Phi}(\xi) \\ &+ \Delta A_1 x_{r\Phi}(\xi_1) + \Delta A_2 x_{r\Phi}(\xi_2), \end{aligned} \tag{4-21}$$

where $\Delta A_0 = A_0 - \bar{A}_0$, $\Delta A_1 = A_1 - \bar{A}_1$ and $\Delta A_2 = A_2 - \bar{A}_2$.

4-1-1 Linearization of the error dynamics with uncertain weight on bit

Following the same design process as in the nominal case, the linearization of the system will be performed at an equilibrium point, writing all the evolution equations in terms of the errors e_i and δ_i, for $i = \Theta, \Phi$. While linearizing, additional difficulties are encountered due to the fact that for the robust case, the equilibrium is not at $e_i = 0$ and $\delta_i = 0$. The latter is caused by the fact that vector P_{cl} does not vanish for $e_i = \delta_i = 0$ due to the presence of parameter uncertainty (among other effects, this causes the feedforward to be inexact, which leads to non-constant perturbations related to the ξ-dependent desired trajectory). This problem is approached in two ways: firstly, by considering the same "equilibrium" point as in the nominal case and secondly, by finding the (quasi-)equilibrium point at different locations along the desired trajectory, thereby obtaining quasi-static solutions for the equilibrium equations.

Prior to performing the linearization, it is important to recall the dependencies of the terms in the system matrices with respect to the states, to have a clear view of where coupling terms may appear. In the case of the inclination, the state matrices and vectors are linear and dependent on constant (uncertain) terms, meaning that these terms will remain the same. On the contrary, vectors $B_{0\Phi}$ and $B_{1\Phi}$ are dependent on states of the inclination dynamics. Let us first analyze $B_{0\Phi}$, which contains elements in terms of Θ, $\check{\Theta}$, Θ' and $\check{\Theta}'$. As in (3-31) and (3-33), Θ and $\check{\Theta}$ can be expressed in terms of e_Θ and δ_Θ. In the case of the derivatives, this need to be substituted from the system dynamics in Equation (2-40), for the case with uncertain weight on bit Π. For notational coherence, we denote these vectors corresponding

to the system where nominal weight on bit $\bar{\Pi}$ a $\bar{B}_{0\Phi}$ and $\bar{B}_{1\Phi}$ and we consider the real ones without the ($^-$) symbol. The dependencies of vectors $B_{0\Phi}$ and $B_{1\Phi}$ can then be expressed in terms of the states of the system as:

$$\begin{aligned} &B_{0\Phi}(e_\Theta(\xi), e_\Theta(\xi_1), e_\Theta(\xi_2), \delta_\Theta(\xi), \delta_\Theta(\xi_1), \delta_\Theta(\xi_2), \Delta\Gamma^*_\Theta(\xi), z_{2\Theta}(\xi)) \\ &B_{1\Phi}(e_\Theta(\xi), \delta_\Theta(\xi)). \end{aligned} \tag{4-22}$$

In order to perform the linearization, an equilibrium point for the system given by Equation (4-18) needs to be found. In the case for $\Pi = \bar{\Pi}$, the errors $e_i(\xi)$, $e_i(\xi_1)$ and $e_i(\xi_2)$ (defined as the difference between the state vector in (2-41) and its desired value), and the observer errors $\delta_i(\xi)$, $\delta_i(\xi_1)$ and $\delta_i(\xi_2)$ (defined as the difference between the state vector in (2-41) and its estimate) for $i = \Theta, \Phi$, were both chosen to be equal to zero. As well in the robust linearized system, the gravity-related terms in the output are disregarded, in accordance with [24]. In the case of the nominal system, it was possible to find a unique solution for the determined system of equilibrium equations given in (3-34). Defining all errors and derivatives of system (4-18) equal to zero results in the equilibrium equations:

$$\begin{aligned}
0 =&(B_{0\Theta} - B_{1\Theta}\bar{b}_0)\Delta\Gamma^*_\Theta - (B_{1\Theta}\bar{b}_1)z_{2\Theta} + F_{p\Theta} + (-B - B_{1\Theta}\bar{b}_1)u_{r\Theta},\\
0 =&-\bar{b}_0\Delta\Gamma^*_\Theta - \bar{b}_1 z_{2\Theta},\\
0 =&\gamma z_{1\Theta} - \gamma z_{2\Theta},\\
0 =&(B_{0\Theta} - B_{1\Theta}\bar{b}_0 - L_\Theta\Delta D_\Theta)\Delta\Gamma^*_\Theta + (-B - B_{1\Theta}\bar{b}_1)z_{2\Theta} - Bq_\Theta + F_{r\Theta} + (-B - B_{1\Theta}\bar{b}_1)u_{r\Theta},\\
0 =&\zeta\begin{bmatrix} l_{1\Theta} & l_{2\Theta}\end{bmatrix}\Delta D_\Theta\Delta\Gamma^*_\Theta + \zeta\begin{bmatrix} l_{1\Theta} & l_{2\Theta}\end{bmatrix}(\Delta C_\Theta x_{r\Theta} + \Delta D_\Theta\Gamma^*_{\Theta d}),\\
0 =&(B_{0\Phi} - B_{1\Phi}\bar{b}_0)\Delta\Gamma^*_\Phi - (B_{1\Phi}\bar{b}_1)z_{2\Phi} + F_{p\Phi} + (-B - B_{1\Phi}\bar{b}_1)u_{r\Phi},\\
0 =&-\bar{b}_0\Delta\Gamma^*_\Phi - \bar{b}_1 z_{2\Phi},\\
0 =&\gamma z_{1\Phi} - \gamma z_{2\Phi},\\
0 =&(B_{0\Phi} - B_{1\Phi}\bar{b}_0 - L_\Phi\Delta D_\Phi)\Delta\Gamma^*_\Phi + (-B - B_{1\Phi}\bar{b}_1)z_{2\Phi} - Bq_\Phi + F_{r\Phi} + (-B - B_{1\Phi}\bar{b}_1)u_{r\Phi},\\
0 =&\zeta\begin{bmatrix} l_{1\Phi} & l_{2\Phi}\end{bmatrix}\Delta D_\Phi\Delta\Gamma^*_\Phi + \zeta\begin{bmatrix} l_{1\Phi} & l_{2\Phi}\end{bmatrix}(\Delta C_\Phi x_{r\Phi} + \Delta D_\Phi\Gamma^*_{\Phi d}).
\end{aligned}$$

(For a nominal point for which $\delta_\Theta = 0$) (4-23)

In this equation it has to be noticed that, since $\Theta = \breve{\Theta}$, then $B_{1\Theta} = B_{1\Phi}$. Nevertheless, vector $B_{0\Phi}$ is still different from $B_{0\Theta}$, because of its dependency on the derivatives of the inclination and its estimate.

It can be seen as well that the system is overdetermined, since it possesses less unknowns than equations, and in general this type of systems has no solution. The main reason for this discrepancy, is that the fifth and tenth equations of (4-23) are added compared to the ones in (3-34). This is because disturbances appear due to the Δ-matrices that represent the difference between the real and nominal system. Two approaches can be taken to find an "equilibrium" around which the system could be linearized. Considering that the variation of Π is slow and is small enough such that it does not significantly change the related equilibrium (for the corresponding constant value of Π), an initial approach is to consider the same linearization point as in the nominal case given in (3-35). The problem of this approach is that this linearization would only be valid for variations of Π along the trajectory that do not make the system diverge to much from its linearized version. The second approach is that instead of taking $e_i(\xi) = 0$ and $\delta_i(\xi) = 0$, retain the errors at the current value of ξ as part of the

equations to obtain a determined system of equations (since $e_i(\xi)$ and $\delta_i(\xi)$ would add up to ten unknowns). There are several problems with this second approach. One of them is, that the error at current ξ for the equilibrium point could be different from zero, caused by the fact that the feedforward input is designed based on the nominal version of the system, which does not represent the real dynamics if there is a discrepancy with respect to the active weight on bit Π. This could potentially cause that the equilibrium point of the system may not be where all the error and observer error dynamics are equal to zero, which would mean that the system would not evolve exactly at the reference trajectory. Another problem of this approach is that the equilibrium point may result in terms dependent on trajectory for certain coordinates, because both the $B_{0\Phi}$ and vector P_{cl} are ξ-dependent when considering parameter uncertainty. This could render the controller design much more complex, since in order to guarantee stability, the controller should be, strictly speaking, stable for all possible values of ξ along the trajectory.

A comparison between this two approaches was performed. In the case where the equilibrium point of the system yields uncertainty, in order to find quasi-static solutions, the error dynamics $e_i(\xi)$ and the observer error dynamics $\delta_i(\xi)$ where kept as variables in the equilibrium equations. This approach is discussed in more detail in Appendix B. It has been decided to use the linearized system around the same equilibrium point as in the nominal case for analysis and controller design. The reasoning behind this is that, according to the simulation results, the variations in Π do not result in steady-state solutions that are located far away from the nominal equilibrium solution of the closed-loop system. Additionally, under normal drilling conditions, the weight on bit Π should not change greatly, as this variation is mainly due to a reduction on the sharpness of the bit, the properties of the interaction between the borehole and the drilling system, and controlled changes on the applied hook-load.

Once more, the linearization is performed according to Equation (3-37) (in this case using the actual value of Π) and defining the perturbation vector as in (3-38). The linearized system (considering that matrix $A_{0\Phi}$ may be ξ-dependent) is given by

$$\bar{X}'(\xi) = \bar{A}_{0cl}\bar{X}(\xi) + \bar{A}_{1cl}\bar{X}(\xi_1) + \bar{A}_{2cl}\bar{X}(\xi_2), \tag{4-24}$$

where the linearized system matrices $\bar{A}_{0cl}$, $\bar{A}_{1cl}$ and $\bar{A}_{2cl}$, are given by:

$$\bar{A}_{0cl} = \begin{bmatrix} \bar{A}_{0\Theta} & 0 \\ \bar{A}_{0c} & \bar{A}_{0\Phi} \end{bmatrix}, \qquad \bar{A}_{1cl} = \begin{bmatrix} \bar{A}_{1\Theta} & 0 \\ \bar{A}_{1c} & \bar{A}_{1\Phi} \end{bmatrix}, \qquad \bar{A}_{2cl} = \begin{bmatrix} \bar{A}_{2\Theta} & 0 \\ \bar{A}_{2c} & \bar{A}_{2\Phi} \end{bmatrix}, \tag{4-25}$$

and sub-matrices defined as:

$$\bar{A}_{0i} = \left[\begin{array}{cccc:cc} A_0 & (B_{0i} - B_{1i}\bar{b}_0) & 0 & -B_{1i}\bar{b}_1 & 0 & 0 \\ 0 & -\bar{b}_0 & 0 & -\bar{b}_1 & 0 & 0 \\ \zeta\left[k_{1i},0,0\right] & 0 & 0 & 0 & -\zeta\left[k_{1i},0,0\right] & 0 \\ \gamma K_i & 0 & \gamma & -\gamma & -\gamma K_i & 0 \\ \hdashline (\Delta A_0 - L_i\Delta C_i) & (B_{0i} - B_{1i}\bar{b}_0 - L_i\Delta D_i) & 0 & (-B - B_{1i}\bar{b}_1) & A_0 - L_i\bar{C}_i & -B \\ \zeta\left[l_{1i},l_{2i}\right]\Delta C_i & \zeta\left[l_{1i},l_{2i}\right]\Delta D_i & 0 & 0 & \zeta\left[l_{1i},l_{2i}\right]\bar{C}_i & 0 \end{array}\right],$$

$$\bar{A}_{0c} = \left[\begin{array}{cccc:cc} p_{0e1}(\xi) & p_{0e2}(\xi) & 0 & p_{0e3}(\xi) & p_{0e4}(\xi) & p_{0e4}(\xi) \\ 0 & 0 & 0 & 0 & 0 & 0 \\ 0 & 0 & 0 & 0 & 0 & 0 \\ 0 & 0 & 0 & 0 & 0 & 0 \\ \hdashline p_{0\delta1}(\xi) & p_{0\delta2}(\xi) & 0 & p_{0\delta3}(\xi) & p_{0\delta4}(\xi) & p_{0\delta5}(\xi) \\ 0 & 0 & 0 & 0 & p_{0q}(\xi) & 0 \end{array}\right],$$

$$\bar{A}_{1i} = \left[\begin{array}{cccc:cc} A_1 & 0 & 0 & 0 & 0 & 0 \\ 0 & 0 & 0 & 0 & 0 & 0 \\ 0 & 0 & 0 & 0 & 0 & 0 \\ 0 & 0 & 0 & 0 & 0 & 0 \\ \hdashline \Delta A_1 & 0 & 0 & 0 & A_1 & 0 \\ 0 & 0 & 0 & 0 & 0 & 0 \end{array}\right], \qquad \bar{A}_{1c} = \left[\begin{array}{cccc:cc} p_{1e1}(\xi) & 0 & 0 & 0 & p_{1e2}(\xi) & 0 \\ 0 & 0 & 0 & 0 & 0 & 0 \\ 0 & 0 & 0 & 0 & 0 & 0 \\ 0 & 0 & 0 & 0 & 0 & 0 \\ \hdashline p_{1\delta1}(\xi) & 0 & 0 & 0 & p_{1\delta2}(\xi) & 0 \\ 0 & 0 & 0 & 0 & 0 & 0 \end{array}\right],$$

$$\bar{A}_{2i} = \left[\begin{array}{cccc:cc} A_2 & 0 & 0 & 0 & 0 & 0 \\ 0 & 0 & 0 & 0 & 0 & 0 \\ 0 & 0 & 0 & 0 & 0 & 0 \\ 0 & 0 & 0 & 0 & 0 & 0 \\ \hdashline \Delta A_2 & 0 & 0 & 0 & A_2 & 0 \\ 0 & 0 & 0 & 0 & 0 & 0 \end{array}\right], \qquad \bar{A}_{2c} = \left[\begin{array}{cccc:cc} p_{2e1}(\xi) & 0 & 0 & 0 & p_{2e2}(\xi) & 0 \\ 0 & 0 & 0 & 0 & 0 & 0 \\ 0 & 0 & 0 & 0 & 0 & 0 \\ 0 & 0 & 0 & 0 & 0 & 0 \\ \hdashline p_{2\delta1}(\xi) & 0 & 0 & 0 & p_{2\delta2}(\xi) & 0 \\ 0 & 0 & 0 & 0 & 0 & 0 \end{array}\right].$$

The definition of the p-coefficients inside the coupling matrix $\bar{A}_{0c}$ will depend on the chosen linearization point. It is important to note, that these coefficients are all dependent on ξ and the actual value of Π, but as in the previous case, these coefficients are all multiplied by the states corresponding to the inclination which, if a proper controller design is performed, will eventually converge to their equilibrium values. Since the inclination dynamics are still independent from the azimuth dynamics, the controller for those dynamics can be designed independently in order to achieve asymptotic stability of the inclination error dynamics. This means that the states of the inclination error dynamics will eventually converge to their equilibrium values, deeming the influence of the perturbation terms that couple the inclination dynamics with the azimuth dynamics inside the $\bar{A}_{0c}$ matrix, to be zero as well.

There are two key differences with respect to the nominal case. First, looking at the structure of matrices $\bar{A}_{0i}$, it can be concluded that the separation principle between controller and observer (for both the inclination and azimuth error dynamics) no longer holds, since there is mutual coupling between the tracking error dynamics and the observer error dynamics in both the inclination and azimuth error dynamics. This means that it is not possible to design controller and observer gains separately as in the nominal case. Secondly, in the specific case of $\bar{A}_{0\Phi}$, it has to be pointed out that this matrix is ξ-dependent. This is due to the fact that vector $B_{0\Phi}$ depends on Θ' and $\check{\Theta}'$, which are not equal due to the difference between Π and $\bar{\Pi}$, i.e.:

$$\begin{aligned} \Theta' - \check{\Theta}' =& (\beta_1 - \bar{\beta}_1)\Theta_d + (\beta_2 - \bar{\beta}_2)\langle\Theta\rangle_{1d} + (\beta_3 - \bar{\beta}_3)\langle\Theta\rangle_{2d} + (\beta_4 - \bar{\beta}_4)\Theta_{1d} + (\beta_5 - \bar{\beta}_5)\Theta_{2d} \\ &+ B^T(B_{0\Theta} - B_{1\Theta}\bar{b}_0)\Delta\Gamma^*_\Theta + B^T(-B_{1\Theta}\bar{b}_1 - B)u_{r\Theta} + B^T(-B_{1\Theta}\bar{b}_1 - B)z_{2\Theta} \\ &+ B^T(B_{0\Theta} - B_{1\Theta}\bar{b}_0)\Delta\Gamma^*_{\Theta d}, \end{aligned} \tag{4-26}$$

where the β and $\bar{\beta}$ terms are defined as in (3-40) for the real and nominal values of Π,

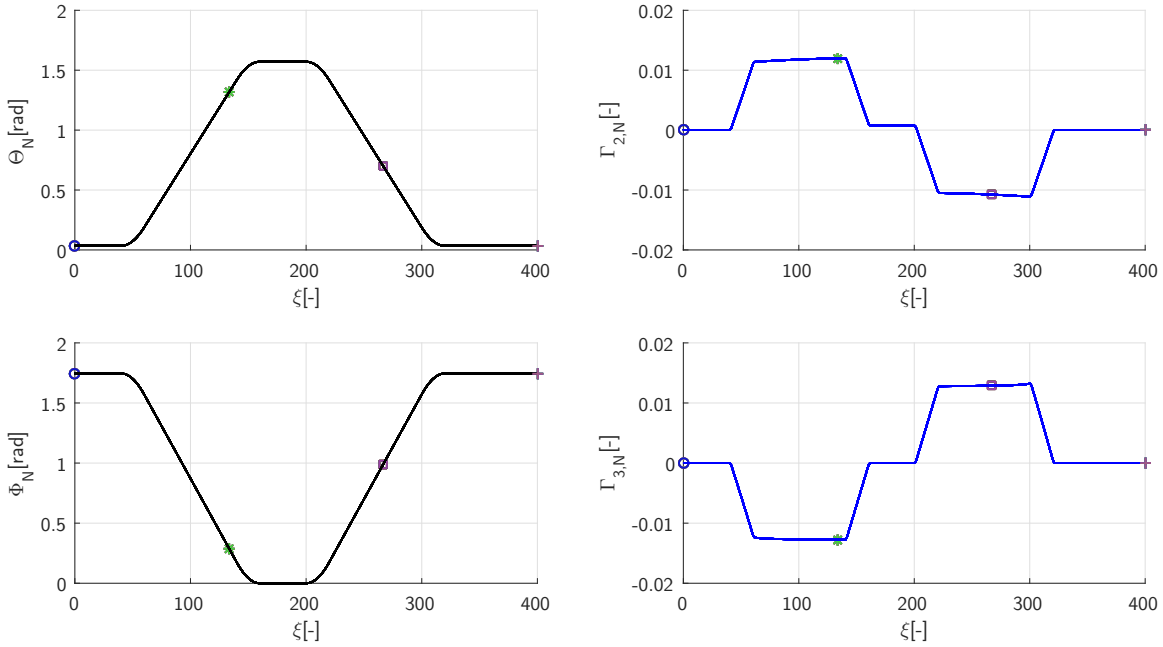

Figure 4-1: Points of the trajectory used to linearize the system.

respectively. In the nominal case, this difference became equal to zero at the equilibrium where $e_i = 0$ and $\delta_i = 0$, which is not the case when taking into account uncertainty on Π. These two differences render the robust controller synthesis much more challenging than the controller design for the nominal case, as will be explained in detail in further sections.

4-1-2 Robust stability analysis

As it has been mentioned before, the system is linearized around the equilibrium point for the system considering $\Pi = \bar{\Pi}$ given by (3-35), due to the fact that under normal drilling conditions the active weight on bit should not vary to much, and also supported by the discussion provided in Appendix B.

The point on the trajectory is not a problem in the case of the inclination dynamics, since the system matrices corresponding to its states are independent from ξ. On the other hand, in the case of the azimuth, there is still dependency on ξ (even if these dynamics are isolated from the inclination error dynamics, due to the presence of vector $B_{0\Phi}$ in $\bar{A}_{0\Phi}$). Because of this, it has been decided to do robust stability analysis for several points along the trajectory. The trajectory is shown in Figure 4-1, along with the marked points chosen for linearization.

The analysis is done by computing the right-most pole of the closed-loop linearized total system dynamics given by Equation (4-24), implementing the controller designed in Chapter 3. These right-most poles, are computed for a variation of active weight of bit $\Pi \in [0.5\bar{\Pi}, 1.5\bar{\Pi}]$ and for the specified values of ξ depicted in Figure 4-2.

Taking a close look at Figure 4-2, it shows that indeed there is a (slight) variation in the location of the right-pole of the closed-loop linearized system. This variation, may be originated due to the persistence of terms related to the designed trajectory, mostly the ones coming from

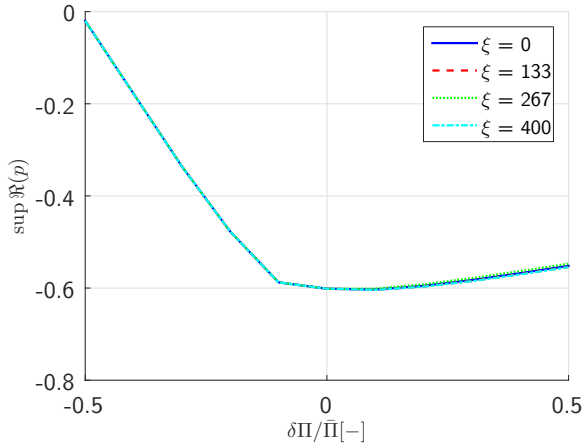

Figure 4-2: Robust stability test for several points along the desired trajectory.

the Δ-matrices and the perturbation vector P_{cl}. Nevertheless, this difference is mostly seen for larger values of Π and does not represent a significant change in the stability properties of the system due to the point on the trajectory. Although the lines corresponding to different points along the trajectory differ, the variation due to the point in the trajectory is rather small. It can be noticed as well, that for smaller values of Π, stability may be compromised (reaching up to a rightmost real part at -0.02). For this reason, a robust controller design is pursued.

4-2 Robust controller design

Following the line of thought given in the previous section for the controller synthesis, the linearization point used in the robust case is chosen to be the same as in the nominal case. The controller synthesis will be performed by isolating the inclination and azimuth dynamics, and computing controller and observer gains together (due to the absence of the separation principle) for both dynamics. In the case of the inclination dynamics, there is no dependency on ξ, which allows to design this gain independently from trajectory. On the other hand, the azimuth is dependent on the designed trajectory, but as it has been shown, the effect of this dependency is not significant, for which it has been decided to do the synthesis of the controller by using the isolated dynamics of the azimuth on one specific point of the trajectory ($\xi = 200$ in this case).

In accordance to the previously conducted robust stability analysis, a control strategy that can guarantee that the right-most pole of the closed-loop system is sufficiently far in the left-half of the complex plain, despite variations of the uncertain parameter Π, is developed in this section.

Initially, the system matrices of the system are analyzed, as in the nominal case. Despite the fact that the separation principle does not longer hold, the same structure with unidirectional coupling from the inclination dynamics to the azimuth dynamics is present. In a similar fashion as in Section 3-4-1, Figure 4-3 shows the series interconnection between the inclination and the azimuth dynamics

This independence of the inclination (along with the fact that the perturbation terms in matrix $\bar{A}_{0c}$ in Equation (4-24) from inclination to azimuth are bounded due to the trajectory design), allows to investigate once again, the stability by only looking at the poles of the block diagonal elements in the matrices $\bar{A}_{0cl}$, $\bar{A}_{1cl}$ and $\bar{A}_{2cl}$. Then as in the nominal case, if we can guarantee that the perturbation coming from the inclination dynamics is bounded and converging to zero for $\xi \to \infty$ and, secondly, the internal azimuth error dynamics are asymptotically stable, then the total system dynamics are asymptotically stable.

Following this argument, we take a look at the poles of the isolated closed-loop error systems formed by:

$$X'_{\Theta}(\xi) = \bar{A}_{0\Theta}X_{\Theta}(\xi) + \bar{A}_{1\Theta}X_{\Theta}(\xi_1) + \bar{A}_{2\Theta}X_{\Theta}(\xi), \tag{4-27}$$

$$X'_{\Phi}(\xi) = \bar{A}_{0\Phi}X_{\Phi}(\xi) + \bar{A}_{1\Phi}X_{\Phi}(\xi_1) + \bar{A}_{2\Phi}X_{\Phi}(\xi), \tag{4-28}$$

where the state vectors X_{Θ} and X_{Φ} correspond to the states related to the inclination and azimuth, respectively, and matrices $\bar{A}_{0i}$, $\bar{A}_{1i}$ and $\bar{A}_{2i}$ are defined as in Equation (4-25).

It has been considered that the linearization point chosen along the trajectory does not affect significantly the location of the right-most pole of the closed-loop system (as depicted in Figure B-1). Figure 4-4 shows the plot of the right-most poles of the closed-loop dynamics of Θ and Φ, as in (4-27) and (4-28), against the variation of Π for the linearized system around the nominal equilibrium point at $\xi = 200$.

It can be noticed, that the poles, located closer to zero, are the ones corresponding to the inclination dynamics. In the case of the azimuth dynamics, the closest pole to the imaginary axis is roughly located around -0.2, which can be considered as sufficiently far from the origin in order to guarantee robust stability. However, it would be beneficial for performance to be able to place these poles corresponding to the azimuth dynamics also further into the left-half complex plane.

Since the separation principle (between controller and observer gains) no longer holds, the computation of error and observer gains has to be performed considering the closed-loop poles of the total dynamics of the system in Equations (4-27) and (4-28). The values of ζ and γ are chosen to be the same as in the nominal case, following the same arguments as in the previous section. The objective functions to be optimized (without considering uncertainty on Π yet) can be described as:

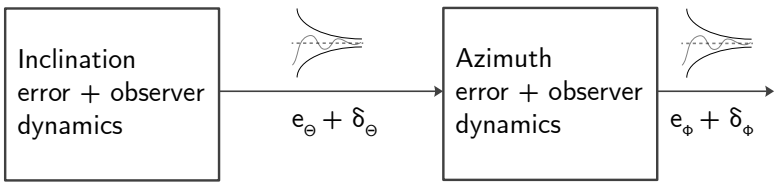

Figure 4-3: Cascaded structure for stability of the system with uncertainty on Π.

$$J_{1r}(K_\Theta, L_\Theta) = \max_{j\in[1,2,\ldots,\infty]} \{\mathfrak{Re}(\lambda_{j\Theta}(K_\Theta, L_\Theta, \bar{\Pi}))\}, \tag{4-29}$$

$$J_{2r}(K_\Phi, L_\Phi) = \max_{j\in[1,2,\ldots,\infty]} \{\mathfrak{Re}(\lambda_{j\Phi}(K_\Phi, L_\Phi, \bar{\Pi}))\}, \tag{4-30}$$

where λ_{ji}, for $i = \Theta, \Phi$, represents the closed-loop pole j of system (4-27) and (4-28), respectively. Strictly speaking, in order to ensure robust stability against uncertainty of Π, the optimization based on the objective functions given by Equations (4-29) and (4-30) should be done for all possible values of Π, which renders the optimization computationally unfeasible. An approach similar to the one given in [23] is taken, where the objective function is defined for a grid of values of Π given by $\Pi = \bar{\Pi} + \delta\Pi_i$, with $\delta\Pi_i$:

$$\delta\Pi_i = -\delta\Pi_{max} + \frac{i-1}{m-1} 2\delta\Pi_{max}, \qquad \text{for } i \in \{1, 2, ..., m\}, \tag{4-31}$$

where m represents the number of grid points for which the closed-loop poles will be calculated. An important remark is that m has to be chosen uneven and higher than two in order to include nominal weight on bit $\bar{\Pi}$ into the objective function. Then the minimization of the following objective functions (which correspond to (4-29) and (4-30) considering uncertain weight on bit) will be pursued:

$$\Psi(K_\Theta, L_\Theta) = \max_{i\in[1,2,\ldots,m]} (J_{1r}(K_\Theta, L_\Theta, \bar{\Pi} + \delta\Pi_i)), \tag{4-32}$$

$$\Psi(K_\Phi, L_\Phi) = \max_{i\in[1,2,\ldots,m]} (J_{2r}(K_\Phi, L_\Phi, \bar{\Pi} + \delta\Pi_i)). \tag{4-33}$$

Despite the fact that the objective functions are defined for a grid of Π, this is still computationally much more expensive than in the nominal case, since the optimization has to be done for five parameters (gains k_{1i}, k_{2i}, k_{1i}, l_{1i} and l_{2i} for $i = \Theta, \Phi$) at the same time. Stability is guaranteed for both observer and controller dynamics, since all the poles of the system are moved further to the left-hand side of the complex plane. This design strategy is applied in order to improve robust stability of the system, verifying afterwards the transient response of the system in order to analyze further improvement.

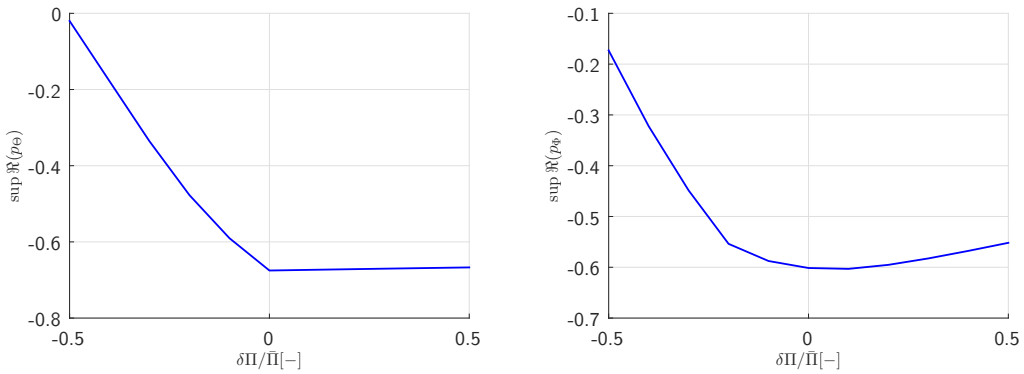

Figure 4-4: Robust stability test for inclination (left) and azimuth (right) dynamics.

Table 4-1: Robust controller settings and gains.

Dynamics	Objective right-most pole	Controller gains (K_i)	Observer gains (L_i)
Inclination (Θ)	-0.7	$[-123987,\ 27068,\ 4104]$	$\begin{bmatrix} 121 & 3192 \\ 0 & 0 \\ 0 & 0 \end{bmatrix}$
Azimuth (Φ)	-0.4	$[-13595,\ 1071,\ 1202]$	$\begin{bmatrix} -1058 & 3243 \\ 0 & 0 \\ 0 & 0 \end{bmatrix}$

In a similar way as in the nominal case, the desired length scale has to be chosen for the dynamics of the system, because the inclination error and observer dynamics have to converge to zero *faster* than the azimuth dynamics. It has been decided to relax the right-most pole location of the inclination dynamics (with respect to the location of the right-most pole of the inclination observer dynamics in the nominal case), in order to reduce computational time. The value of the objective real part of the right-most pole is set to be smaller than -0.7. In the case of the azimuth, this parameter has set to be -0.4, to have a slower convergence than the inclination dynamics.

4-3 Simulation results of the robust controller design

A summary of the settings chosen and the corresponding gains (knowing that the values of ζ and γ are the same as in the nominal case) are given in Table 4-1.

It can be observed, that the gains corresponding the tracking error controller (K_i) for the robust controller design, have much larger values than the ones of the nominal controller. This may have an effect on the control input applied to the system (namely the RSS force). In the case of the observer gains (L_i), they possess values comparable to the ones of the nominal case. Using these gains, the same robust stability test is performed for the closed-loop linear system and compared with the results of the nominal controller design. The comparison is depicted in Figure 4-5.

As shown in the figure, there is a substantial improvement in the level of robustness in accordance to the design. Furthermore, it can be seen that the plots start to become "flat", i.e. independent of Π, (more evident in the case of the azimuth); this can be considered a positive effect, since they start behaving closer to the specified objective right-most pole for every possible value of Π. In other words, despite the fact that both dynamics are intrinsically stable, if for some value of Π the right-most pole of the azimuth dynamics was *faster* than the one of the inclination, this could result in poor performance or even instability.

4-3-1 Time domain simulations of the robust controller

To perform the time domain simulations, the value of Π is set to the value of $0.5\bar{\Pi}$. The initial conditions of the system are set to $\Theta_0 = 20°$ and $\Phi_0 = 80°$, following the same reference trajectory as in the nominal case. Figure 4-6 shows the error between the reference

trajectory and the values of the inclination and azimuth along length ξ (up to 80, since the error converges to zero before this value), for both the nominal and the robust controller.

It is clear that the performance of the robust controller is significantly better than that of the nominal controller. Observing the inclination response, the overshoot is less in the case of the robust controller. The difference of performance becomes more evident in the case of the azimuth response, since the nominal controller transient response possesses a high level of oscillations, this is precisely one of the undesired behaviors of the system, namely borehole rippling. It can be seen that the robust controller manages to avoid this rippling and reaches steady state much faster. Regarding steady state behavior, both controllers manage to reach zero steady state errors.

An important aspect is the order of magnitude of the RSS force, since the feedback gains are much larger in the robust controller. Figure 4-7 shows the RSS force applied for both controllers along the trajectory.

For the inclination, the applied RSS force is bigger than in the nominal case, since the initial control action is corresponding to the value of the gains. On the other hand, since the azimuth nominal controller induces severe transient rippling, it uses high levels of RSS force to compensate for this large variations of the errors. The amount of RSS force applied by the robust controller is indeed smaller, since it manages to keep the error within a smaller range. Despite the fact that these values seem big (compared to the ones displayed with no presence of uncertainty), it has to be kept in mind that the values for the initial conditions of the system were chosen extremely far away from the reference (i.e., $e_\Theta(0) = 19°$, $e_\Phi(0) = -20°$). This means that the control action will reduce significantly for more conventional initial values (as seen in the nominal case for initial conditions close to the reference trajectory).

4-3-2 Simulation results for non-neutral bit walk model

In this section, the previously design robust output-feedback controller for the neutral bit walk case, will be tested on the non-neutral bit walk system. Unfortunately due to time constraints, it was not possible to perform a dedicated controller design that could account for the effect of the bit walk tendency.

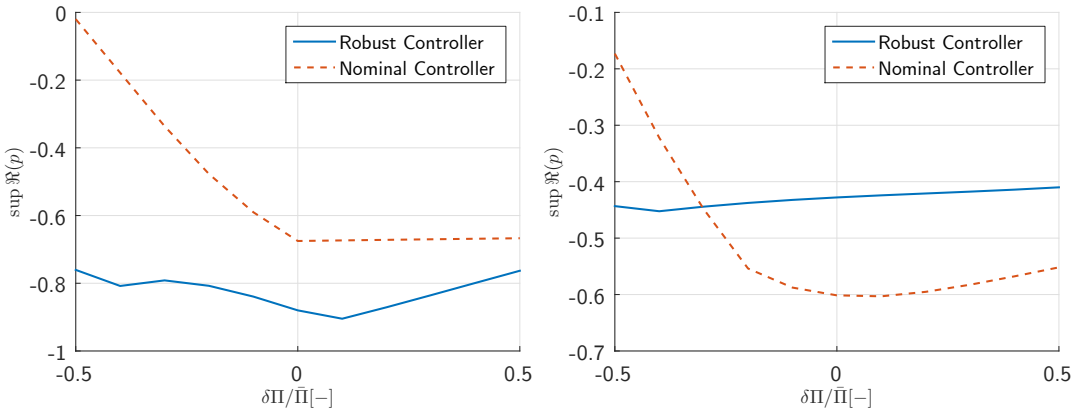

Figure 4-5: Robust stability comparison for inclination (left) and azimuth (right) dynamics.

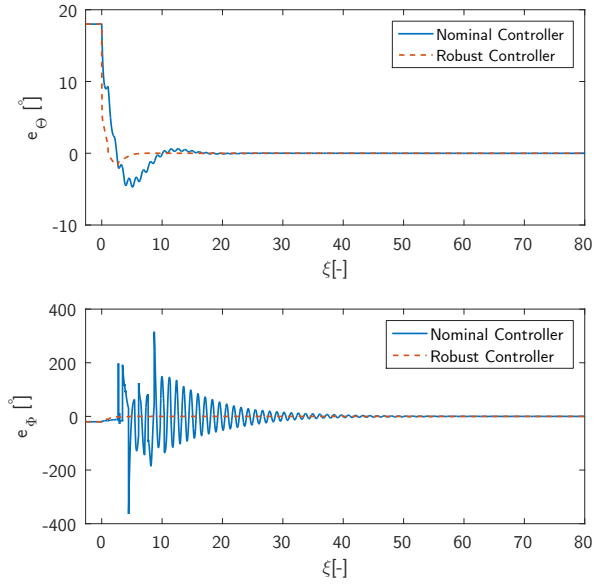

Figure 4-6: Comparison between the errors of nominal and robust controllers for $\Pi = 0.5\bar{\Pi}$.

The previously developed strategy is designed, based on the situation when $\varpi = 0$, but in practice this is usually not the case. As it was mentioned, the variation of this parameter can cause many undesired effects to the borehole geometry. This bit walk tendency is one of the main factors that cause the so-called borehole spiraling.

In order to see how the strategy developed in this research copes with this effect, the controller is tested via simulation. As an initial step, the output equations of the system given by (4-2) and (4-3) are no longer valid, since now the output is affected by the bit walk tendency. The process to obtain these output equations is equivalent to the one performed in Section 2-1-1. As it was done for the neutral bit walk system, one could obtain the BHA inclination and azimuth making use of the particular solution of the Euler-Bernoulli equations of the beam, given by (2-7), substituting s for the sensor locations. The complete derivation of these equations is not given here, but it is important to notice that coefficients $\mathcal{A}_{ij}$ and $\mathcal{B}_{ik}$ for $i = 0, 1, 2$, $j = 0, 1, 2, 3$ and $k = 0, 1, 2$, coming from the particular solution of the BHA remain the same. The solutions for the BHA inclination at the bit ($\hat{\theta}$ and $\hat{\phi}$), given by Equations (2-30) as:

$$\theta = \frac{a_1 + a_2 a_3}{1 - a_2 a_4}, \qquad \phi = \frac{a_3 + a_1 a_4}{1 - a_2 a_4}.$$

where the auxiliary variables a_i for $i = 1, ..., 4$ are given in the same as in Section 2-1, and are now used considering $\varpi \neq 0$. This is where the key difference with respect to the neutral bit walk model output equations is seen. The effect of this parameter originates coupling between the inclination and azimuth outputs and adds nonlinear terms to these equations as well (besides the ones related to gravity).

Using the non-neutral bit walk output equations, the previously design strategy will be tested. Since the controller was designed considering uncertain active weight on bit Π, the simulation will be performed for the extreme case when $\Pi = 0.5\bar{\Pi}$. Considering the initial conditions, despite the fact that the robust controller managed to track the reference for large initial estimation errors ($\Theta - \check{\Theta} = 19°$ and $\Phi - \check{\Phi} = -20°$), it is believed that the effect of the

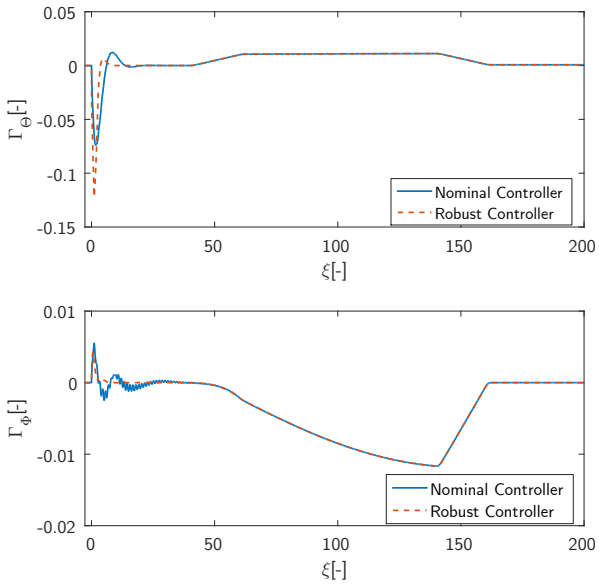

Figure 4-7: Comparison between the inputs of nominal and robust controllers.

bit walk angle can destabilize the system, even if there are no estimation errors. Because of this the initial conditions are decided to remain close to the reference as $\Theta_0 = 1°$ and $\Phi_0 = 100°$. The simulation is performed for $\varpi \in \{-20°, -25°, -30°\}$. Only considering negative values is believed to be enough, since the open-loop simulation results in Section 2-3, showed a symmetrical behavior between negative and positive values of the bit walk angle. The controller settings are the ones shown in Table 4-1 and Figure 4-8 shows the errors of the system (the results of the nominal controller applied to the system are not shown for the sake of clarity, since they are unstable even for small variations of ϖ).

Several conclusions can be drawn from these results. The most evident one is that indeed there is a great effect of the bit walk angle on the response of the system, reflected as a high amount of oscillating transient behavior. However, it was noticed that if the nominal controller values implemented to the closed-loop system, it became completely unstable; meaning that the robust controller design helps to at least render the system stable, for a certain range of values of ϖ. Taking a close look to the tracking error dynamics plot at $\varpi = -20°$, it can be noticed that the oscillations of the transient response vanish as they approach steady state. Nevertheless, as the value of the bit walk angle increases, the oscillating effect becomes larger and, for the extreme case of $\varpi = -30°$, unstable. In all three cases, it can be seen that the oscillations of the azimuth tracking error dynamics are more and of larger values of those corresponding to the inclination. This may be due to the fact that the azimuth observer, is dependent of the inclination error dynamics (along with all the other introduced couplings due to $\varpi \neq 0$), which could mean that there are nonlinear components of the inclination observer affecting the dynamics of the azimuth.

As a general conclusion, the strategy derived in this research, can be valuable to start the design of a controller that is able to cope with non-neutral bit walk tendency, making use only of local measurements. Although, despite the fact that the newly designed controller can manage to stabilize the system for a range of values of Π, it is almost certain that considering the bit walk tendency in the controller design (as previous works have shown [5]) will improve

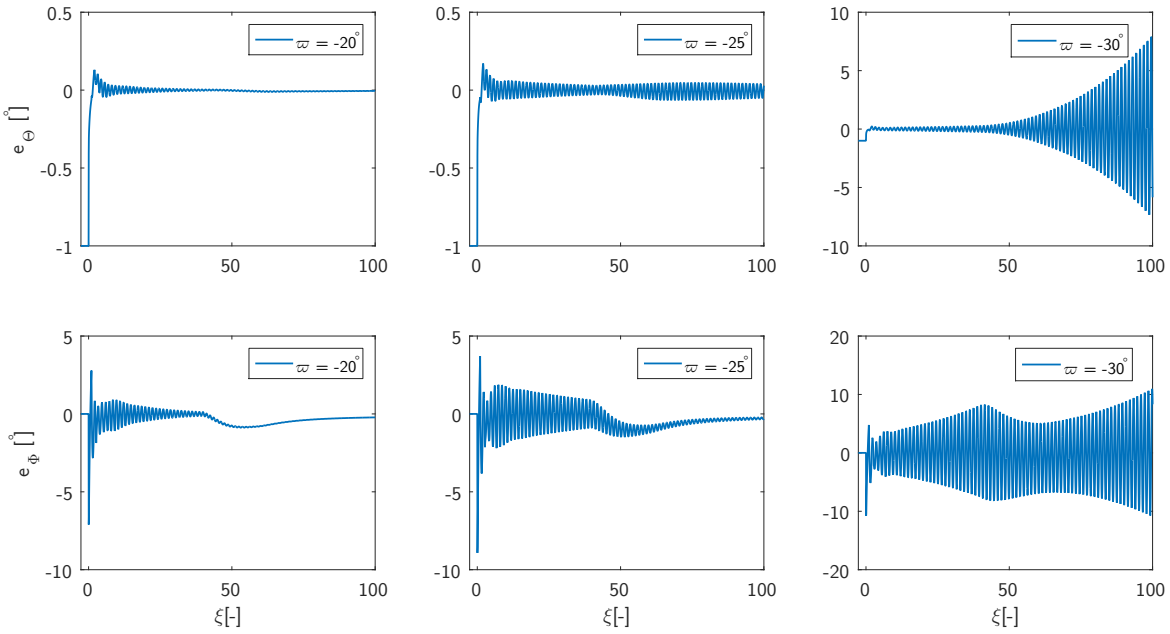

Figure 4-8: Simulation results of the neutral bit walk robust output-feedback controller for $\Pi = 0.5\bar{\Pi}$, $\Theta_0 = 1°$, $\Phi_0 = 100°$ and $\varpi \in \{-20°, -25°, -30°\}$.

the overall performance of the system.

4-4 Discussion

In summary, an output-feedback controller was successfully derived for a 3D directional drilling system, able to track a complex borehole geometry and robust against uncertainty related to the active weight on bit Π. The controller relies only on local measurements of the BHA. This design proved to diminish the amount of negative effects in the borehole such as spiraling, rippling and kinking.

After performing the nominal controller design, robust stability against uncertainty on weight on bit was considered. The key element of this analysis, was to make the explicit difference between the nominal weight on bit $\bar{\Pi}$ and the real one Π. An equivalent procedure to the nominal case was performed, to arrive to the linear error dynamics of the system. In order to ensure stability, the gains for the controller and observer were synthesized by optimizing right-most pole location of the closed-loop isolated dynamics of the subsystems comprised by the tracking and observer error dynamics.

Robustness was tested for this newly designed controller, showing great improvement with respect to its nominal counterpart. Simulations of the tracking problem were performed for the same borehole geometry, finding that there was a significant change, with respect to the nominal controller, for the extreme case where $\Pi = 0.5\bar{\Pi}$, showing an important reduction of oscillations and overshoot. Furthermore, it yield much better performance against initial estimation errors.

Despite this improvement in design, it remains to take a decisive step to tackle the non-neutral bit walk case. Some of the difficulties of this scenario can be derived from this study (bilateral

coupling, nonlinear effects), and a similar methodology can be used to derived a controller that takes into account this effect.

Chapter 5

Conclusions and recommendations

5-1 Conclusions

Several conclusions can be derived from this thesis project. The initial goal to derive a controller that was able to steer a 3D directional drilling system, only making use of local measures of the inclination of the BHA was achieved.

In the nominal case, we developed an input transformation (based on the one proposed in [5]) that decouples the inclination and azimuth dynamics only after the inclination observer error dynamics converge to zero. To analyze stability, the system was linearized around the equilibrium where both the tracking error and the observer error were equal to zero (considering that the assumption on small tracking and observer errors is reasonable under normal drilling conditions).

Analyzing the closed-loop tracking error dynamics and observer error dynamics, it was found that the azimuth dynamics were perturbed by the observer error dynamics of the inclination. However, the inclination dynamics are independent from the azimuth dynamics, which results in a series interconnection between the two. Moreover, if this coupling perturbation is not considered, in both inclination and azimuth the separation principle between observer and controller was proved to hold. This inspired to use a cascaded structure for the error dynamics to aid in the task of the controller design. A "length" scale was proposed for the convergence of controller and observer dynamics for the two orientation variables to guarantee the stability (and transient performance) of the system, making use of the aforementioned structure.

The controller was synthesized considering four isolated error systems, for which stability was ensured if the right-most pole of the union of the closed-loop eigenvalues of this subsystems was on the left-half of the complex plane. Furthermore, performance was considered by proposing a "length" scale for the convergence of controller and observer dynamics for the two orientation variables, to guarantee that the observer dynamics of the inclination would not affect the transient of the azimuth, making use of the aforementioned cascaded structure. This synthesis was done by optimizing the location of the right-most pole of each subsystem, and implementing a low-pass filter and integral action based on the works of [5]. Simulations

were subsequently performed, and it was seen that the controller managed to track a proposed complex borehole geometry, even in the presence of large initial estimation errors.

As a next step, robust stability against uncertainty in the active weight on bit Π was analyzed. This analysis (which was performed by linearizing the uncertain error system dynamics once again) showed, that stability may be compromised if the value Π was sufficiently low. Also, the analysis of the closed-loop error dynamics of the system showed, that there was still a unilateral coupling from the inclination dynamics to the azimuth dynamics. However, the separation principle between observer and controller design did not hold anymore, for both the inclination and azimuth dynamics. To tackle this situation, a similar cascaded structure was proposed, now considering the tracking and observer error dynamics of the inclination as one subsystem which perturbed the azimuth tracking and observer error dynamics.

The synthesis of this controller was done by considering two decoupled subsystems of the inclination and azimuth dynamics, both comprising the controller and observer gains. Furthermore, a "length" scale was also proposed in order to guarantee a *faster* convergence of the inclination error dynamics. The low-pass filter and integral action were applied in the same way as in the nominal controller, and they were synthesized once again, by optimizing the location of the right-pole of the closed-loop error dynamics of each subsystem. This controller, was proved to be robust against uncertainty related to the active weight on bit Π. Simulation results showed a significant improvement in the transient performance of the system, reducing almost completely the oscillations present while using the nominal controller. Also, the system showed a much more homogeneous right-most pole location for both isolated error subsystems for a range of values of $\Pi \in [0.5\bar{\Pi}, 1.5\bar{\Pi}]$, which means that the controller design provided a stable and well-behave controller, with a higher degree of independence with respect to the active weight on bit.

5-2 Recommendations

Despite the positive results achieved, several tasks were left pending. Here we point out the ones that are considered the most important.

Extending the current design to the case of non-neutral bit walk tendency. Unfortunately, due to lack of time, it was not possible to extend this design strategy to the non-neutral bit walk case. However, from this controller design several guidelines on where to start the analysis of this case can be obtained. As a first step, the output equations of the system were derived in this research. These resulted in two nonlinear bilaterally coupled equations. The robust controller derived was tested, in order to get insight on how the coupling affects this system. It was shown that the presence of bit walk tendency greatly affects the performance of the system. In order to proceed with a controller design similar to the one taken here, one could make use of the linearized system derived in [5], which takes into account the presence of a bit walk angle different to zero, and proceed then to obtain a linearized version of the output equations. This process will most likely result in a system that couples inclination and azimuth dynamics bilaterally. Once again, one could analyze the system matrices to understand how the coupling acts on both the inclination and azimuth dynamics, and possibly make uses of tools such as the RGA.

Analyze the coupling effect of the bit walk angle. Despite the fact that this research shows some insight with respect to the effect of ϖ, the true consequences of this will not be known until the closed-loop error dynamics of the system are derived. This closed-loop error dynamics may yield a strong coupling, for which the input transformation is not even capable to generate a unilateral coupling from inclination to azimuth. This coupling has to be formally studied, which can be done in several ways. One could take a similar thinking process as in this research, were the matrix structure was analyzed, and lead to the proposed cascaded system. However, if the system matrices yield a high level of complexity, one could make use of either time domain simulations, to study the effects of the coupling, or make use of frequency domain tools, such as the Relative Gain Array.

Alternative angle parameterization. In [5], one of the final recommendations was to derive the borehole evolution equations, making use of different angle parameterization to avoid the singularity present at $\Theta = 0°$. This was actually attempted in this research, although it proved to be more challenging than expected, which is why it was not included in this report. The attempt consisted in using an alternative angle parameterization proposed in [19]. This description, was considered to simplify the analysis of a phenomenon called bit tilt saturation, and it is valid for small changes in the curvature. The model was derived making use of this description (which replaces the azimuth angle Φ with a pseudo-azimuth Δ), and open-loop simulations were performed. The results of the simulations were not positive since there was a discrepancy between the responses of both models. It is believed that this discrepancy has to do with how the average of the pseudo-azimuth acts in the model.

Analyze the applicability of the developed strategy to models that consider a wider range of nonlinear effects. Although the PD model has proven to be one of the most advanced in the field, it does not consider certain effects present in the system. Some work has already been done in the development of a switching model that takes into account bit tilt saturation in [19] for a 3D directional drilling system, and currently research is being done to develop a hybrid model that considers the presence of non-ideal stabilizer contact. One could try to work on developing this control strategy for this novel system description, in order to improve performance in a real scenario.

Appendix A

BHA profile and influence coefficients

The coefficients originated from the model of the BHA profile are given in this appendix. These coefficients are obtained by imposing $6(n+1)$ constraints to the general solution of Equations (2-5). The BHA is divided in $n+1$ beams connected by this set of constraints, considering the segments between stabilizers, the segment from the first stabilizer and the RSS and the segment between the RSS and the bit as the total number of sections of the BHA. These coefficients depend on the dimensionless parameters distance between stabilizers $\varkappa_i$ for $i = 1, .., n$, distance from bit to RSS Λ, external loads Υ, Γ_2 and Γ_3 and the variables corresponding to the angles at the bit $\hat{\theta}$ and $\hat{\phi}$ and the average inclination and azimuth angles $\langle\Theta\rangle_i$ and $\langle\Phi\rangle_i$ for $i = 1, 2$.

A-1 Profile coefficients

$$\mathcal{A}_{i3} = \frac{1}{2}\Upsilon \sin\langle\Theta\rangle_1, \qquad \text{for } i \in [0,1,2],$$

$$\begin{aligned}\mathcal{A}_{02} =& \frac{3}{8(4\varkappa_2+3)}\Big(24\Gamma_2\Lambda^3 - 36\Gamma_2\Lambda^2 + 8\Gamma_2\Lambda^3\varkappa_2 - 24\Gamma_2\Lambda^2\varkappa_2 + 16\Gamma_2\varkappa_2 + 12\Gamma_2 + 16\hat{\theta}\varkappa_2 + 24\hat{\theta} \\ & - 6\Upsilon\sin\langle\Theta\rangle_1 + 3\Upsilon\varkappa_2^3\sin\langle\Theta\rangle_1 - 10\Upsilon\varkappa_2\sin\langle\Theta\rangle_1 - 16\langle\Theta\rangle_1\varkappa_2 - 48\langle\Theta\rangle_1 + 24\langle\Theta\rangle_2\Big),\end{aligned}$$

$$\begin{aligned}\mathcal{A}_{12} =& \frac{3}{8(4\varkappa_2+3)}\Big(24\Gamma_2\Lambda^3 - 36\Gamma_2\Lambda^2 + 8\Gamma_2\Lambda^3\varkappa_2 - 24\Gamma_2\Lambda^2\varkappa_2 + 16\hat{\theta}\varkappa_2 + 24\hat{\theta} - 6\Upsilon\sin\langle\Theta\rangle_1 \\ & + 3\Upsilon\varkappa_2^3\sin\langle\Theta\rangle_1 - 10\Upsilon\varkappa_2\sin\langle\Theta\rangle_1 - 16\langle\Theta\rangle_1\varkappa_2 - 48\langle\Theta\rangle_1 + 24\langle\Theta\rangle_2\Big),\end{aligned}$$

$$\begin{aligned}\mathcal{A}_{22} =& -\frac{3}{8\varkappa_2(4\varkappa_2+3)}\Big(12\Gamma_2\Lambda^3 - 12\Gamma_2\Lambda^2 + 8\hat{\theta} + \Upsilon\sin\langle\Theta\rangle_1 + 10\Upsilon\varkappa_2^3\sin\langle\Theta\rangle_1 + 22\Upsilon\varkappa_2^2\sin\langle\Theta\rangle_1 \\ & + 12\Upsilon\varkappa_2\sin\langle\Theta\rangle_1 - 24\langle\Theta\rangle_1 + 16\langle\Theta\rangle_2\Big),\end{aligned}$$

$$\begin{aligned}\mathcal{A}_{01} =& -\frac{3}{4(4\varkappa_2+3)}\Big(12\Gamma_2\Lambda^3 - 24\Gamma_2\Lambda^2 + 12\Gamma_2\Lambda + 8\Gamma_2\Lambda^3\varkappa_2 - 24\Gamma_2\Lambda^2\varkappa_2 + 16\Gamma_2\Lambda\varkappa_2 + 16\hat{\theta}\varkappa_2 \\ & + 16\hat{\theta} - \Upsilon\sin\langle\Theta\rangle_1 + \Upsilon\varkappa_2^3\sin\langle\Theta\rangle_1 - 2\Upsilon\varkappa_2\sin\langle\Theta\rangle_1 - 16\langle\Theta\rangle_1\varkappa_2 - 24\langle\Theta\rangle_1 + 8\langle\Theta\rangle_2\Big),\end{aligned}$$

$$\begin{aligned}\mathcal{A}_{11} =& -\frac{3}{4(4\varkappa_2+3)}\Big(12\Gamma_2\Lambda^3 - 24\Gamma_2\Lambda^2 + 8\Gamma_2\Lambda^3\varkappa_2 - 24\Gamma_2\Lambda^2\varkappa_2 + 16\hat{\theta}\varkappa_2 + 16\hat{\theta} - \Upsilon\sin\langle\Theta\rangle_1 \\ & + \Upsilon\varkappa_2^3\sin\langle\Theta\rangle_1 - 2\Upsilon\varkappa_2\sin\langle\Theta\rangle_1 - 16\langle\Theta\rangle_1\varkappa_2 - 24\langle\Theta\rangle_1 + 8\langle\Theta\rangle_2\Big),\end{aligned}$$

$$\begin{aligned}\mathcal{A}_{21} =& \frac{3(\varkappa_2+1)}{4\varkappa_2(4\varkappa_2+3)}\Big(12\Gamma_2\Lambda^3 - 12\Gamma_2\Lambda^2 + 8\hat{\theta} + \Upsilon\sin\langle\Theta\rangle_1 + 10\Upsilon\varkappa_2^3\sin\langle\Theta\rangle_1 + 22\Upsilon\varkappa_2^2\sin\langle\Theta\rangle_1 \\ & + 12\Upsilon\varkappa_2\sin\langle\Theta\rangle_1 - 24\langle\Theta\rangle_1 + 16\langle\Theta\rangle_2 - 2\Upsilon\varkappa_2(\varkappa_2+1)(\varkappa_2+3)\sin\langle\Theta\rangle_1\Big),\end{aligned}$$

$$\mathcal{A}_{00} = \hat{\theta},$$

$$\mathcal{A}_{10} = \frac{1}{2}\left(2\hat{\theta} - 3\Gamma_2\Lambda^2\right),$$

$$\mathcal{A}_{20} = \frac{3\left(-\frac{3}{2}\varkappa_2 - 1\right)}{8\varkappa_2(4\varkappa_2+3)}\Big(12\Gamma_2\Lambda^3 - 12\Gamma_2\Lambda^2 + 8\hat{\theta} + \Upsilon\sin\langle\Theta\rangle_1 + 10\Upsilon\varkappa_2^3\sin\langle\Theta\rangle_1 + 22\Upsilon\varkappa_2^2\sin\langle\Theta\rangle_1 + 12\Upsilon\varkappa_2\sin\langle\Theta\rangle_1 - 24\langle\Theta\rangle_1 + 16\langle\Theta\rangle_2\Big) - \frac{3}{4}\Gamma_2\Lambda^3 + \frac{3\Gamma_2\Lambda^2}{4} - \frac{\hat{\theta}}{2} - \frac{3}{16}\Upsilon\sin\langle\Theta\rangle_1 + \frac{3}{2}\langle\Theta\rangle_1 + \frac{9}{8}\Upsilon(\varkappa_2+1)^2\sin\langle\Theta\rangle_1.$$

These coefficients were obtained by using the same procedure as the one in Appendix B of [23]. In the case of the general solution of the BHA profile equation (2-5) with respect to the azimuth, the same constraints can be applied, with the main difference that there are no gravitational effects on the azimuth and that all the RSS forces will be scaled by the term $\frac{1}{\sin\langle\Theta\rangle_1}$. The profile coefficients of the azimuth BHA angle equation in (2-7) are given by:

$$\mathcal{B}_{02} = \frac{3}{8(4\varkappa_2+3)}\Big(24\frac{\Gamma_3}{\sin\langle\Theta\rangle_1}\Lambda^3 - 36\frac{\Gamma_3}{\sin\langle\Theta\rangle_1}\Lambda^2 + 8\frac{\Gamma_3}{\sin\langle\Theta\rangle_1}\Lambda^3\varkappa_2 - 24\frac{\Gamma_3}{\sin\langle\Theta\rangle_1}\Lambda^2\varkappa_2 + 16\frac{\Gamma_3}{\sin\langle\Theta\rangle_1}\varkappa_2 + 12\frac{\Gamma_3}{\sin\langle\Theta\rangle_1} + 16\hat{\phi}\varkappa_2 + 24\hat{\phi} - 16\langle\Phi\rangle_1\varkappa_2 - 48\langle\Phi\rangle_1 + 24\langle\Phi\rangle_2\Big),$$

$$\mathcal{B}_{12} = \frac{3}{8(4\varkappa_2+3)}\Big(24\frac{\Gamma_3}{\sin\langle\Theta\rangle_1}\Lambda^3 - 36\frac{\Gamma_3}{\sin\langle\Theta\rangle_1}\Lambda^2 + 8\frac{\Gamma_3}{\sin\langle\Theta\rangle_1}\Lambda^3\varkappa_2 - 24\frac{\Gamma_3}{\sin\langle\Theta\rangle_1}\Lambda^2\varkappa_2 + 16\hat{\phi}\varkappa_2 + 24\hat{\phi} - 16\langle\Phi\rangle_1\varkappa_2 - 48\langle\Phi\rangle_1 + 24\langle\Phi\rangle_2\Big),$$

$$\mathcal{B}_{22} = -\frac{3}{8\varkappa_2(4\varkappa_2+3)}\Big(12\frac{\Gamma_3}{\sin\langle\Theta\rangle_1}\Lambda^3 - 12\frac{\Gamma_3}{\sin\langle\Theta\rangle_1}\Lambda^2 + 8\hat{\phi} - 24\langle\Phi\rangle_1 + 16\langle\Phi\rangle_2\Big),$$

$$\mathcal{B}_{01} = -\frac{3}{4(4\varkappa_2+3)}\Big(12\frac{\Gamma_3}{\sin\langle\Theta\rangle_1}\Lambda^3 - 24\frac{\Gamma_3}{\sin\langle\Theta\rangle_1}\Lambda^2 + 12\frac{\Gamma_3}{\sin\langle\Theta\rangle_1}\Lambda + 8\frac{\Gamma_3}{\sin\langle\Theta\rangle_1}\Lambda^3\varkappa_2 - 24\frac{\Gamma_3}{\sin\langle\Theta\rangle_1}\Lambda^2\varkappa_2 + 16\frac{\Gamma_3}{\sin\langle\Theta\rangle_1}\Lambda\varkappa_2 + 16\hat{\phi}\varkappa_2 + 16\hat{\phi} - 16\langle\Phi\rangle_1\varkappa_2 - 24\langle\Phi\rangle_1 + 8\langle\Phi\rangle_2\Big),$$

$$\mathcal{B}_{11} = -\frac{3}{4(4\varkappa_2+3)}\Big(12\frac{\Gamma_3}{\sin\langle\Theta\rangle_1}\Lambda^3 - 24\frac{\Gamma_3}{\sin\langle\Theta\rangle_1}\Lambda^2 + 8\frac{\Gamma_3}{\sin\langle\Theta\rangle_1}\Lambda^3\varkappa_2 - 24\frac{\Gamma_3}{\sin\langle\Theta\rangle_1}\Lambda^2\varkappa_2 + 16\hat{\phi}\varkappa_2 + 16\hat{\phi} - 16\langle\Phi\rangle_1\varkappa_2 - 24\langle\Phi\rangle_1 + 8\langle\Phi\rangle_2\Big),$$

$$\mathcal{B}_{21} = \frac{3(\varkappa_2+1)}{4\varkappa_2(4\varkappa_2+3)}\Big(12\frac{\Gamma_3}{\sin\langle\Theta\rangle_1}\Lambda^3 - 12\frac{\Gamma_3}{\sin\langle\Theta\rangle_1}\Lambda^2 + 8\hat{\phi} - 24\langle\Phi\rangle_1 + 16\langle\Phi\rangle_2)\Big),$$

$$\mathcal{B}_{00} = \hat{\phi},$$

$$\mathcal{B}_{10} = \frac{1}{2}\left(2\hat{\phi} - 3\frac{\Gamma_3}{\sin\langle\Theta\rangle_1}\Lambda^2\right),$$

$$\mathcal{B}_{20} = \frac{3\left(-\frac{3}{2}\varkappa_2 - 1\right)}{8\varkappa_2(4\varkappa_2+3)}\left(12\frac{\Gamma_3}{\sin\langle\Theta\rangle_1}\Lambda^3 - 12\frac{\Gamma_3}{\sin\langle\Theta\rangle_1}\Lambda^2 + 8\hat{\phi} - 24\langle\Phi\rangle_1 + 16\langle\Phi\rangle_2\right) - \frac{3}{4}\frac{\Gamma_3}{\sin\langle\Theta\rangle_1}\Lambda^3 + \frac{3}{4}\frac{\Gamma_3}{\sin\langle\Theta\rangle_1}\Lambda^2 - \frac{\hat{\phi}}{2} + \frac{3}{2}\langle\Phi\rangle_1.$$

A-2 Influence coefficients

The influence coefficients are constants related entirely to the BHA configuration. They depend on distance between stabilizers $\varkappa_i$ for $i = 1, 2$ and distance from bit to RSS Λ. The complete procedure to obtain these coefficients is given in [3].

$$\mathcal{F}_b = -\frac{6+4\varkappa_2}{3+4\varkappa_2},$$

$$\mathcal{F}_w = \frac{6+10\varkappa_2-3\varkappa_2^3}{12+16\varkappa_2},$$

$$\mathcal{F}_r = \frac{-3-4\varkappa_2+\Lambda^2(9+6\varkappa_2)-2\Lambda^3(3+\varkappa_2)}{3+4\varkappa_2},$$

$$\mathcal{F}_1 = \frac{6}{3+4\varkappa_2},$$

$$\mathcal{M}_b = \frac{4(1+\varkappa_2)}{3+4\varkappa_2},$$

$$\mathcal{M}_w = \frac{-1-2\varkappa_2+\varkappa_2^3}{12+16\varkappa_2},$$

$$\mathcal{M}_r = \frac{\Lambda(1-\Lambda)(3+4\varkappa_2-\Lambda(3+2\varkappa_2))}{3+4\varkappa_2},$$

$$\mathcal{M}_1 = -\frac{2}{3+4\varkappa_2}.$$

Appendix B

Discussion about equilibrium of the system with uncertainty on Π

In this appendix the detailed discussion related to the equilibrium point chosen for the system is given. It aims to explain the aforementioned approach, which keeps the errors e_i and δ_i, for $i = \Theta, \Phi$ different to zero, in order to provide a determined set of equilibrium equations. The resulting system of equations is the one given by

$$
\begin{aligned}
0 =& A_0 e_\Theta + (B_{0\Theta} - B_{1\Theta}\bar{b}_0)\Delta\Gamma^*_\Theta - (B_{1\Theta}\bar{b}_1)z_{2\Theta} + F_{p\Theta} + (-B - B_{1\Theta}\bar{b}_1)u_{r\Theta},\\
0 =& -\bar{b}_0\Delta\Gamma^*_\Theta - \bar{b}_1 z_{2\Theta},\\
0 =& \zeta\begin{bmatrix} k_{1\Theta} & 0 & 0\end{bmatrix} e_\Theta - \zeta\begin{bmatrix} k_{1\Theta} & 0 & 0\end{bmatrix}\delta_\Theta,\\
0 =& \gamma K_\Theta e_\Theta + \gamma z_{1\Theta} - \gamma z_{2\Theta} - \gamma K_\Theta \delta_\Theta,\\
0 =& (\Delta A_0 - L_\Theta \Delta C_\Theta)e_\Theta + (B_{0\Theta} - B_{1\Theta}\bar{b}_0 - L_\Theta\Delta D_\Theta)\Delta\Gamma^*_\Theta + (-B - B_{1\Theta}\bar{b}_1)z_{2\Theta}\\
&+ (\bar{A}_0 - L_\Theta\bar{C}_\Theta)\delta_\Theta - Bq_\Theta + F_{r\Theta} + (-B - B_{1\Theta}\bar{b}_1)u_{r\Theta},\\
0 =& \zeta\begin{bmatrix} l_{1\Theta} & l_{2\Theta}\end{bmatrix}(\Delta C_\Theta e_\Theta + \Delta D_\Theta\Delta\Gamma^*_\Theta + \bar{C}_\Theta\delta_\Theta + \Delta C_\Theta x_{r\Theta} + \Delta D_\Theta\Gamma^*_{\Theta d}),\\
0 =& A_0 e_\Phi + (B_{0\Phi} - B_{1\Phi}\bar{b}_0)\Delta\Gamma^*_\Phi - (B_{1\Phi}\bar{b}_1)z_{2\Phi} + F_{p\Phi} + (-B - B_{1\Phi}\bar{b}_1)u_{r\Phi},\\
0 =& -\bar{b}_0\Delta\Gamma^*_\Phi - \bar{b}_1 z_{2\Phi},\\
0 =& \zeta\begin{bmatrix} k_{1\Phi} & 0 & 0\end{bmatrix} e_\Phi - \zeta\begin{bmatrix} k_{1\Phi} & 0 & 0\end{bmatrix}\delta_\Phi,\\
0 =& \gamma K_\Phi e_\Phi + \gamma z_{1\Phi} - \gamma z_{2\Phi} - \gamma K_\Phi \delta_\Phi,\\
0 =& (\Delta A_0 - L_\Phi \Delta C_\Phi)e_\Phi + (B_{0\Phi} - B_{1\Phi}\bar{b}_0 - L_\Phi\Delta D_\Phi)\Delta\Gamma^*_\Phi + (-B - B_{1\Phi}\bar{b}_1)z_{2\Phi}\\
&+ (\bar{A}_0 - L_\Phi\bar{C}_\Phi)\delta_\Phi - Bq_\Phi + F_{r\Phi} + (-B - B_{1\Phi}\bar{b}_1)u_{r\Phi},\\
0 =& \zeta\begin{bmatrix} l_{1\Phi} & l_{2\Phi}\end{bmatrix}(\Delta C_\Phi e_\Phi + \Delta D_\Phi\Delta\Gamma^*_\Phi + \bar{C}_\Phi\delta_\Phi + \Delta C_\Phi x_{r\Phi} + \Delta D_\Phi\Gamma^*_{\Phi d}).
\end{aligned}
\tag{B-1}
$$

This set of equations has a unique solution. Due to the complexity of the expressions, these were solved using the Symbolic Math Toolbox of MATLAB [30]. The found solution, is indeed

ξ-dependent, and the error and observer error dynamics of the orientation at the bit (e_{i0} and δ_{i0}, for $i = \Theta, \Phi$) result equal to zero. The location of the equilibrium at $e_{i0} = \delta_{i0} = 0$, in theory, would yield the convergence of the average inclination and azimuth errors. Despite this fact, the equilibrium point found by solving (B-1), in the case of the average errors ($e_{\langle i \rangle_1}$, $e_{\langle i \rangle_2}$, $\delta_{\langle i \rangle_1}$ and $\delta_{\langle i \rangle_2}$) appears to be ξ-dependent. It is believed that the combination of the terms involving reference points, for specific values of trajectory, should make the equilibrium points equal to zero. In other words, if the values of desired trajectory are substituted in the equilibrium solutions for each specific point shown in Figure 4-1, the equilibrium solutions of the average inclination and azimuth tracking errors and observer errors will be equal to zero.

Due to the difficulty to analytically prove that the solution of the average states at the equilibrium is equal to zero, the solution found using MATLAB is compared with the equilibrium point given in the nominal case via simulation. This is done by testing the stability of the system, computing the right-most pole of the closed-loop linearized system in (4-24) (using the controller based on the nominal system) for $\Pi \in [0.5\bar{\Pi}, 1.5\bar{\Pi}]$, substituting the value of ξ at the desired trajectory point in the system matrices (i.e., computing quasi-static solutions of the system along the trajectory in Figure 4-1) for both linearization points (around Π and $\bar{\Pi}$). The result of this comparison is shown in Figure B-1.

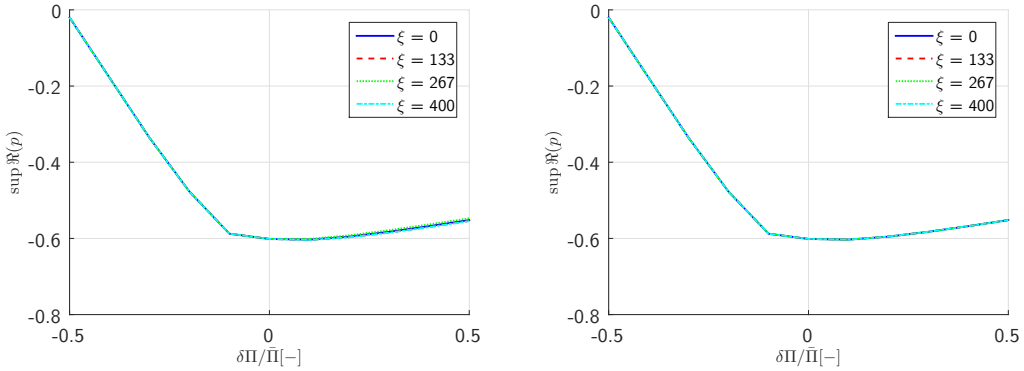

Figure B-1: Robustness test for the linearization point around $\bar{\Pi}$ (left) and Π (right).

An interesting result comes out of this test. First of all, taking a close look at the plot corresponding to the equilibrium point using real active weight on bit Π (plot on the right in Figure B-1), it can be seen that the lines in this plot are exactly on top of each other, meaning that the change on the location of the right-most pole of the closed-loop system for different values of Π is the same, irrespective of the point chosen in the trajectory where the linearization was performed. Secondly, the plot corresponding to the equilibrium point used in the nominal case (left plot in Figure B-1), it can be seen that the shift in the location of the right-most closed-loop pool is not significant (there is only a slight change in the location of the right-most pole for larger values of Π).

In summary, the effect of the chosen linearization point is thought not to be determinant for the behavior of the system.

Bibliography

[1] "Bit of best fit." http://www.drillingcontractor.org. Accessed: 2015-10-18.

[2] J. Marck and E. Detournay, "Influence of Rotary-Steerable-System Design on Borehole Spiraling," *SPE Journal*, no. April, pp. 1–10, 2015.

[3] L. Perneder, *A three-dimensional Mathematical model of directional drilling*. PhD thesis, University of Minnesota, 2013.

[4] L. Perneder and E. Detournay, "Steady-state solutions of a propagating borehole," *International Journal of Solids and Structures*, vol. 50, no. 9, pp. 1226–1240, 2013.

[5] F. Monsieurs, "Model-based decoupled control of a 3D directional drilling system," Master's thesis, Eindhoven University of Technology, 2015.

[6] G. Downton, T. S. Klausen, A. Hendricks, and D. Pafitis, "New Directions in Rotary Steerable Drilling," *Oilfield Review*, pp. 18–29, 2000.

[7] E. Felczak, N. D. Godwin, R. Hawkins, S. Jones, and F. Slayden, "The Best of Both Worlds — A Hybrid Rotary Steerable System," *Oilfield Review*, pp. 36–44, 2012.

[8] J. Marck, E. Detournay, A. Kuesters, and J. Wingate, "Analysis of Spiraled-Borehole Data by Use of a Novel Directional-Drilling Model," *SPE Drilling & Completion*, vol. 29, no. 3, pp. 267 – 278, 2014.

[9] N. P. Callas, "Predicting borehole trajectories," *Oil and Gas Journal*, vol. 79, no. 34, pp. 129–133, 1981.

[10] K. K. Millheim, "Computer simulation of the directional drilling process," in *International Petroleum Exhibition and Technical Symposium*, no. SPE 9990, (Beijing, China), pp. 483–496, Society of Petroleum Engineers, March 1982.

[11] S. Rafie, "Mechanistic approach in designing BHA's and forecasting welbore position," in *IADC/SPE Drilling Conference*, (Dallas, Texas, U.S.A.), pp. 161–170, Society of Petroleum Engineers, February-March 1988.

[12] J. Matheus, M. Ignova, and P. Hornblower, "A hybrid approach to closed-loop directional drilling control using rotary steerable systems," *SPE Latin American and Caribbean Petroleum Engineering Conference Proceedings*, vol. 3, pp. 1996–2005, 2014.

[13] G. C. Downton, "Directional drilling system response and stability," in *16th IEEE International Conference on Control Applications*, (Singapore), pp. 1543–1550, October 2007.

[14] G. Downton and M. Ignova, "Stability and response of closed loop directional drilling system using linear delay differential equations," *Control Applications (CCA)*, pp. 893–898, 2011.

[15] N. Panchal, M. T. Bayliss, and J. F. Whidborne, "Robust Linear Feedback Control of Attitude for Directional Drilling Tools," *Journal of Modeling and Simulation*, vol. 4, pp. 41–47, 2010.

[16] N. Panchal, M. T. Bayliss, and J. F. Whidborne, "Vector Based Kinematic Closed-Loop Attitude Control-System for Directional Drilling," *Proc.\ 2012 IFAC Workshop on Automatic Control in Offshore Oil and Gas Production*, no. 4020, pp. 78–83, 2012.

[17] J. Marck and E. Detournay, "Analysis of Spiraled-Borehole Data by Use of a Novel Directional-Drilling Model," *SPE Journal*, no. September 2014, pp. 268–278, 2014.

[18] G. Neubert, M. and Heisig, "Advanced trajectory simulation of directional wellbores.," *Energy Week Conference and Exhibition: incorporating ETCE*, no. 3, pp. 45–52, 1997.

[19] J. Marck, *A Nonlinear Dynamical Model of Borehole Spiraling.* PhD thesis, University of Minnesota, 2015.

[20] N. Panchal, M. T. Bayliss, and J. F. Whidborne, "Minimum strain energy waypoint-following controller for directional drilling using OGH curves," *Interntional Conference on Control Applications, Denver, 28-30 September*, pp. 887–892, 2011.

[21] M. Bayliss, C. Bogath, and J. Whidborne, "MPC-Based Feedback Delay Compensation Scheme for Directional Drilling Attitude Control," *Drilling Conference and Exhibition, 17-19 March*, 2015.

[22] H. Sun, Z. Li, N. Hovakimyan, and T. Ba, "L 1 Adaptive Control for Directional Drilling Systems," *Proceedings of the IFAC Workshop on Automic Control in Offshore and Gas Production, 6-11 July*, pp. 72–77, 2012.

[23] N. Kremers, "Model-based robust control of a directional drilling system," Master's thesis, Eindhoven University of Technology, 2013.

[24] N. Kremers, E. Detournay, and N. Van De Wouw, "Model-based robust control of directional drilling systems," *IEEE Transactions on Control Systems Technology*, vol. 24, no. 1, pp. 226–239, 2016. cited By 1.

[25] L. Perneder, E. Detournay, and C. Earth, "Anomalous Behaviors of a Propagating Borehole," *SPE 151377*, 2012.

[26] L. Perneder and E. Detournay, "Equilibrium Inclinations of Straight Boreholes," *SPE Journal*, no. June, pp. 395–405, 2013.

[27] B. Heijke, "A hybrid model of a 2D directional drilling system," Master's thesis, Delft University of Technology, 2016.

[28] L. Perneder, E. Detournay, and G. Downton, "International Journal of Rock Mechanics & Mining Sciences Bit / rock interface laws in directional drilling," *International Journal of Rock Mechanics and Mining Sciences*, vol. 51, pp. 81–90, 2012.

[29] E. Detournay, T. Richard, and M. Shepherd, "Drilling response of drag bits : Theory and experiment," *International Journal of Rock Mechanics and Mining Sciences*, vol. 45, pp. 1347–1360, 2008.

[30] MATLAB, *version 8.5.0.197613 (R2015a)*. Natick, Massachusetts: The MathWorks Inc., 2015.

[31] W. Michiels and S.-I. Niculescu, *Stability and Stabilization of Time-Delay Systems*. Philadelphia, PA, USA: Society for Industrial and Applied Mathematics, 2007.

[32] S. Chen, G. J. Collins, and M. B. Thomas, "Reexamination of PDC Bit Walk in Directional and Horizontal Wells," *SPE Journal*, no. March, pp. 4–6, 2008.

Glossary

List of Acronyms

RSS	Rotary Steerable System
ROP	Rate of Penetration
BHA	Bottom Hole Assembly
MWD	Measurement While Drilling
PDC	Polycrystalline Diamond Compact
MPC	Model Predictive Control
MIMO	Multiple Input Multiple Output
RGA	Relative Gain Array
LTI	Linear Time Invariant

List of Symbols

Greek Symbols

α	Lumped inclination-related terms in the azimuth dynamics.
χ	Angular steering resistance.
δ	Observer error dynamics.
$\Delta\Gamma$	Error coordinate for the RSS input.
η	Lateral steering resistance.
Γ	Scaled RSS force.
γ	Low-pass filter gain.

Λ	Scaling factor for the location of the RSS
λ_{jKi}	Closed-loop pole i of tracking error dynamics.
λ_{jLi}	Closed-loop pole i of observer error dynamics.
Φ	Borehole azimuth.
ϕ	BHA azimuth.
Φ_i	Azimuth of the i-th stabilizer.
Π	Scaled active weight on bit.
ρ	Density.
Θ	Borehole inclination.
θ	BHA inclination.
Θ_i	Inclination of the i-th stabilizer.
Υ	Scaled distributed weight.
$\varkappa_i$	Dimensionless length of i-th section.
ϖ	Bit walk angle.
$\vec{\Omega}$	Angular velocity vector of the bit.
$\vec{\omega}$	Spin vector of the bit.
$\vec{\varphi}$	Angular penetration.
ξ	Dimensionless length.
ξ_i	Dimensionless location of stabilizer i.
ζ	Integral part gain.
$\langle\Phi\rangle_i$	Average borehole azimuth of i-th stabilizer.
$\langle\Theta\rangle_i$	Average borehole inclination of i-th stabilizer.

Latin Symbols

$(\vec{e}_x, \vec{e}_y, \vec{e}_z)$	Fixed coordinate system.
$(\vec{I}_1, \vec{I}_2, \vec{I}_3)$	Basis for the borehole axis.
$(\vec{i}_1, \vec{i}_2, \vec{i}_3)$	BHA basis.
ℓ_i	Length of BHA section i.
$\hat{F}_1, \hat{F}_2, \hat{F}_3, \hat{M}_2, \hat{M}_3$	Forces and moments acting on the bit.
$\mathcal{A}_{ij}$	Coefficients of inclination angle for general solution of BHA profile.
$\mathcal{B}$	Borehole axis.
$\mathcal{B}_{ik}$	Coefficients of azimuth angle for general solution of BHA profile.
$\mathcal{C}_1$	Chord linking the bit and the first stabilizer.
$\mathcal{C}_{ij}$	Constant coefficients of the inclination output equations.
$\mathcal{D}$	BHA axis.
$\mathcal{D}_{ik}$	Constant coefficients of the azimuth output equations.
$\mathcal{F}_b$, $\mathcal{F}_r$, $\mathcal{F}_w$, $\mathcal{F}_i$	Coefficients related to force influence.
$\mathcal{M}_b$, $\mathcal{M}_r$, $\mathcal{M}_w$, $\mathcal{M}_i$	Coefficients related to moment influence.

$\vec{d}$	Axial penetration vector.
$\vec{F}_{rss}$	RSS force in the BHA.
$\vec{R}(S)$	Vector function of borehole axis $\mathcal{B}$ in curvilinear coordinates S.
$\vec{r}(s, L)$	Vector function of the BHA axis in curvilinear coordinates s.
$\vec{v}$	Linear velocity of the bit.
$\vec{w}$	Distributed weight on the BHA.
A	Cross section surface area of the BHA.
A_0, A_1, A_2	System matrices of the neutral bit walk model.
a_i	Auxiliary variables for the borehole evolution equations for $i = 1, ..., 4$.
A_{0cl}, A_{1cl}, A_{2cl}	Closed-loop matrices of the system.
B, B_{0i}, B_{1i}	System vectors of the neutral bit walk model.
b_i	Auxiliary variables for the derivatives of the Θ and Φ for $i = 1, ..., 8$.
$d_1, d_2, d_3, \varphi_2, \varphi_3$	Set of scalar penetration variables.
e	Tracking error dynamics.
E_y	Young's module.
F_*	Characteristic force
G_1	Bluntness coefficient of the bit/rock interaction.
H_0, H_1, H_2, H_3	Bit/rock interface geometry and rock properties coefficients.
I	Area moment of inertia.
I_r	Inner radius of the BHA.
K_i	State-feedback gain.
L	Total length of borehole.
L_*	Characteristic length.
L_i	Observer feedback gain matrix.
L_{BHA}	Length of the BHA.
n	Number of stabilizers.
O_r	Outer radius of the BHA.
P_{cl}	Perturbation vector of closed-loop system dynamics.
S	Curvilinear coordinate from drill rig to bit.
s_i	Location of the i-th stablizer.
u_i	Sum of the feedback and feedforward inputs.
W	Normalized weight of the BHA.
w	Uniform distributed weight.
W_y	Normalized output-related weight of the BHA.
W_{act}	Active weight on bit.
W_{app}	Applied weight on bit.
x_i	State vector.
x_{ri}	Reference vector.
z_{1i}	Integral action state.

z_{2i}	Low-pass filter state.

Subscripts

$_\Phi$	Borhole azimuth dynamics.
$_\Theta$	Borehole inclination dynamics.
$_d$	Desired value.
$_r$	Reference trajectory.

Superscripts

*	Transformed RSS force.

Diacritic Symbols

$\bar{}$	Evaluated at nominal active weight on bit.
$\check{}$	Estimated value.
$\hat{}$	Evaluated at the bit.